Understanding the molecular mechanisms of arrhythmogenic right ventricular cardiomyopathy caused by TMEM43 p.S358L mutation

© Zachary G. Porter, B.Sc.

A thesis submitted to the School of Graduate Studies in partial fulfillment of the requirements for the degree of

Master of Science in Medicine (Cancer & Development)

Division of BioMedical Sciences, Faculty of Medicine

Memorial University of Newfoundland

October 2022

St. John's, Newfoundland and Labrador

Abstract

Arrhythmogenic right ventricular cardiomyopathy (ARVC) is a genetic cardiac disease characterized by fibrofatty infiltration of the myocardium, life-threatening arrhythmias, and sudden cardiac death. Newfoundland and Labrador is home to a substantial founder population with an autosomal dominant mutation in the transmembrane protein 43 (*TMEM43*) gene (c.1073C>T; p.S358L), responsible for ARVC type 5. Although we know that this mutation causes ARVC, there is limited information on the TMEM43 protein life cycle, protein-protein interactions, and function. Additionally, it is unknown how the p.S358L mutation affects TMEM43 function, contributes to ARVC, or why it affects only the heart despite being widely expressed. Here I investigate the intracellular trafficking of wild-type TMEM43 in human induced pluripotent stem cells (iPSCs) and iPSC-cardiomyocytes (iPSC-CMs). I find that TMEM43 resides primarily in early endosomes in iPSCs. Interestingly, although TMEM43 remains localized to early endosomes in early contracting iPSC-CMs, it shifts toward the nuclear envelope as iPSC-CMs are cultured *in vitro* for an extended period of time. CRISPR-Cas9 genetic ablation of the *TMEM43* gene has no apparent effects on several intracellular organelles previously shown to be affected by the TMEM43-S358L mutation. However, *TMEM43-/-* iPSC-CMs exhibit subtle calcium handling aberrations pointing toward a pro-arrhythmic phenotype. Finally, primary ARVC patient dermal fibroblasts show significant changes in the expression of extracellular matrix proteins, which may play a role in the fibrosis seen in ARVC. Together, these studies begin to unravel the basic life cycle and function of the TMEM43 protein in a human-derived cellular model of ARVC.

Lay Summary

Arrhythmogenic right ventricular cardiomyopathy (ARVC) is an inherited heart disease that causes heart failure, requiring a heart transplant, or sudden cardiac death. Newfoundland and Labrador has a large population with ARVC due to a specific mutation in the *TMEM43* gene. Genes are the "blueprint" for building proteins, which are essential components that make up a cell, and mutations are mistakes in the blueprint that can affect protein function and cause cell damage. Cells are what make up the human body. Children of ARVC affected parents have a 50% chance of acquiring the disease, and the disease is more severe in males than females. Despite being linked to ARVC, the function of TMEM43 protein in heart cells is unknown. My study focused on uncovering the unknown characteristics of the TMEM43 protein and how heart cells are affected when TMEM43 is not present. A better understanding of normal TMEM43 function will shed light on how the mutated protein causes ARVC.

Co-authorship Statement

TMEM43-/- induced pluripotent stem cells used in this study were generated by Dr. Jessica Esseltine, Robert Flemmer, and Hooman Sadighian. Dr. Kathy Hodgkinson recruited all ARVC patients that donated skin biopsies for this project. The skin biopsies were collected by Dr. David Pace. Dr. Esseltine helped isolate fibroblasts from the patient skin biopsies and prepare data figures. Rebecca Frohlich and Grace Christopher assisted in training me in stem cell culture techniques. Camila Fuchs performed the blinded analysis of calcium traces presented in Figure 11G.

Acknowledgments

I want to express my appreciation and gratitude to Dr. Jessica Esseltine, as her guidance, support, and enthusiasm have been invaluable to my success in this degree. I am very grateful she took me on as a graduate student. Jess was always supportive through the highs and lows of my studies. She has been my greatest mentor as a graduate student. I am grateful for my committee members, Dr. Kathy Hodgkinson and Dr. Jules Dore, who offered their expertise to help me complete my degree. I would also like to thank all the graduate students, faculty members, and staff members who have helped me along the way.

I am grateful for my lab mates, especially Rebecca Frohlich and Hooman Sadighian, who have sacrificed their time to help train and support me throughout my Master's program. Finally, I would like to thank my family and friends who have been so supportive throughout my MSc program.

This research was made possible by funding from the Faculty of Medicine, Memorial University, and the Stem Cell Network Grant FY21 / ECI-7 to Jessica L. Esseltine. In addition, the School of Graduate Studies and the Stem Cell Network Grant FY21 / ECI-7 to Jessica L. Esseltine were sources of support for my stipend during my full-time program.

The authors declare that the research in this thesis was conducted in the absence of any financial or personal relationships with any organization that could be interpreted as a conflict of interest.

Table of Contents

List of Abbreviations

ANOVA – Analysis of variance

ANF – Atrial natriuretic factor

ARVC – Arrhythmogenic right ventricular cardiomyopathy

AV – Atrioventricular

BMP – Bone morphogenic protein

BMP4 – Bone morphogenic protein 4

BFA – Brefeldin A

BSA – Bovine serum albumin

cTnT – Cardiac muscle troponin T

Cx – Connexin

Cx37 – Connexin37

Cx40 – Connexin40

Cx43 – Connexin43

Cx45 – Connexin45

DSC2 – Desmocollin2

DSG2 – Desmoglein2

DSP – Desmoplakin

DCM – Dilated cardiomyopathy

DMEM – Dulbecco's modified eagle medium

E8 – Essential 8 medium

EEA1 – Early endosome antigen 1

ECG – Electrocardiogram

ECM – Extracellular matrix

FABP4 – Fatty acid-binding protein 4

FBS – Fetal bovine serum

FGF – Fibroblast growth factor

FGF8 – Fibroblast growth factor 8

FACS – Fluorescence-activated cell sorting

GAPDH – Glyceraldehyde 3-phosphate dehydrogenase

GATA4 – GATA binding protein 4

GSK3β – Glycogen synthase kinase-3β

HRP – Horseradish peroxidase

HCM – Hypertrophic cardiomyopathy

iPSC – Induced pluripotent stem cell

iPSC-CM – Induced pluripotent stem cell-derived cardiomyocyte

LINC – LInker of Nucleoskeleton and Cytoskeleton

LTCC – L-Type calcium channels

LAMP1 – Lysosomal-associated membrane protein 1

MESP1 – Mesoderm posterior 1

mEGFP – Monomeric enhanced green fluorescent protein

MEF2C – Myocyte-specific enhancer factor 2C

MLC2A – Myosin light chain 2A

MLC2V – Myosin light chain 2V

MRI – Magnetic resonance imaging

NF-κβ – Nuclear factor

NFAT – Nuclear factor of activated T-cells

PPARγ – Peroxisome proliferator-activated receptor-γ

PBS – Phosphate-buffered saline

PDE – Phosphodiesterase

PKP2 – Plakophilin2

PKG – Plakoglobin

Rab – Ras-like proteins in brain

sgRNA – Single guide RNAs (sgRNA)

SDS-PAGE – Sodium dodecyl sulfate-polyacrylamide gel electrophoresis

RPM – Rotations per minute

RYR2 – Ryanodine receptor 2

SERCA – Sarcoendoplasmic reticulum ATPase pump

SR – Sarcoplasmic reticulum

qPCR – Semi-quantitative reverse transcription-polymerase chain reaction

SA – Sinoatrial

TBX5 – T-Box transcription factor 5

TGFβ – Transforming growth factor beta

x g – Times gravity

TMEM43 – Transmembrane protein 43

TMEM43-S358L – Transmembrane protein 43 (*c.1073C>T*; p.S358L)

TBS-T – Tris buffered saline with tween 20

WNT – Wingless/int family of genes

WT – Wild type

List of Tables

List of Figures

1 Introduction

1.1 The Heart

The heart is a vital organ that pumps blood through the circulatory system to deliver oxygen and nutrients to all the body's cells and help facilitate the movement of metabolic waste to the excretory organs, where it can be removed from the body. The heart is involved in regulating blood pressure and heart rate with the help of the nervous system and the endocrine system[1]. Thus, proper heart function is essential in maintaining homeostasis within the body and diseases of the heart are especially deleterious to human health.

1.2 Heart Development

The heart is derived from the embryonic mesoderm germ layer. The heart is formed from bilateral fields created during the gastrulation process[2]. Cardiac progenitor cells of the late gastrulation embryo are often called the cardiac crescent because of the shape of the region they form. This cardiac crescent extends laterally along the embryo and eventually fuses with the midline to form the primitive linear heart tube. The primitive cardiomyocytes begin to contract, and the heart tube morphologically changes as the heart starts to twist in a process called cardiac looping. The process of cardiac looping marks the beginning of ventricular and atrial formation[3]. The heart's conduction system develops simultaneously during the formation of the heart tube and cardiac looping. By the end of the second week of embryonic development, the differentiating cardiomyocytes begin to establish electrical conduction properties and display peristaltic contractions when the heart tube is formed. These processes form the general structure of the heart and will continue to develop into a

mature adult heart[3]. Heart development begins very early in embryonic development with both the electrical system and chambers of the heart forming simultaneously.

1.2.1 Structure of the Adult Heart

The heart is a hollow muscular organ composed of 4 chambers: the left and right atria and ventricles. The heart's left and right atria receive blood from the pulmonary and systemic circulations and eject the blood into the ventricles. The ventricles pump the blood back into the pulmonary and systemic circulation. The heart is a dual pump separated by the septum in which the left atria and ventricle make up the left pump, while the right atria and ventricle make up the right pump. The left pump receives oxygenated blood from the pulmonary circulation and pumps it into the systemic system. The right pump receives deoxygenated blood from the systemic circulation and pumps it into the pulmonary system to be reoxygenated and remove carbon dioxide[4]. The two-pump system in the heart allows for blood to be pumped into the pulmonary and systemic circulation simultaneously with every heart beat.

The walls of the heart are composed of three distinct layers: the endothelium, myocardium, and epicardium. The innermost endothelial layer lines the entire circulatory system and is involved in several physiological processes such as blood coagulation mechanisms, vasodilation and constriction, angiogenesis, platelet-leukocyte interactions, and inflammation[5]. The middle myocardium layer is composed of cardiac muscle (cardiomyocytes) responsible for pumping blood via synchronized contraction[6]. Finally, the external epicardium plays a role in tissue regeneration and houses tissue-resident fibroblasts which are mainly responsible for the production and maintenance of

extracellular matrix proteins for structural stability and mechanical stability[7]. Additionally, cardiac fibroblasts have an integral role in cardiac remodeling and scar formation after events such as myocardial infarctions[8]. These three layers of the heart wall work together to provide structure and strength to the heart allowing for efficient blood pumping.

1.2.2 Cardiomyocyte Cell Fate Specification

Cardiomyocyte cell fate specification begins with embryonic stem cell specification to embryonic mesoderm. The embryonic splanchnic mesoderm gives rise to cardiac progenitor cells. The progenitor cells form the cardiac crest, where they differentiate into the different cardiac cell types[9] (Figure 1). The formation of the cardiac progenitor cells begins the process that ultimately leads to all the cardiac cell types in the heart.

Pluripotent stem cells are the starting point of cardiomyocyte cell fate specification. Pluripotent stem cells express the regulatory factors Oct4, Nanog, and Sox2 that maintain pluripotency and play a role in cell fate specification. High levels of Oct4 in the absence of bone morphogenetic protein 4 (BMP4) signaling promote self-renewal, while high levels of Oct4 in the presence of BMP4 specify mesendoderm[10]. Activating the nodal/activin A and wingless/int family of genes (WNT) signaling pathways in stem cells leads to mesoderm germ lineage commitment[11,12,13]. The expression of brachyury and Mixl-1 can identify the developed mesoderm tissue. During mouse development, brachyury is expressed in the primitive streak, tailbud, and notochord[14,15]. Brachyury knock-out embryos do not form a differentiated notochord[16]. Mixl-1 is expressed in the primitive streak,[17] and knock-out models develop defects in mesoderm-derived structures such as thickened primitive streak, absence of heart tube and gut, and deficient paraxial

Figure 1 Transcription factors and signaling pathways involved in pluripotent stem cells specification to cardiomyocytes

Embryonic stem cells express pluripotent markers Oct4, Nanog, and Sox2 and are the starting point in cardiomyocyte cell specification. Activation of nodal/Activin A and WNT signaling pathways initiate mesoderm germ lineage specification. Mesoderm cells can be identified by the mesoderm markers brachyury and Mixl-1. Notch inhibition and activation of FGF and BMP signaling cause the commitment of mesoderm to cardiac mesoderm. Cardiac mesoderm cells express MESP1/2 and Flk-1. Downregulation of Transforming Growth Factor Beta (TGFβ), WNT, and BMP signaling occur when cardiac mesoderm transitions into cardiac progenitor cells. Cardiac progenitor cells express the markers Nkx2.5, GATA binding protein 4 (GATA4), T-box transcription factor 5 (TBX5), and myocyte-specific enhancer factor 2C (MEF2C). BMP signaling is upregulated a second time during the differentiation of cardiac progenitors into cardiomyocytes. Mature cardiomyocytes express Nkx2.5, cardiac muscle troponin T (cTnT), α-actin, myosin light chain 2A (MLC2A), and myosin light chain 2V (MLC2V). Cell progression from mesoderm to cardiac mesoderm to cardiomyocytes is a time-sensitive process. Figure 1 was created using BioRender Premium software, *biorender.com*.

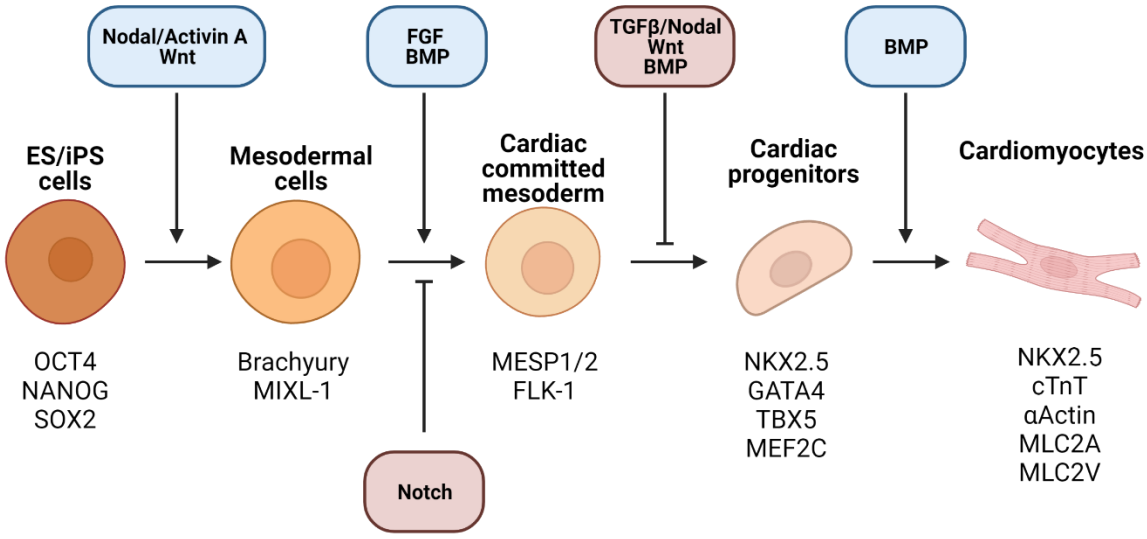
Nodal/Activin A
Wnt
FGF
BMP
TGFβ/Nodal
Wnt
BMP
BMP
ES/iPS cells
Mesodermal cells
Cardiac committed mesoderm
Cardiac progenitors
Cardiomyocytes
OCT4
NANOG
SOX2
Brachyury
MIXL-1
MESP1/2
FLK-1
NKX2.5
GATA4
TBX5
MEF2C
NKX2.5
cTnT
αActin
MLC2A
MLC2V
Notch

mesoderm[18]. Transitioning from mesoderm to cardiac mesoderm requires the activation of fibroblast growth factor (FGF) and BMP signaling pathways[19]. In addition, inhibition of notch signaling helps promote cardiac specification of the mesoderm[20]. The earliest marker of cardiac mesoderm induction in cardiac specification is the transcription factor mesoderm posterior 1 (MESP1), expressed at embryonic days 6.5-7.5 in mice[21]. MESP1-positive cells give rise to cardiac cells[22], and cardiac precursor cells in MESP1 knockout mice fail to migrate properly, leading to abnormal heart morphogenesis[22]. The tyrosine kinase receptor Flk-1 is another marker of early cardiac mesoderm. Cell populations that express Flk-1 have the potential to differentiate into cardiac, endothelial, and vascular smooth muscle cell types[23]. In addition to the role of FGF and BMP signaling pathways, cardiac mesoderm populations are depended on MESP1 and Flk-1 in the developmental timeline as knockout models demonstrate significant abnormalities. These developmental discoveries observed in model organisms now enable scientists to direct the cell fate specification of pluripotent stem cells *in vitro* toward cardiac progenitors and cardiomyocytes (Figure 1).

For cardiac-committed mesoderm to become cardiac progenitor cells, transforming growth factor β (TGFβ)/Nodal, WNT, and BMP signaling must be inhibited in the cells. Cardiac progenitor cells can be identified by the expression of the transcription factor Nkx2.5. Nkx2.5 is highly expressed in early cardiac progenitor cells through to the adult heart[24] and plays a role in cardiac looping and growth of the heart[25]. Additionally, the LIM homeodomain transcription factor Islet1 marks proliferating undifferentiated cardiac progenitor cells[26]. Islet1 is essential for cardiac progenitor cell specification and normal development as homozygous Islet1 knockout mice die around embryonic day 10 from heart

deformation[26]. WNT signaling acts through β-catenin and fibroblast growth factor 8 (FGF8)[27,28]. WNT/β-catenin signaling plays a biphasic role in cardiac differentiation. Early WNT activity leads to downstream activation of BMP and FGF signaling. For example, in the pluripotent mouse cell line P19CL6, WNT/β-catenin activation triggered BMP signaling and FGF8 expression. BMP signaling and FGF8 play a role in committing to cardiac mesoderm[29]. As cardiac mesoderm cells transition towards cardiac progenitors, WNT/β-catenin inhibition suppresses Nkx2.5 expression. For example, in a zebrafish model, when WNT/β-catenin was inhibited during gastrulation, there was a decrease in Nkx2.5 expression. Once WNT signaling is inhibited in cardiac progenitors, WNT signaling in surrounding mesoderm helps to define the boundary and proper size of the heart-forming field[30]. Thus, the precise activation and inhibition of WNT/ β-catenin at discreet developmental time points are essential to ensure the proper development of cardiac progenitor cells.

Bone morphogenic protein signaling is also upregulated during the differentiation of cardiac progenitor cells to cardiomyocytes. BMPs are transiently inhibited at the cardiac mesoderm stage to allow differentiation into cardiac progenitors and then upregulated again during cardiac progenitor differentiation to cardiomyocytes. BMP signaling is modulated by extracellular factors (e.g., Noggin), intracellular factors (e.g., Peptidyl-prolyl cis-trans isomerase, microRNAs, phosphatases, and inhibitory smads), or co-receptors in the plasma membrane (e.g., Endoglin)[31]. BMP signaling has been shown to promote the expression of myofibrillar genes, such as Nkx2.5 and GATA4, and inhibit fibroblast growth factor signaling[32,33]. Mature cardiomyocytes can be identified by unique transcription factors and

proteins. Cardiomyocytes express Nkx2.5, cardiac troponin T, α-actin, myosin light chain 2a, and myosin light chain 2v. These proteins are essential for cardiomyocyte development and function. For example, Nkx2.5-deficient mice die at embryonic day 9-10 due to arrested heart morphogenesis and growth delays[34]. Additionally, cardiac troponin T-deficient mice could not assemble sarcomeres in cardiomyocytes leading to a lack of heart contractions and embryonic lethality[35]. When all developmental processes occur correctly, cardiomyocytes have the ability to contract synchronously and efficiently by the stimulation of the heart's electrical conduction system, discussed later.

1.3 Electrical Conduction of the Heart

The synchronized contraction of the heart muscle is coordinated through the generation of electrical action potentials initiated by the autorhythmic pacemaker cells of the sinoatrial (SA) node. The cardiac conduction system is comprised of the SA node, atrioventricular (AV) node, the bundle of His, the left and right bundle branches, and the Purkinje fiber network[36]. After the SA node has generated an action potential, the electrical impulse moves quickly throughout the atrial myocardium. The electrical stimulation causes synchronous contraction of the atria. The impulses then slow down when they reach the AV node, allowing the ventricles to fill before contraction. From there, the electrical impulse travels rapidly down the left and right branches of the bundle of His and throughout the ventricular myocardium through the Purkinje fibres. This system allows synchronous contraction of the left and right ventricles. Contractions begin at the heart's inferior tip (apex) and move towards the superior surface of the heart (base) to produce an apex-to-

base contraction within each ventricle[36]. Every part of the conduction system is integral to ensure the heart contracts synchronously and efficiently at a physiological normal pace.

Action potentials generated in the SA node are the starting point for excitation-contraction coupling in cardiomyocytes. Unlike the pacemaker cells of the conduction system, cardiomyocytes within the working myocardium require external stimulation to generate an action potential. The cardiomyocyte action potential is divided into 5 phases: the initial fast depolarization (phase 0), early repolarization (phase 1), the plateau phase (phase 2), late repolarization (phase 3), and finally, the resting phase when the membrane potential across the sarcolemma (cardiomyocyte cell membrane) is at baseline (phase 4). The primary ion currents involved in cardiomyocyte depolarization are inward sodium currents, inward calcium currents, and outward potassium currents. Depolarization during phase 0 of the action potential is mainly due to inward sodium currents[37]. Phase 1 repolarization occurs when the sodium currents are inactivated, and transient outward potassium currents are activated. The plateau phase results from an influx of calcium into the cell through L-type calcium channels and the release of calcium from the sarcoplasmic reticulum. Similar to phase 1 repolarization, cardiomyocyte repolarization in phase 3 is caused by potassium currents[37]. The electrical conduction system in the heart is unique due to its ability to generate action potentials independent of electrical stimulation from the autonomic nervous system. The electrical stimulation of the heart is only one facet of a contraction, as the electrical signal must be converted to a mechanical force through excitation-contraction coupling to drive contraction.

1.3.1 Cardiomyocyte Excitation-Contraction Coupling

Cardiomyocyte excitation-contraction coupling is the process where a cardiomyocyte can bridge the electrical stimulus of an action potential with the mechanical contraction of the sarcomeres within the cell. Excitation-contraction coupling begins when an action potential reaches the sarcolemma and activates the L-type calcium channels (LTCCs) in the transverse tubules. Activated LTCCs allow an influx of calcium ions into the cell, which activates the ryanodine receptor 2 (RYR2) on the sarcoplasmic reticulum[37]. Activated RYR2 then releases more calcium ions into the cytoplasm from the sarcoplasmic reticulum (calcium induced-calcium release, Figure 2)[38,39]. The excitation-contraction coupling process converts an electrical stimulus to a mechanical contraction generated by the cardiomyocytes.

The contraction of a cardiomyocyte is dependent on the concentration of calcium ions in the cytoplasm. When the intracellular calcium concentration is low, troponin stabilizes tropomyosin on the myosin-binding site. Troponin has three subunits: one that binds to actin, one that binds to tropomyosin, and a third that can bind to calcium. However, when the calcium concentration increases via sarcoplasmic reticulum release, calcium binds to troponin and causes a conformational change in troponin and tropomyosin. This movement exposes the myosin binding site, allowing cross-bridge interaction between thin and thick filaments[6]. This significant increase in calcium concentration within the cell causes the cardiomyocyte to contract. Efficient contraction of the myofibril depends on the sarcomere. The sarcomere is a structure that is continuously repeated in the myofibril. Sarcomeres are composed of thick filaments and thin filaments. The thick filament is made up of many

Figure 2 Calcium induced-calcium release is the linker between cardiomyocyte excitation and contraction

(A) At the resting state, L-type calcium channels in the sarcolemma are closed. The intracellular calcium concentration is low due to most calcium being located in the sarcoplasmic reticulum (SR). The sarcomere is in its relaxed position. The ryanodine receptor type 2 (RYR2) is inactive. (B) Depolarization of the sarcolemma due to an action potential (AP) activates L-type calcium channels in the T-tubules letting calcium into the cell. The intracellular calcium binds to RYR2 on the SR. The binding of calcium activates the receptor, initiating calcium release from the SR into the cytosol (calcium-induced calcium release). The intracellular calcium can then interact with the sarcomere to initiate cardiomyocyte contraction by binding to troponin C. After binding, tropomyosin shifts, revealing the myosin head binding site on actin and initiates cross-bridging. Cross-bridging between thick and thin filaments of the sarcomere causes contraction. (C) Calcium is cleared from the cytosol primarily through sodium-calcium exchanger channels and SERCA channels in the SR. Once calcium is cleared from the cytosol, tropomyosin shifts back to cover the myosin head binding site, stopping cross-bridging and, therefore, contraction. L-type calcium channels have closed and are now ready to be activated by another action potential. Figure 2 was created using BioRender Premium software, *biorender.com*.

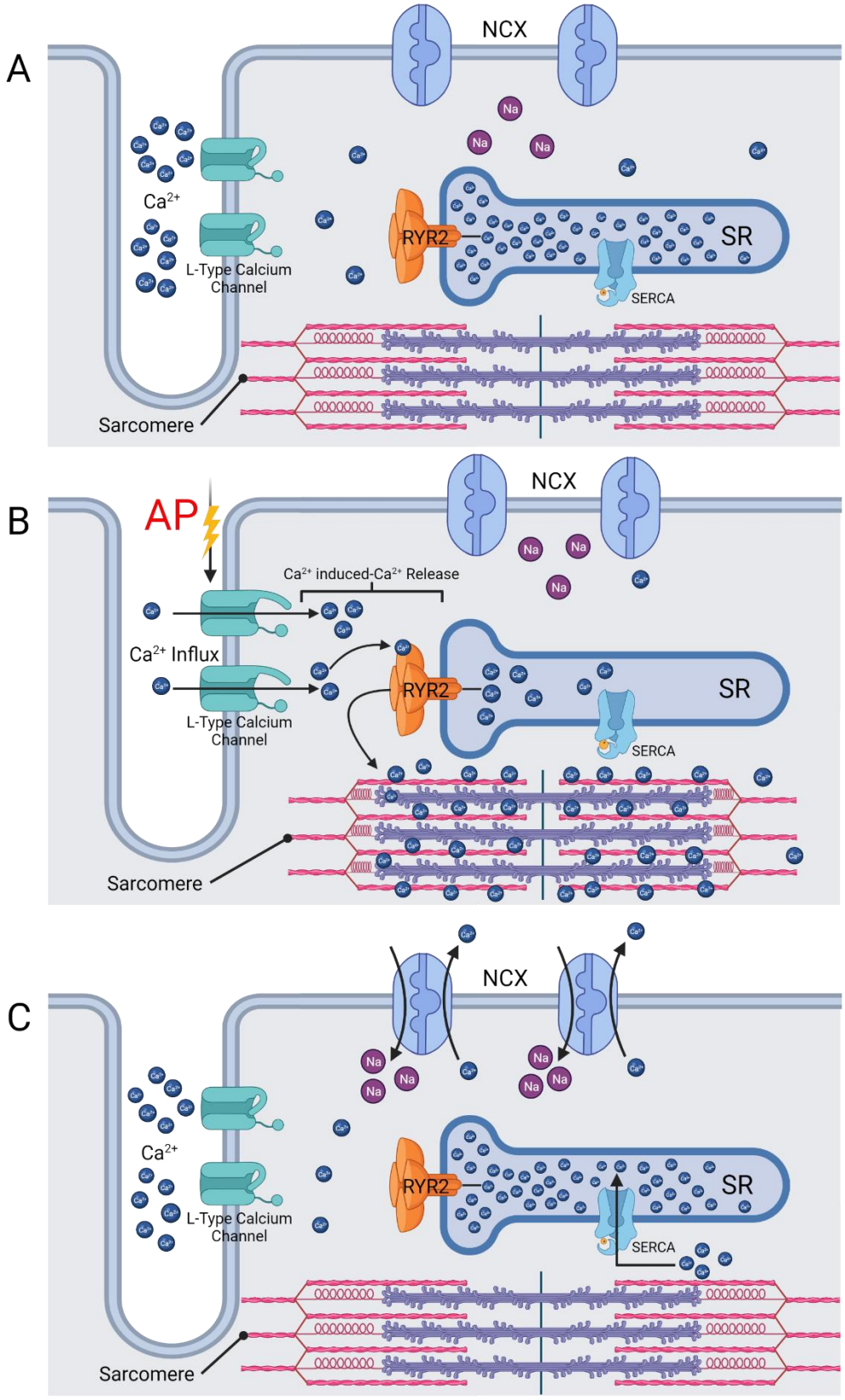
A
NCX
Na
Na
Na
Ca2+
L-Type Calcium Channel
RYR2
SR
SERCA
Sarcomere
B
AP
NCX
Na
Na
Na
Ca2+ induced-Ca2+ Release
Ca2+ Influx
L-Type Calcium Channel
RYR2
SR
SERCA
Sarcomere
C
NCX
Na
Na
Na
Na
Na
Na
Ca2+
L-Type Calcium Channel
RYR2
SR
SERCA
Sarcomere

myosin proteins, while the thin filaments are comprised of an actin helix, troponin, and tropomyosin[6]. The sarcomeres are joined together laterally by a protein-dense region at the end of a sarcomere called the Z-disc. The Z-disc contains α-actinin, γ-filamin, and myotilin, responsible for cross-linking the thin filament actin protein of adjacent sarcomeres. The sarcomeres are connected to other organelles via intermediate filaments to maintain cellular integrity and efficient translation of contractile force. In addition, the costamere links the sarcomere to the sarcolemma by the Z-disc and M-band[40]. In the resting state, tropomyosin blocks the myosin-binding site on actin, preventing cross-bridging and contraction from occurring. Contraction of the sarcomere occurs when tropomyosin reveals the myosin-binding site on actin, and the head domain of the myosin protein interacts with actin. This process pulls the thin filaments inward to the center of the sarcomere from both ends resulting in net shortening of the sarcomere[6]. Calcium plays a major role in the initiation of cross-bridging and contraction as the binding of calcium starts the chain of events that lead to sarcomere contraction. The coordinated contraction of connected sarcomeres in myofibrils generate the force needed for heart contraction.

After contraction, the cardiomyocytes must relax during diastole. The calcium released into the cytoplasm through calcium-induced calcium release must now be removed from the cytoplasm. Calcium is pumped out of the cell by sodium-calcium exchanger channels[41] and pumped back into the sarcoplasmic reticulum by the sarcoendoplasmic reticulum ATPase pump (SERCA)[42]. As calcium is cleared from the cytosol, the troponin-tropomyosin complex moves back to the resting position, stopping contraction[6]. This whole process is repeated for every muscle contraction in the heart. Thus, appropriate excitation-

contraction coupling across every single cardiomyocyte is essential for the coordinated contractile activity of the heart organ as a whole.

1.3.2 Intercalated Discs

For the atria and ventricles to be properly excited and contract synchronously, the electrical signals delivered from the SA and AV nodes must be able to efficiently propagate from cardiomyocyte to cardiomyocyte. The intercalated disc is a highly organized cell-cell adhesion structure that confers strength and electrical conduction between cardiomyocytes. The intercalated disc comprises three major protein junctional complexes: gap junctions, desmosomes, and adherens junctions (Figure 3). Gap junctions propagate electrical signals across cardiomyocytes while desmosomes and adherens junctions anchor cardiomyocytes together and provide strength to the cardiac muscle. Together, this structure facilitates the propagation of action potentials and strengthens the working myocardium.

1.3.3 Desmosomes

Desmosomes are intercellular junctions most commonly found in cells that experience significant mechanical strain. Desmosomes provide cells with strong adhesion forces to resist being pulled apart. Tissues such as the working myocardium and epidermis tend to be enriched with desmosomes to combat the constant mechanical forces they experience[43]. Desmosome proteins include the cadherins, armadillo, and plako gene families. Proteins from the cadherins family (desmoglein, desmocollin) link neighboring cells together. The N-terminal domain couples the two halves of the desmosome in the intercellular space, while the C-terminal domain interacts with armadillo proteins (plakoglobin, plakophilin) within the cell. The desmosomal plaque protein, desmoplakin,

Figure 3 Intercalated discs are cellular adhesion structures that electrically connect cardiomyocytes and provide strength to the working myocardium

The intercalated disc is composed of three main structures. Gap junctions allow the flow of ions from one cell to the next. Desmosomes provide strong adhesion forces to prevent neighboring cardiomyocytes from being pulled apart. Adherens junctions connect actin filaments from adjacent cardiomyocytes, which provides structural strength to the cardiomyocytes. Figure 3 was created using BioRender Premium software, *biorender.com*.

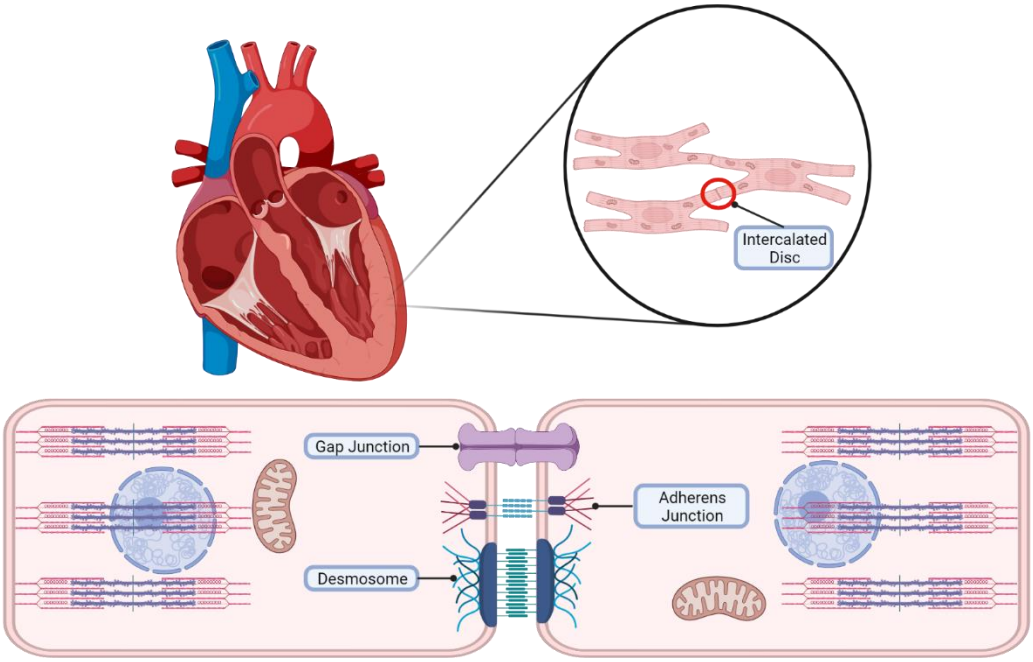
Intercalated Disc
Gap Junction
Adherens Junction
Desmosome

anchors the cell's intermediate filaments to the desmosome junction[43,44]. While complex stratified tissues, such as the epidermis, express several different isoforms of cadherin and armadillo proteins, cardiac tissue expresses only desmoglein-2 (DSG2), desmocollin2 (DSC2), and plakophilin2 (PKP2). These proteins, along with plakoglobin (PKG) and desmoplakin (DSP), anchor the intermediate filament desmin to the cardiac myocyte plasma membrane[45]. The importance of proper desmosome function can be highlighted by diseases associated with desmosome protein mutations. Mutations in cadherins proteins have been shown to cause skin and autoimmune diseases such as striate palmoplantar keratodermas[46], dermatitis[47], and pemphigus vulgaris[48]. Additionally, mutations in DSG2 have been associated with arrhythmogenic right ventricular cardiomyopathy (ARVC) 10[49]. Mutated armadillo proteins display similar disease phenotypes as cadherins, including skin abnormalities such as ectodermal dysplasia/skin fragility syndrome[50]. Patients with ARVC9 have had mutations in armadillo proteins, most notably PKP2[51]. Thus, desmosomes provide strength to the heart wall and mutated desmosomal proteins can lead to compromised myocardial integrity and subsequent cardiac disease.

1.3.4 Adherens Junctions

Adherens junctions connect actin filaments from adjacent cardiomyocytes, which provides structural strength to the cardiomyocytes. They act as the anchor point for myofibrils which enables the transmission of contractile force from one cell to the next. Adherens junctions are constructed from cadherins and catenins[52]. N-cadherin is a member of the classical cadherin family and is the only isoform expressed in the heart. This protein mediates calcium-dependent cell adhesison[53]. N-cadherin is located in the cell membrane

and is attached to actin filaments by multiple adherens junction proteins. The extracellular domain of N-cadherins interacts to form homodimers in the intercellular space linking neighboring cells.[54]. The intercalated disc structure completely breaks down in N-cadherin-deficient mice, leading to sudden arrhythmic death. Haploinsufficiency of N-cadherin negatively affected gap junctions and increased arrhythmogenicity in this model[55]. The other main component of adherens junctions is catenin proteins. The catenin family includes α-catenin, β-catenin, γ-catenin, and p120 catenin. β-catenin binds directly to the cytoplasmic C-terminal of N-cadherin and, through the association with α-catenin, connects to the actin cytoskeleton. β-catenin additionally has a role in signaling pathways as it is an integral component in the WNT signaling pathway during cardiac development[29]. Alternatively, if β-catenin is inhibited from linking N-cadherin and the actin cytoskeleton, γ-catenin can make the link with the help of α-actinin[54]. β-catenin and PKG (γ-catenin) double knockout mice exhibited dissolution of intercalated discs and developed cardiomyopathy, fibrous tissue replacement, and conduction abnormalities that lead to sudden cardiac death[56]. p120-catenin binds to the cytoplasmic domain of N-cadherin close to the membrane, where it can modulate adhesion and cell shape[54]. Additionally, p120-catenin binds to accessory proteins that connect adherens junctions to microtubules[54]. The studies discussed in this section support that adherens junctions are an integral component of the intercalated disc as the knockout models develop cardiac disease and are lethal.

1.3.5 Gap Junctions

Gap junctions are intercellular channels that allow the direct transfer of small molecules between adjacent cells. Gap junction channels are comprised of the multigene

family of proteins called connexins (Cx)[57]. There are 21 unique connexin proteins in humans, all encoded by a separate gene[58]. Six connexin subunits oligomerize to form a hemichannel that can then dock with a hemichannel on an adjacent cell to form a contiguous gap junction channel. Gap junctional dysregulation underlies dozens of inherited and acquired diseases. Mutations in the prototypical Cx43 causes the pleiotropic human disease oculodentodigital dysplasia. This rare genetic disease affects the development of multiple organs in the human body, and there are more than 70 mutations in the Cx43 gene associated with oculodentodigital dysplasia[59]. Some of the common phenotypes seen include syndactyly and camptodactyly, enamel hypoplasia, microcornea and microphthalmos, and craniofacial abnormalities[60]. Although connexins are expressed across nearly every cell and tissue type, their function is especially critical in cardiac cell electrical coupling.

Gap junctions are essential for the propagation of electrical action potentials from the SA node to the working myocardium and from one cardiomyocyte to the next within the heart wall[61]. Mouse and human hearts express Cx37, Cx40, Cx43, and Cx45 across various cell types. Specifically, cardiomyocytes express Cx40, Cx43, and Cx45, while endothelial cells are coupled by Cx37 and Cx40[62]. Cx45 is preferentially expressed in the SA node and the AV node and co-expressed in the bundle of His and the Purkinje fibers with Cx43. The ventricular myocardium is primarily coupled by Cx43, while both Cx43 and Cx40 are expressed in the atria[63]. Cx43 is a vital protein for heart development in mice, as Cx43 homozygous mutation is lethal due to a defect in the right ventricular outflow tract[64].

Dysregulated gap junctional intercellular communication within the heart results in several pathologies and can ultimately result in cardiovascular diseases.

1.4 Cardiovascular Disease

Heart diseases are the second leading cause of death in Canada. About 1 in 12 Canadians (or 2.4 million) over the age of 20 live with heart disease, and every hour, 12 Canadians with diagnosed heart disease die. From 2001 to 2013, there has been a decline in heart disease in the Canadian population, going from 221,800 to 158,700 newly diagnosed Canadian adults. The death rate per 1000 people has decreased by 23% during this span. The different types of cardiovascular diseases include stroke, peripheral vascular disease, heart failure, cardiomyopathy, rheumatic heart disease, arrhythmia, and congenital heart disease. Factors contributing to the development of these conditions include family history, lifestyle behaviors, and environmental factors, such as air pollution[65,66]. Heart disease is a multifactorial condition and although there has been a decline in heart disease in Canada, it is still a prevalent issue.

1.5 Arrhythmias

On average, a healthy human heart will beat between 60 and 100 times per minute. However, each individual is different, and their heart rate will vary slightly. An arrhythmia is diagnosed when the heart rhythm is outside the patient's normal range. Arrhythmias occur when the electrical conduction pathway in the heart is not functioning correctly. Several different types of arrhythmias can occur and are classified based on the speed and rhythm of the heart rate associated. The two main categories of arrhythmias include bradycardia and tachycardia.

Bradycardia is defined as a heart rate below 60 beats per minute while at rest[67]. A low resting heart rate does not always mean there is something wrong. Physically fit young adults or trained athletes could have a low resting heart rate without any complications. However, if one has a low heart rate and the heart is not pumping sufficient blood around the body, then bradycardia may be possible. Common causes of bradycardia include sinus-node dysfunction[68] and atrioventricular-conduction disturbances[69]. Common problems associated with sinus-node dysfunction include sinus arrest, sinus exit block, sinus bradycardia, and tachycardia-bradycardia syndrome[70]. Atrioventricular-conduction disturbances can result from injuries to this area, such as infarction, infection, or catheter-related trauma.

On the other hand, tachycardia is defined as a heart rate above the normal range, leading to inadequate blood pumping. Tachycardias can be split up further into arrhythmias that originate above the ventricles (supraventricular) and those that occur in the ventricles. Atrial fibrillation is the most common type of supraventricular arrhythmia. It is characterized by an extremely high heart rate and contraction of the atria that does not let the heart chambers fill with blood correctly. Atrial fibrillation is a common arrhythmia seen in various inherited cardiomyopathies[71]. Atrial flutter is an arrhythmia that causes the atria to beat up to 300 times per minute and lacks an isoelectric baseline between defections[72]. The final type of supraventricular arrhythmia is paroxysmal supraventricular tachycardia, characterized by sudden onset of tachycardia and abrupt termination[73]. All types of supraventricular tachycardia are serious and should be addressed, although atrial fibrillation is the most common.

Ventricular arrhythmias are classified as either ventricular tachycardia or ventricular fibrillation and are a significant clinical problem in patients with heart diseases, including ischemic and nonischemic cardiomyopathies. Ischemic cardiomyopathy refers to myocardial damage brought upon by a lack of blood flow to the heart. In contrast, nonischemic cardiomyopathy is a myocardium disease associated with mechanical or electrical dysfunction leading to inappropriate hypertrophy or dilation[74,75]. Many different mechanisms lead to ventricular tachycardia, including abnormal automaticity, triggered activity, and various forms of reentry. Reentry is caused by continuous excitation of the ventricle cardiomyocytes during a complete excitation-contraction cycle[76]. Several of these mechanisms can be linked to disturbances in cell electrophysiology—for example, mutations in ion transporters, channels, and pumps[76]. The occurrence of ventricular tachycardia appears to be the manifestation of multiple cardiac factors at once, including ineffective ion channel arrangement and function, intracellular ion dynamics, cardiac innervation, and metabolic and signaling pathways[76]. The occurrence of ventricular tachycardia leading to ventricular fibrillation often leads to sudden cardiac death. It is the cause of greater than half of all cardiac deaths and up to 15% of mortality in the United States[77]. Ventricular arrhythmias are commonly associated with various cardiomyopathies and are a significant contributor to sudden cardiac death in the population.

1.6 Cardiomyopathies

Cardiomyopathies are a category of heart muscle diseases that prevent the heart from pumping a sufficient amount of oxygen-rich blood around the body[78]. According to the American Heart Association, cardiomyopathies can be classified as either primary or

secondary. Primary cardiomyopathies are concentrated to the heart, while secondary cardiomyopathies are systemic diseases that affect the heart[79]. Primary cardiomyopathies can develop from genetic, mixed (genetic and nongenetic), and acquired etiologies[79]. Primary cardiomyopathies, including dilated cardiomyopathy, hypertrophic cardiomyopathy, and restrictive cardiomyopathy, all present with similar symptoms, such as heart failure and decreased ejection fraction. However, the phenotypes and etiologies of each disease can vary[80,81,82]. ARVC is considered a primary cardiomyopathy. Ventricular arrhythmias and symptoms such as palpitations, light-headedness, and syncope are common with ARVC. Patients with ARVC may experience sudden cardiac death[83]. ARVC is a heterogenous disease partly due to the multiple mutations that cause the disease. Although there is a unified clinical diagnosis for ARVC patients, the disease presentation can change depending on what gene mutation is present. For example, ARVC patients with a *DSP* variant are more likely to be associated with left ventricular dysfunction[84], and patients with a *PKP2* variant are more likely to be associated with ventricular tachycardia[85]. In summary, primary cardiomyopathies develop due to many different etiologies, including multiple different gene mutations. The first symptom of patients with ARVC can be sudden cardiac death, while other primary cardiomyopathies present and progress differently.

Acquired cardiomyopathies are often the result of a different health condition. These conditions include long-term hypertension, heart tissue damage from a heart attack, long-term rapid heart rate, viral infections, metabolic disorders such as obesity or diabetes, and long-term excessive alcohol consumption and drug use (cocaine or amphetamines)[86]. Inherited cardiomyopathies result from a pathogenic mutation that has been passed down

from a parent. There are hundreds of genetic variants that have been associated with cardiomyopathic diseases[87]. A genetic variant can be characterized by the penetrance and disease expression in the patient. Penetrance is the percentage of mutation carriers that clinically express the disease. Disease expressivity describes the differences observed in the clinical phenotype of two patients with the same genetic phenotype[88]. The challenge we face with these genetic mutations is their variable penetrance and variable disease expression (severity) from patient to patient.

Diagnosis of cardiomyopathies during the early stages of the disease can be challenging since patients will often be asymptomatic or have minimal symptoms[89]. Genetic screening for known mutations associated with cardiomyopathy is an important part of the early detection of the disease. However, not all cardiomyopathies have a robust genetic characterization. Approximately 40% of all patients clinically diagnosed with ARVC do not have an identified mutation[90], and approximately 40-50% of hypertrophic cardiomyopathy patients do not have an identified mutation[91]. Besides genetic testing, cardiomyopathies can be diagnosed by testing the patients using electrocardiogram (ECG), echocardiogram, magnetic resonance imaging (MRI), right ventricle angiography, and endomyocardial biopsies[92,93]. These diagnostic tools have been invaluable in the detection and treatment of patients with cardiomyopathy.

A patient that has been diagnosed with cardiomyopathy can have different pathologies. Due to myocyte death and fibrosis, dilated cardiomyopathy hearts are characterized by dilation of ventricles and a significant decrease in ventricle wall thickness compared to a healthy heart. This phenotype is seen in ARVC, which will be discussed

further in the next section. With progressive dilation of the ventricles, there is a decrease in contractility, leading to an ejection fraction of less than 0.45 and ineffective pumping[81]. Hypertrophic cardiomyopathy presents with thickening of the left ventricle due to myocyte hypertrophy. Diastolic dysfunction is common in this disease due to the increased interstitial fibrosis and delayed relaxation time[89]. Although the underlying structural changes of dilated and hypertrophic cardiomyopathy are different, each pathology ultimately results in reduced blood pumping efficiency.

1.6.1 Arrhythmogenic Right Ventricular Cardiomyopathy

Arrhythmogenic right ventricular cardiomyopathy (ARVC) is characterized by fibro-fatty replacement of the myocardium in the right ventricle and thinning of the ventricular wall, and can predispose the patient to life-threatening arrhythmias and progressive dysfunction of the right ventricle[94] (Figure 4). There has been considerable interest in ARVC as it has been shown to cause sudden cardiac death in young athletes[95]. Although ARVC has been historically characterized by fibro-fatty replacement in the right ventricle, there is a growing body of evidence that suggests ARVC affects the left ventricle as well[96,97]. Genetics play a significant role in the different types of ARVC as there have been at least 16 different genes associated with the clinical ARVC phenotype. Although specific genes have been identified as contributing factors to developing ARVC, studying the disease and learning the molecular mechanisms behind the disease have been hampered by several factors. The rarity of the disease combined with the wide range of clinical presentations in patients makes diagnosis difficult[96]. Unfortunately, sudden cardiac death can be the first symptom, adding additional complications to studying the disease.

Figure 4 Fibrofatty invasion of the ventricular myocardium and thinning of the left and right ventricle wall are hallmark characteristics of ARVC

Increased fibrosis from cardiac fibroblasts and the infiltration of adipocytes into the myocardium inhibit proper electrical propagation due to the insulative properties of the scar tissue and adipocytes. Thinning of the ventricle walls due to cardiomyocyte death weakens the heart and decreases the blood pumping efficiency of the ventricles. Figure 4 was created using BioRender Premium software, *biorender.com*.

Healthy Heart

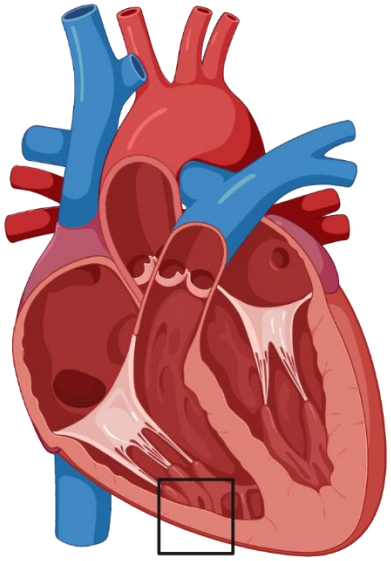

ARVC Heart

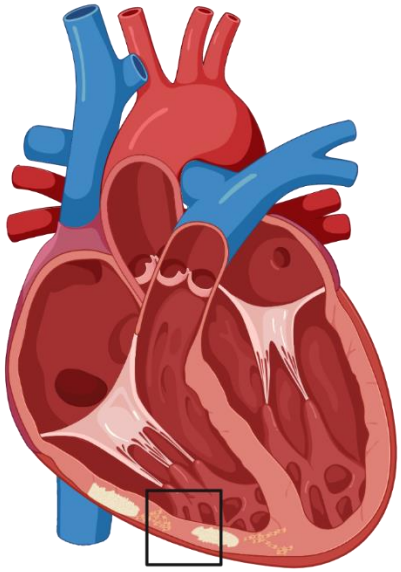

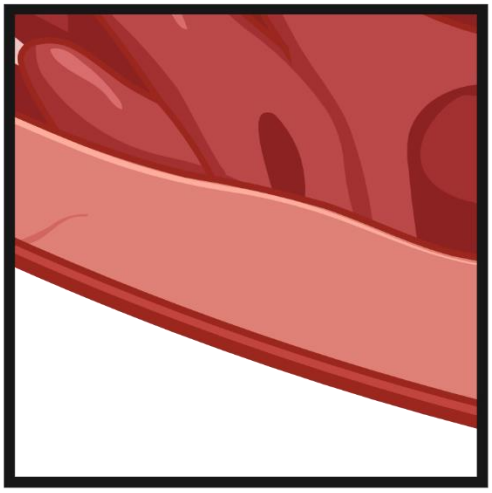

Fibrofatty Invasion

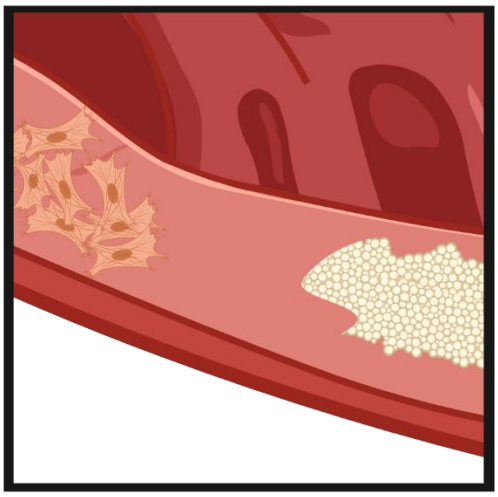

The official name of ARVC is arrhythmogenic right ventricular dysplasia, established by Online Mendelian Inheritance in Man. However, the disease has since been reclassified as cardiomyopathy. Arrhythmogenic right ventricular dysplasia is now predominantly referred to as ARVC. For this thesis, the disease will be referred to as ARVC.

1.6.2 ARVC Diagnosis

The current clinical criteria for ARVC diagnosis include global or regional dysfunction and structural alterations of the right ventricle, tissue characterizations of the tissue wall, repolarization abnormalities, depolarization/conduction abnormalities, ventricular arrhythmias, and family history[93]. Techniques such as ECGs, echocardiogram, magnetic resonance imaging (MRI), right ventricle angiography, and endomyocardial biopsies are employed to determine if a patient meets all the criteria to be diagnosed[93]. ECGs are universal, easy to perform, and allow for the discovery of heart abnormalities in patients[93]. Patterns in the QRS-T segment of the heart's electrical conduction are often variable due to the progressive degradation of subepicardial fibers and conduction defects in the patients as they age. Differences in the ECG readings depend on the severity and location of the disease, where early stages of the disease abnormalities may not be detected, but more severe late-stage ARVC will present with more abnormalities[93]. T-wave inversions in the right precordial leads (extending up until V5 and V6) are highly prevalent in ARVC adult patients. Inverted T-waves in the inferior leads are possible and can indicate ARVC, as inverted T-waves in the inferior leads can occur when there is fibro-fatty invasion in the left ventricle[98].

Non-invasive imaging techniques are integral to help diagnose and manage ARVC. Two-dimensional echocardiography is the most widely available imaging method for patients with ARVC or suspected of having ARVC. This technique can be used to identify regional ventricle wall motion abnormalities that are associated with right ventricular dilation or dysfunction. MRI is a powerful tool to assess ventricle volume, wall thickness, morphology, myocardial adipose, fibrous matter, and regional movement. Due to the dilation seen in this disease, it can be increasingly difficult to see the fibrofatty tissue in the right ventricle wall due to constraints in the spatial resolution of lower power MRI[99]. Finally, cardiac computed tomography is another technology that can help diagnose patients. Cardiac computed tomography has excellent spatial resolution and could play a role in distinguishing between ARVC and other causes of ventricular arrhythmias, such as coronary heart disease[100]. The techniques described play an important role in identifying patients with ARVC, including those of the population located in Newfoundland.

1.7 ARVC Molecular Mechanisms

As outlined in section 1.6.1, ARVC pathology involves both arrhythmogenesis (cardiomyocyte) and cardiomyopathy (fibroblasts). Desmosomal genes make up most ARVC-related mutations; however, ARVC is associated with mutations in cytoskeletal proteins (Titin, Alpha-T-catenin) and nuclear envelope proteins (TMEM43, Lamin A/C)[93]. Mutations in desmosomal proteins are part of a prominent mechanism associated with ARVC. Without the proper desmosomal protein function, the intercalated discs responsible for cell-to-cell adhesion of cardiomyocytes break down[49,101]. This jeopardizes the strength and stability of the cardiomyocytes in the heart. Detachment of cardiomyocytes from each

other can lead to cell death and remodeling of the heart tissue. The poor electrical properties of the scar tissue that replaces the myocytes can lead to arrhythmias and sudden cardiac death[102]. Mutations in desmosomes support the mechanism of intercalated disc breakdown; however, the effects of mutations in nuclear envelope proteins on intercalated discs and how they contribute to ARVC is unclear.

In addition to the arrhythmogenesis of ARVC, cardiomyopathy plays an equally important role in the disease. Cardiac fibroblasts are mainly recognized for their ability to maintain structural integrity through proliferation and maintenance of the extracellular matrix. Activated myocardial fibroblast cells in the remodeling heart become highly invasive and proliferative and actively remodel the cardiac interstitium through increased secretion of extracellular matrix-degrading metalloproteinases and collagen turnover[103]. These remodeling processes are essential in the initial repair of cardiac tissue after injury. However, long-term activation of these cardiac fibroblasts can accumulate collagen, resulting in cardiac fibrosis and, eventually, a loss of cardiac function[103]. The fibrosis produced by the cardiac fibroblasts plays an integral role in weakening the ventricular myocardium in ARVC hearts. Together, the pathogenic phenotype of ARVC is likely multifactorial in development and progression.

Increasing evidence points toward improper protein trafficking and degradation as potential contributors to cardiomyopathy etiology. The heart is a highly metabolic organ, and stringent protein quality control is necessary to maintain the heart and prevent disease. In inherited cardiomyopathies, deregulated protein quality control could result from the inherited mutation itself or as a compensatory mechanism to counteract the cellular stress

caused by the mutant protein. For example, in HCM caused by an α-actinin 2 mutation, human cardiomyocytes displayed diffuse cytoplasmic vacuolization with perinuclear halos[104]. Cytoplasmic vacuolization can indicate dysfunction of protein degradation. Similarly, abnormal lysosomes were found in mice hearts when modeling inherited DCM with the nebulette-K60N mutation[105]. Abnormal lysosomes could also indicate compromised protein degradation or quality control, as the lysosomal pathway is a crucial process for degrading macromolecules[106]. In heart samples of ARVC patients, there was a significant decrease in levels of DSG2 and DSC2 compared to the control despite having normal transcript levels, suggesting that there is an increased level of protein turn-over[107]. In addition, mutated plakoglobin related to ARVC stably transfected into HEK293 cells displayed ubiquitylation and preferential localization in the cytoplasm[108]. These studies point toward protein turnover as a factor in arrhythmogenic cardiomyopathies.

1.8 Founder Effect in Newfoundland

Newfoundland is known to be a genetically isolated population; thus, founder effects occur [109]. The founder effect is a phenomenon of a loss of genetic variability when a subset of a larger population is used to establish a new settlement. Heritable diseases can become enriched within this founder population; thus, genetically isolated populations often provide an excellent resource for identifying pathological mutations[110,111,112]. Newfoundland has three main founder populations: the Irish, English, and Aboriginal founders, with a large portion of the founder population coming from Irish settlers[113,109,114]. This makes the province an important resource for mapping the genetic causes of autosomal dominant and recessive diseases. Newfoundland families have been referenced as a

significant contributor in elucidating the genetic cause of 60 entries in Online Mendelian Inheritance of Man[115]. Newfoundland's 60 entries are 10-fold that of the other Atlantic provinces (Nova Scotia, New Brunswick, Prince Edward Island).

1.9 Transmembrane Protein 43

A founder population in Newfoundland carrying a mutation in the *TMEM43* gene (*c.1073C>T*; p.S358L) is associated with high ARVC penetrance and an increased occurrence of sudden cardiac death[116,117]. The *TMEM43* gene contains 13 exons on chromosome 3 (3p25.1)[118]. *TMEM43* mRNA is expressed in the ovary, spleen, small intestine, thymus, colon, prostate, leukocytes, testis, liver, heart, and placenta[118]. The *TMEM43* gene encodes for the poorly characterized Transmembrane Protein 43 (TMEM43). The human TMEM43 protein is 400 amino acids in length with a molecular mass of 44.8 kDa. TMEM43 has four transmembrane domains with a large hydrophilic domain located between domains one and two[118]. Although the specific *TMEM43* gene mutation that causes ARVC5 has been identified, many characteristics of TMEM43 protein are unknown.

Studies have reported TMEM43 localized to the nuclear envelope[119,120], endoplasmic reticulum[118,121], and adherens junctions[122] in different systems. For example, TMEM43 localization to the nuclear envelope in mouse embryonic fibroblasts is dependent on A-type Lamins. TMEM43 is incorrectly trafficked to the endoplasmic reticulum in Lamin A/C-deficient mouse embryonic fibroblasts[118]. In addition to WT TMEM43 being differentially localized across cell types, the TMEM43-S358L mutant protein can be mislocalized compared to the wild type. For example, Christensen *et al.* demonstrated that wild-type

TMEM43 localizes at the sarcolemma in the control myocardium, whereas TMEM43-S358L mutant protein localized to the cytoplasm in heart tissue from ARVC5 patients[123]. In contrast to the Christensen *et al.* study, TMEM43 was shown to be localized to the nuclear envelope of mouse myocardium, while TMEM43-S358L was re-distributed to intracellular puncta[124]. These reports suggest that the cell type and model system may influence TMEM43 localization and affect the consequences of mutating the protein.

Just as the intracellular localization of TMEM43 is unclear, different studies suggest different roles for the protein. TMEM43 is thought to help maintain nuclear envelope structure by organizing protein complexes in the inner nuclear membrane[118]. TMEM43 interacts with emerin and lamin A/C primarily in the LInker of Nucleoskeleton and Cytoskeleton (LINC) complex[125]. These interactions help to position emerin in the inner nuclear membrane[118]. Bengtsson and Otto proposed that TMEM43 may have a similar function as a family of proteins called tetraspanins based on their similarities[118]. Both have a large extracellular or luminal domain contributing to binding other integral membrane proteins; tetraspanins can self-oligomerize and have the potential to disrupt membrane organization. Due to these similarities, they hypothesized that mutated forms of TMEM43 could contribute to dystrophic diseases[118]. For example, TMEM43 has been reported to be associated with diseases including emery-dreifuss muscular dystrophy 7[126], auditory neuropathy spectrum disorder[127,128], and ARVC5[116]. Merner *et al.* identified the TMEM43-S358L mutation in an ARVC patient population in Newfoundland and Labrador[116]. Since this discovery, the TMEM43-S358L mutation has been identified in non-Newfoundland and Labrador ARVC5 populations[129], and multiple studies have reported the presence of

the TMEM43-S358L mutant in ARVC5 patients and described its clinical manifestations and disease progession.[117,130–132]. The characterization of the ARVC5 population was possible due to the extended family history available in Newfoundland and Labrador. Family history has proven to be powerful when mapping genetic disease pathways and developing treatment protocols. Characterization of the ARVC5 population in Newfoundland and Labrador revealed that this genetic subtype has some differences from the majority of ARVC. Few patients had T wave inversion and epsilon waves commonly found in ARVC[117]. ARVC5 is more severe in males than females, leading to shorter survival time and earlier development of poor R wave progression, left ventricular enlargement, and ectopy in males[117]. Although the function of TMEM43 is unclear, the evidence of TMEM43-S358L playing a role in disease is convincing, and the ARVC5 population in Newfoundland and Labrador will surely aid in understanding ARVC5 disease mechanisms.

The ARVC5 population found in Newfoundland and Labrador is a very useful resource for research in this field. Newfoundland and Labrador has the best-characterized population of ARVC patients[116]. There are 15 families in this population, and each family has many generations. Tracking the inheritance of ARVC5 is possible because there are multiple generations in each family, and the group is a homogenous population arising from a genetic isolate that harbors the TMEM43-S358L mutation[116]. Many ARVC studies examine small families to determine gene-specific penetrance and cardiac characteristics[133]. However, the ARVC5 population in Newfoundland and Labrador is large, and all affected individuals have the TMEM43-S358L mutation providing mutation-

specific data on the clinical manifestations of ARVC5. The complete penetrance of ARVC5 allows for quick identification of carriers allowing the study of patient phenotype and disease progression. A single gene mutation with complete penetrance is unique to ARVC5 as most other types of ARVC display incomplete penetrance[133]. Many patients are available to donate samples for research, and unaffected individuals in each family become very valuable as control subjects when studying cardiac features.

The mechanism responsible for fibrofatty accumulation observed in ARVC5 hearts is unknown. However, the *TMEM43* gene contains a peroxisome proliferator-activated receptor-γ (PPARγ) response element, which may contribute to the fibrofatty replacement of the myocardium.[116] PPARγ is an adipocyte growth factor associated with fibroadipocyte progenitor cell differentiation into myocardial adipocytes[134]. TMEM43-S358L mutation has been shown to enhance the nuclear factor-κβ (NF-κβ)-TFGβ signaling cascade in heart tissue and primary cardiomyocyte cells[135]. The hyperactivation of NF-κβ-TFGβ signaling cascade was shown to drive pro-fibrotic gene expression, specifically TGFβ1, and enhance downstream signaling of NF-κβ-TFGβ. Thus, the TMEM43-S358L mutant may drive ARVC5 fibrofatty development by influencing multiple signaling cascades. However, the cellular origin of this fibrofatty remodeling remains unclear. For example, researchers have not yet identified whether ARVC5 cardiomyocytes are reprogrammed toward adipocyte lineages or whether the cardiomyopathy is a result of aberrant cardiac fibroblast activity.

In addition to cell culture studies, TMEM43's role in ARVC has been examined in mouse models. TMEM43 knockout mice displayed no apparent cardiac abnormalities or dysfunction even under stress induced via transverse aortic constriction[125]. TMEM43-

S358L knock-in mice in the same study demonstrated normal cardiac function and morphology[125]. However, cardiomyocyte-specific TMEM43-S358L overexpressing mice died at a young age and displayed cardiomyocyte death and fibrofatty invasion[124]. Inhibition of glycogen synthase kinase-3β (GSK3β) improved cardiac function in these mice. In a recent study, TMEM43-S358L knock-in rats recapitulated the human ARVC phenotype by displaying ventricular arrhythmias and fibrotic myocardial replacement[121]. TMEM43-S358L was modified by N-linked glycosylation in rat cardiomyocytes and patient-derived induced pluripotent stem cell derived-cardiomyocytes (iPSC-CMs). Endoplasmic reticulum stress increased the amount of N-linked glycosylation on TMEM43-S358L and promoted the movement to the nuclear envelope from the endoplasmic reticulum[121]. Most rodent models do not experience sudden cardiac death or sex-related differences, which are prominent in humans with ARVC. Given the inherent electrophysiological differences between rodents and humans, creating a human-oriented model of ARVC5 is essential to fully uncover the cellular changes underlying the TMEM43-S358L mutation.

1.10 Disease modeling using iPSCs and CRISPR-Cas9

Stem cells are unspecialized cells with the ability to differentiate into specific terminal cell types, including cardiomyocytes. Induced pluripotent stem cells (iPSC) are reprogrammed stem cells derived from a terminally differentiating somatic cell type such as dermal fibroblasts[136] (Figure 5). iPSC reprogramming requires only four transcription factors, Oct4, Sox2, Klf4, and c-Myc ("Yamanaka Factors")[136]. After transfection with

Figure 5 Generation and genetic editing of induced pluripotent stem cells from a terminally differentiated cell type

Somatic cell types such as dermal fibroblasts can be reprogrammed to become pluripotent stem cells by expressing OCT4, SOX2, KLF4, and C-MYC. iPSCs can undergo gene editing using the CRISPR-Cas9 system to knock out specific genes. Double-stranded DNA breaks are created in the target gene using specific guide RNA and Cas9 endonuclease. Double-stranded breaks repaired using the endogenous non-homologous end joining repair pathway have a high probability of insertion or deletion mutations, that can result in a frameshift mutation, and the introduction of premature stop codons. Subsequent nonsense-mediated decay of the transcript results in a complete depletion of the target protein. Control and genetically engineered iPSCs can then be differentiated into contracting cardiomyocytes through a multi-step protocol. Important steps in the differentiation include activating and inactivating the Wnt pathway. Cardiomyocytes can then be used for disease modeling and drug screening experiments. Figure 5 was created using BioRender Premium software, *biorender.com*.

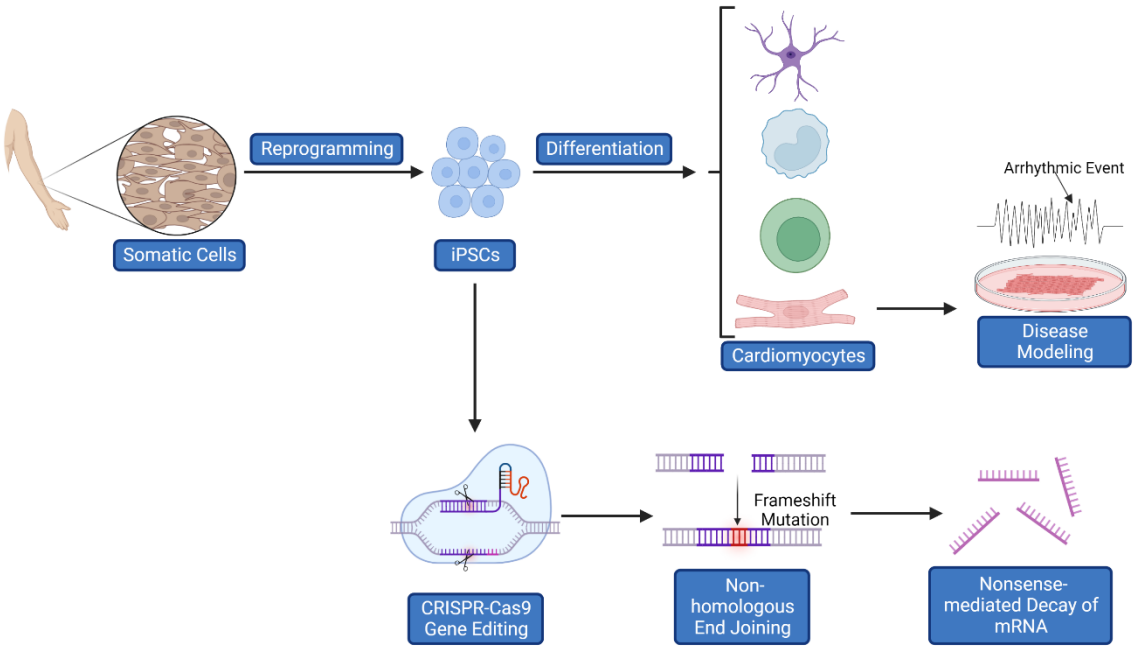
Somatic Cells
Reprogramming
iPSCs
Differentiation
Cardiomyocytes
Arrhythmic Event
Disease Modeling
CRISPR-Cas9 Gene Editing
Non-homologous End Joining
Frameshift Mutation
Nonsense-mediated Decay of mRNA

these Yamanaka Factors, the somatic cells will begin to revert to a pluripotent state, and suitable clones can then be picked to be cultured further.

iPSC technology can be combined with another powerful technique called Clustered regularly interspaced short palindromic repeats (CRISPR)-CRISPR-associated protein 9 (Cas9). CRISPR-Cas9 is a gene editing system derived from a bacterial defense mechanism. The system is comprised of the Cas9 endonuclease and a guide RNA molecule specific to the target gene[137]. CRISPR-Cas9 has proved to be a very useful tool in research as it allows researchers to knock out and modify genes of interest in eukaryotic model systems[138,139]. One of the possible applications of CRISPR-Cas9 is gene ablation in cell culture. Gene ablation is carried out by creating double-stranded DNA breaks in the target gene and allowing the cell to repair the break using non-homologous end joining. Non-homologous end joining is a highly active yet error-prone pathway for DNA repair. The non-homologous end joining pathway often creates insertion or deletion mutations while repairing the DNA. Insertion and deletion mutations can cause a frameshift in the open reading frame of the gene. When a frameshift occurs, premature stop codons can arise and lead to early termination of the protein product[140]. A successful gene ablation experiment will create a premature stop codon in the gene of interest leading to incomplete mRNA products. The cell recognizes the mRNA as incomplete and degrades it through nonsense-mediated decay[141]. Combining iPSCs with CRISPR-Cas9 allows researchers to quickly and efficiently examine the effect of gene mutation in a human model of disease (Figure 5).

As outlined in section 1.2.2, differentiating iPSCs into cardiomyocytes (iPSC-CMs) requires the iPSCs to express specific transcription factors that will make them commit to

a cardiac mesoderm lineage and differentiate into cardiomyocytes. iPSCs are initially treated with glycogen synthase kinase-3 (GSK3) inhibitor, inhibiting both GSK3α and GSK3β. Inhibition of GSK3 activates the WNT/β-catenin pathway and initiates mesoderm germ lineage commitment[142]. The WNT/β-catenin pathway is inhibited via a WNT signaling inhibitor (e.g., Porcupine inhibitor IWP2)[142], in mesoderm cells to initiate the transition from mesoderm to cardiac mesoderm. MESP1 is a transcription factor that promotes the commitment to cardiac mesoderm[22]. Cardiac mesoderm then downregulates TGFβ/Nodal and BMP pathways and upregulates transcription factors Nkx2.5, GATA4, TBX5, and MEF2C to commit to cardiac progenitor cells[143]. BMP signaling is active in cardiac progenitor cells while they differentiate into contracting cardiomyocytes[32]. WNT signaling, BMP signaling, and TGFβ signaling must be activated and inhibited at specific points during differentiation. The activation of one signaling pathway, such as WNT signaling, at the incorrect time during differentiation will prevent the cells from moving forward in the differentiation process[30]. Failure to provide the appropriate signaling molecules at the correct time point will result in an unsuccessful differentiation that contains a heterogeneous cell population that may or may not contain functional cardiomyocytes.

iPSC-CMs have become a popular model for studying human diseases. iPSC-CMs exhibit several characteristics of cardiomyocytes found in the human heart. They contain organized sarcomeres and the proper cell machinery to propagate action potentials and cycle calcium[144]. iPSC-CMs provide a system where patient-specific cells can be generated for disease modeling, personalized drug screening, and regenerative approaches to

personalized medicine[145,146]. There are several advantages to iPSC-CMs over other *in vitro* models, such as immortalized cell lines, human cadaveric tissues, and primary cell cultures of non-human origin. iPSC-CMs generation is minimally invasive (skin punch biopsy or blood draw) and can theoretically provide an unlimited supply of iPSC-CMs. iPSC-CMs account for the patient's genetic background, allowing the assessment of genotype-phenotype associations. Additionally, iPSC-CMs allow the characterization of the cellular physiology of cardiomyocytes *in vitro*[147]. Human-derived models are especially important for cardiovascular research due to the glaring differences between animal and human cardiovascular systems. Small animal models have considerable differences in heart rates, energetics, myofilament composition, ion channel expression, electrophysiology, and calcium handling[147]. For the reasons listed, iPSC model systems can be used to study a wide range of human diseases, especially heart diseases.

However, there are some important differences between iPSC-CMs and normal adult cardiomyocytes. iPSC-CMs are immature, resembling fetal rather than adult cardiomyocytes[144]. Adult cardiomyocytes in the heart are large rod-shaped cells with the presence of long myofibrils allowing for efficient contraction. Meanwhile, iPSC-CMs cultured in 2D monolayers exhibit a flattened heterogenous shape with improper myofibril alignment[144]. The electrophysiology and calcium handling in iPSC-CMs must be considered as there are some notable differences between *in vivo* and *in vitro* cardiomyocytes. Adult cardiomyocytes in the heart are inactive until stimulated by an action potential generated in the heart conduction system, as outlined in section 1.3. Meanwhile, iPSC-CMs contract spontaneously due to high levels of hyperpolarization-

activated cyclic nucleotide-gated channel 4 in the plasma membrane, known as a voltage clock[144]. The calcium dynamics of iPSC-CMs are poorly established compared to adult cardiomyocytes[148]. Cultured iPSC-CMs lack T-tubules and have an increased time to calcium peak and slower decline of calcium signal. The lack of T-tubules results in a special uncoupling of the L-type calcium channels and the ryanodine receptors on the sarcoplasmic reticulum[144]. Despite the limitations of using iPSC-CMs as a model system, they have become a valuable tool used to investigate many inherited cardiomyopathies[147].

1.11 iPSC models of Arrhythmogenic Cardiomyopathies

iPSC-CM models are being used to study pathogenic mutations and have been helpful in understanding the molecular features of different forms of cardiomyopathy. iPSC-CMs have been a popular model for hypertrophic cardiomyopathy since there are many well-characterized genetic mutations that lead to the disease. Lan *et al.* developed an iPSC model that exhibited similar characteristics as hypertrophic cardiomyopathy *in vivo*. Patient-derived iPSC-CMs had an enlarged cellular size and increased frequency of multinucleation. The diseased iPSC-CMs demonstrated changes typical of hypertrophic cardiomyopathy (HCM), such as changed expression levels of atrial natriuretic factor (ANF), increased beta-myosin/alpha-myosin ratio, calcineurin activation, and nuclear translocation of nuclear factor of activated T-cells (NFAT). There was an increase in myofibril content and sarcomere disorganization within the iPSC-CMs. Arrhythmic waveforms were observed in electrophysiological recordings of HCM iPSC-CMs, and irregular calcium transients were observed in the HCM iPSC-CMs, while the control calcium transients were normal. Together, this iPSC-CM model points towards an aberrant

electromechanical function of HCM cardiomyocytes[149]. Similar studies have been done on familial dilated cardiomyopathy (DCM)-derived iPSC-CMs, where researchers demonstrated affected cardiomyocytes had dysregulated calcium handling, impaired contractility, and abnormal distribution of the sarcomeric protein α-actinin[150]. β-adrenergic signaling seems to be a common pathway involved in DCM pathogenesis in iPSC-CM studies[151,150]. Activation of β-adrenergic receptors resulted in compromised contractility, reduced contraction rate, and increased occurrence of abnormal α-actinin distribution. Additionally, one study showed that β-adrenergic signaling response was significantly weakened in DCM iPSC-CMs, and inhibiting phosphodiesterases (PDE) 2A and PDE3A rescued the signal response. These studies suggest that abnormal regulation of β-adrenergic signaling plays a major role in the pathogenesis of DCM. ARVC iPSC-CM models have been generated for many of the known mutations. Hawthorn *et al.*, Caspi *et al.*, Chen *et al.*, Padron-Barthe *et al.*, and Ratnavadivel *et al.* have used iPSC-CMs to investigate mutations in desmosomal proteins[152,153], sarcomere proteins (obscurin)[154], and TMEM43[124,155]. For example, Caspi *et al.* generated ARVC9 patient-derived iPSC-CMs harbouring a frameshift mutation in the *PKP2* gene that creates a premature stop codon (*c.972InsT/N*; p.A324fs335X). Caspi *et al.* demonstrated that ARVC cardiomyocytes have normal sarcomeres and myofibrils, but have an abnormal buildup of lipid droplets within the cytoplasm and upregulate proadipogenic transcription factor peroxisome proliferator-activated receptor-γ[153]. Additionally, ARVC10 cardiomyocytes bearing a DSG2 mutation (*c.1912G>A*; p.G638R) have abnormal action potentials and decreased peak ion currents potentially caused by down-regulated mRNA expression of ion channel genes in the cells[156]. ARVC iPSC-CMs with desmosomal protein mutations demonstrated a decrease in

expression levels of the mutated mRNA and altered organization of other important cellular structures such as gap junctions, and myofibrils. Lipid accumulation and irregular z-bands were found in iPSC-CMs modeling a sarcomeric protein mutation. The expression of adipocytokines and proteins related to adipogenic pathways such as peroxisome proliferator-activated receptor-γ (PPARγ), CCAAT enhancer binding protein α (C/EBPα), and fatty acid-binding protein 4 (FABP4) were increased due to the mutation in obscurin. Only three studies to date describe the generation of iPSCs expressing the TMEM43-S358L mutation[121,124,155]. The p.S358L mutation in TMEM43 has been modeled using expression vectors in iPSC-CMs and ARVC patient-derived iPSC-CMs. iPSC-CMs harboring the TMEM43-S358L mutation showed better contraction dynamics with GSK3β inhibition[124]. Additionally, Shinomiya *et al.* used patient-derived iPSC-CMs and reported that endoplasmic reticulum stress caused N-terminal glycosylation of TMEM43, leading to the abnormal accumulation at the nuclear envelope[121]. The study suggested that this mechanism could be a contributing factor in the pathogenesis in ARVC patients. These studies have proved to be very useful in modeling specific characteristics of ARVC and studying cellular processes that may play a role in ARVC.

iPSC-CMs are now being used more frequently in engineered heart tissue models to study cardiac diseases and drug screening[157,158]. This is a significant advancement as it allows for a more accurate 3D environment and a better representation of *in vivo* human hearts. The continuous advancement of iPSC-CM models in the context of arrhythmogenic cardiomyopathies will surely allow researchers to better encompass many of the factors that are at play in the human heart.

1.12 Rationale and Objectives

Uncovering the fundamental characteristics of the wild-type TMEM43 protein is necessary to understanding the role TMEM43 plays in ARVC. Once we understand the wild-type TMEM43 protein, we can then look at how the TMEM43-S358L mutant affects TMEM43 life cycle, function, and interacting partners. This will be invaluable in mapping out the molecular mechanisms that connect TMEM43 to ARVC5 and treating this disease.

As discussed above, TMEM43-S358L can be mislocalized to different intracellular compartments. Compromised trafficking of the TMEM43-S358L mutant may lead to protein instability due to faulty or damaged protein synthesis. Due to this mutation being autosomal dominant, the mutant protein may interfere with the function of the wild-type protein and other protein interactor partners such as Emerin and Lamins, thus compromising the overall function of the cell. Despite being widely expressed, TMEM43 mutations only seem to affect specific tissues in the body, such as the heart. Thus, altered TMEM43 trafficking across different cell types may play a role in these tissue-specific effects.

This project focuses on determining the subcellular localization and half-life of TMEM43 in different cell types, including patient-derived fibroblasts, wild-type and TMEM43 knockout iPSCs, and iPSC-derived cardiomyocytes (iPSC-CMs). The following three study objectives will address these gaps in knowledge:

1. Determine subcellular localization and half-life of TMEM43 in human iPSCs and iPSC-CMs using immunofluorescent microscopy and Western blotting.

2. Identify the effects of knocking out the *TMEM43* gene on iPSC-CM calcium handling and susceptibility to arrhythmogenicity.
3. Evaluate the significance of the TMEM43-S358L mutation in ARVC5 patient primary dermal fibroblast gene expression.

Given that studies report conflicting observations about TMEM43 localization in the cell and human patients harboring the TMEM43-S358L mutation present with life-threatening arrhythmias, I hypothesize that TMEM43 is localized to distinct subcellular compartments across different cell types and has an indispensable role in cardiomyocyte calcium handling. Furthermore, we hypothesize that ARVC5 patient fibroblasts will exhibit altered expression of extracellular matrix-associated proteins, which may point toward a mechanism of cardiomyopathy in patients.

1.13 Summary of Findings

I show that TMEM43 is stably localized in the early endosomes in undifferentiated human iPSCs. TMEM43 remains localized to early endosomes in early contracting cardiomyocytes, but shifts localization to the nuclear envelope as iPSC-CMs are cultured *in vitro* for an extended period. Several major intracellular organelle structures do not appear to be altered in TMEM43-deficient iPSC-CMs, although these cells do exhibit slightly higher abnormal calcium handling compared to wild-type iPSC-CMs. Finally, TMEM43-S358L patient fibroblasts differentially express extracellular matrix-associated genes compared to control fibroblasts. Taken together, these studies contribute to our knowledge of the TMEM43 life cycle in cardiac development and the effects of TMEM43

deficiency on cardiomyocytes. Patient-derived dermal fibroblast studies provide insight into the consequences of the p.S358L mutation in TMEM43 on gene regulation.

2 Material and Methods

2.1 Human Ethics and Biosafety

These studies are approved by the Newfoundland and Labrador Human Research Ethics Board (HREB #2018.210, HREB #00-176, and HREB #2020.310). The Esseltine laboratory is approved for biosafety containment level 2 research (protocol #M-007). All approvals are reviewed and renewed annually.

2.2 Human AD293 Cell Culture

AD293 cells (Cat # 240085, Agilent, Santa Clara, USA) were cultured in Dulbecco's Modified Eagle Medium (DMEM; Cat # 319-015-CL, Wisent, St-Bruno, CA) supplemented with Fetal Bovine Serum [FBS; (10% v/v), Cat # 10437028, Fisher Scientific, Ottawa, CA] and housed in T-25 culture flasks (Cat # 12-565-348, Fisher Scientific) with medium changes twice a week. Cells were maintained in a cell culture incubator at 37 °C and 5% CO_2. The cells were passaged once they reached 70-80% confluency in the flask. For passaging, cells were first washed with Phosphate-Buffered Saline (PBS; Cat # 311-011-CL, Wisent), then incubated with Trypsin-EDTA (0.05% Trypsin, Cat # 325-044-EL, Wisent; 0.53 mM EDTA, Cat # AM9260G, Thermo Fisher, Waltham, USA) at 37 °C and 5% CO_2 for approximately 4 minutes or until cells began to lift off the flask. Trypsin-EDTA reaction was then quenched using DMEM media supplemented with FBS. Cells were re-plated at a split ratio between 1:6 and 1:20.

2.3 Human Induced Pluripotent Stem Cell Culture

Two control human induced pluripotent stem cell (iPSC) lines were used to evaluate TMEM43 expression. The GM25256-iPSC cell line was derived from dermal fibroblasts

taken from a Japanese 30-year old male with no known illnesses (GM25256, NIGMS Human Genetic Cell Repository). The 43Q-iPSC cell line was derived from dermal fibroblasts taken from a Caucasian 32-year old female with no known illnesses[159]. The heterozygous *GJA1*-EGFP iPSC reporter cell line (WTC/AICS-0, Allen Institute for Cell Science) was derived from the same GM25256 iPSCs described above. This cell line endogenously expresses a connexin43-monomeric enhanced green fluorescent protein (Cx43-mEGFP) created using CRISPR/Cas9 homologous directed repair (HDR) technology. The cell line was confirmed to have the intended mEGFP insertion at the *GJA1* (Cx43) locus.

iPSCs were maintained in either Essential 8 medium (E8; Cat # A1517001, Thermo Fisher) or mTesR-Plus (Cat # 100-0276, Stem Cell Technologies, Vancouver, CA) in 6-well plates pre-coated with the extracellular matrix cocktail Geltrex (Cat # A1413302, Thermo Fisher). For pre-coating, Geltrex was diluted in cold DMEM using a final coating concentration of 0.5 $\mu g/cm^2$. Cells received daily media changes and were passaged every 4 to 5 days or when cells reached approximately 70% confluency. Healthy, undifferentiated iPSCs grow in multicellular colonies with distinct borders. Individual cells should be compact with a large nucleus-to-cytoplasm ratio and prominent nucleoli[160]. Spontaneous differentiation in iPSC cultures can be distinguished by irregularly shaped colonies, colonies that have lost border integrity, or cells with irregular morphology within a colony[160]. iPSCs were passaged using an aggregate passage protocol as follows. Spent media was first aspirated, and any identified regions of spontaneous differentiation removed through aspiration. The well was then washed once with PBS to remove any dead

cells. Gentle cell dissociation reagent (0.5 mM EDTA in PBS) was then added and incubated at room temperature for 2 to 5 minutes. Once the cells started to separate and become round, and the colonies appeared to have holes in them under a microscope, the simple cell dissociation buffer was removed, and 1 mL of E8 was added to quench the reaction. Cells were then gently scraped off the bottom of the well and transferred to a 15 mL conical tube. The cell suspension was then gently triturated to produce desired size cell clumps – approximately 100 µm in diameter[160]. The cells were then re-seeded onto a new 6-well dish that was treated with Geltrex as previously described. The cells were distributed evenly across the entire surface area of the well by rocking the plate several times, side to side and front to back. The plate was then incubated at 37 °C and 5 % CO_2 overnight to allow the cells to adhere to the dish.

2.4 Patient-Derived Primary Fibroblasts

2.4.1 ARVC5 Patient Dermal Biopsy Collection and Classification

Dr. Kathy Hodgkinson recruited ARVC5 dermal biopsy donors, and appointments were scheduled for Dr. David Pace to perform the biopsy procedure. Biopsies were performed on affected and unaffected individuals from the identified ARVC5 population in Newfoundland and Labrador[116], and a total of 15 samples were collected (Figure 6). The disease severity, mutation, and sex status of samples used were not revealed until after all experiments were completed. The patient samples used in this study included an ARVC5 severely affected male (ARVC#1) and their unaffected brother (CNTRL#1), two mildly affected females (ARVC#2 and ARVC#3), and a mildly affected male (ARVC#4).

Figure 6 Characteristics of the ARVC5 population in Newfoundland and Labrador and the patient samples collected for this study

Mutation and clinical status of 496 individuals born at *a priori* 50% risk related to the ARVC5 population in Newfoundland and Labrador. The ARVC5 population consists of 15 families. Subjects were classified by clinical presentation (affected or unaffected), mutation status, and sex. A dermal biopsy was collected from affected and unaffected individuals, and dermal fibroblasts were isolated. ARVC5 patient fibroblast cell lines used in this study include ARVC#1 (severely affected male), ARVC#2 (mildly affected female), ARVC#3 (mildly affected female), ARVC#4 (mildly affected male), and CNTRL#1 (unaffected male) The source of the data in this figure is Merner *et al.* 2008[116]. Figure 6 was created using BioRender Premium software, *biorender.com*.

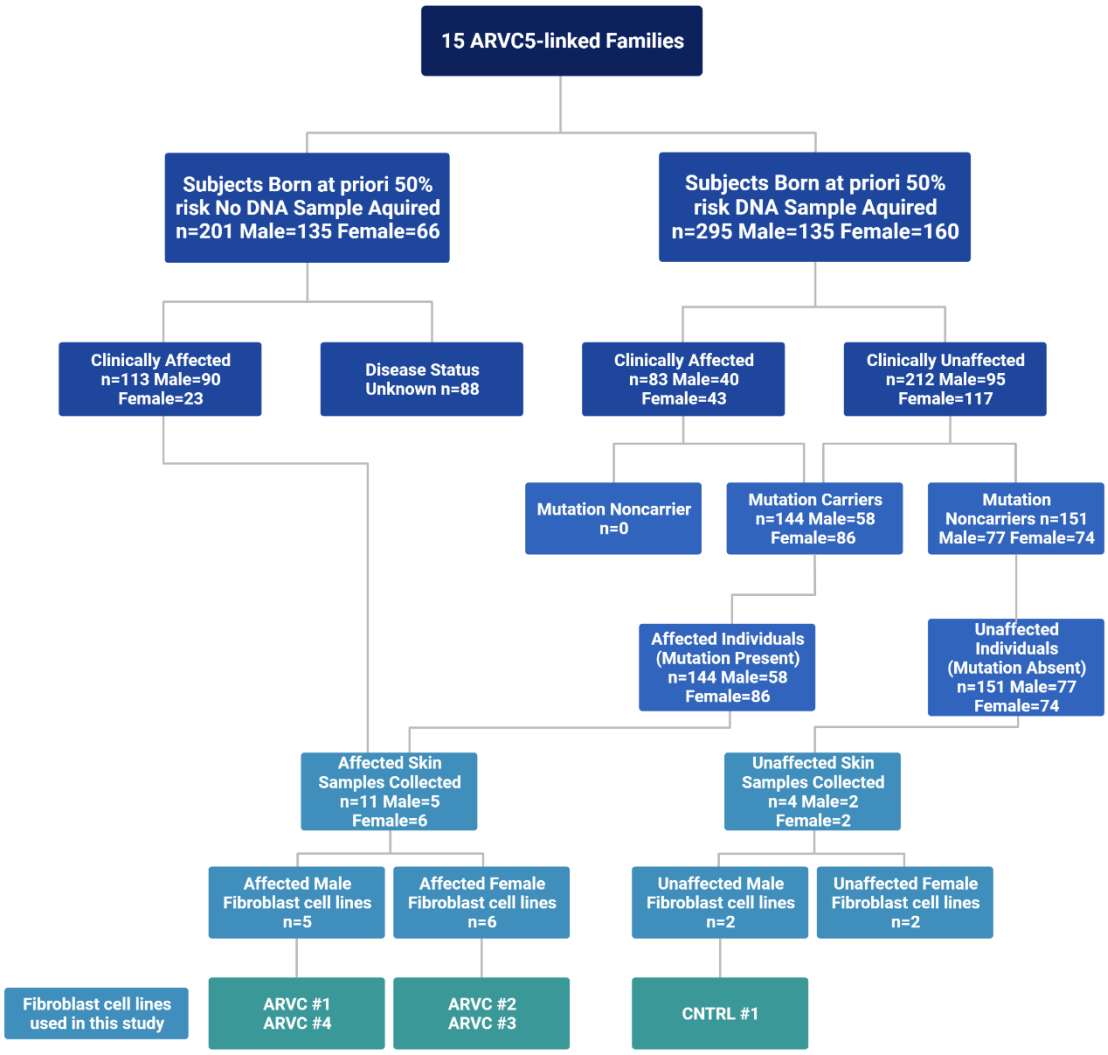
15 ARVC5-linked Families
Subjects Born at priori 50% risk No DNA Sample Aquired n=201 Male=135 Female=66
Subjects Born at priori 50% risk DNA Sample Aquired n=295 Male=135 Female=160
Clinically Affected n=113 Male=90 Female=23
Disease Status Unknown n=88
Clinically Affected n=83 Male=40 Female=43
Clinically Unaffected n=212 Male=95 Female=117
Mutation Noncarrier n=0
Mutation Carriers n=144 Male=58 Female=86
Mutation Noncarriers n=151 Male=77 Female=74
Affected Individuals (Mutation Present) n=144 Male=58 Female=86
Unaffected Individuals (Mutation Absent) n=151 Male=77 Female=74
Affected Skin Samples Collected n=11 Male=5 Female=6
Unaffected Skin Samples Collected n=4 Male=2 Female=2
Affected Male Fibroblast cell lines n=5
Affected Female Fibroblast cell lines n=6
Unaffected Male Fibroblast cell lines n=2
Unaffected Female Fibroblast cell lines n=2
Fibroblast cell lines used in this study
ARVC #1 ARVC #4
ARVC #2 ARVC #3
CNTRL #1

2.4.2 Primary Fibroblast Isolation from Dermal Biopsy Explant

Primary fibroblast isolation was performed using an outgrowth procedure using skin samples from punch biopsies[161,162]. The skin punch biopsies were approximately 4 to 6 mm in diameter and obtained from male and female ARVC5 patients of varying disease severity as described above. Skin samples were stored on ice in DMEM supplemented with 20% FBS (v/v) and 5% penicillin/Streptomycin (v/v; referred to as complete DMEM) while being transferred from the clinic to the laboratory. Samples were immediately processed for fibroblast isolation upon arrival. Skin samples were dissected on the lid of a 10 cm petri dish in complete DMEM. The skin samples were cut into 20 to 24 equal-sized pieces using a sterile scalpel and tissue forceps, ensuring that pieces had sharp straight edges to help facilitate adhesion and cell outgrowth. The pieces were then transferred to a 6-well dish pre-coated with 0.1% porcine gelatin (Cat # G1890, Sigma-Aldrich, St. Louis, USA) with 700 µL of complete DMEM. Samples were incubated at 37 °C and 5% CO_2 with the addition of approximately 200 µL of complete DMEM every two days to replace evaporated medium. After approximately one week in culture, when skin pieces adhered to the dish, the medium volume was increased to 1.5 mL. The medium was replaced every 2 to 3 days. Skin samples were cultured for an additional 2 to 3 weeks to allow cells to become confluent to the point where fibroblasts reached the edges of the wells. Cells were then subcultured into T75 culture flasks, and cell stocks were frozen at early passages. Cells were cryopreserved using the Mr. Frosty™ Freezing Container (Cat # 5100-0036, Thermo Fisher) as per the manufactures instructions. Cells were frozen in FBS (90% v/v) and dimethyl sulfoxide (10% v/v; Cat # BP231-100 Thermo Fisher) and stored at -196°C in a liquid nitrogen dewar.

2.4.3 Primary Fibroblast Culture

Primary fibroblasts were cultured in DMEM supplemented with FBS (20% v/v) in T-25 culture flasks with medium changes every two days. Cells were maintained in an incubator at 37 °C and 5% CO_2. The cells were passaged once they reached 70 to 80% confluency in the flask. Cells were first washed with PBS, then incubated with Trypsin-EDTA (0.05% Trypsin, 0.53 mM EDTA) at 37 °C and 5% CO_2 for approximately 4 to 6 minutes or until cells began to lift off the flask. Trypsin-EDTA reaction was then quenched using DMEM media supplemented with FBS. Cells were re-plated at split ratios of between 1:6 and 1:20. Primary dermal fibroblasts were used for experiments between passages 2 to 10, and all cell lines were passaged-matched in each experiment.

2.5 TMEM43 CRISPR-Cas9 Genetic Ablation

TMEM43 knockout AD293 and iPSC cell lines were created by former Esseltine laboratory members using CRISPR-Cas9 genetic ablation as described previously[163,164]. Two single guide RNAs (sgRNA) targeting human *TMEM43* were designed using the Sanger Institute CRISPR finder [*http://www.sanger.ac.uk/htgt/wge/*; Sanger sgRNA ID 950611662 (5′-TGGCGCCTTACGGACATCCA-3’); Sanger sgRNA ID 950611647 (5′-ACGGCAACCTCATTGGCTGA-3’)]. The sgRNAs were selected based on their predicted efficiency and low predicted off-target effects. The two sgRNAs were cloned into either the pSpCas9(BB)-2A-GFP (PX458) or pSpCas9(BB)-2A-Puro (PX459) V2.0 plasmids (Addgene, Cambridge, USA). Both plasmids contain the gene for the Cas9 protein, the cloning backbone for a sgRNA, and a selection marker (PX458:GFP or PX459:puromycin)[137]. The human AD293 and iPSC cell lines were transfected using the

Mirus TransIT®-LT1 Transfection Reagent (Cat # MIR 2300, Mirus Bio LLC, Madison, USA) according to the manufacturer's instructions. After transfection, cells were selected for puromycin resistance with 2 μg/mL puromycin treatment (Cat # A1113803, Thermo Fisher), and GFP-expressing cells were sorted using fluorescence-activated cell sorting (FACS). The selected clones had TMEM43 protein ablation confirmed via immunofluorescence and Western blotting.

2.6 Cardiomyocyte Differentiation

iPSCs were differentiated into contracting cardiomyocytes using a commercially available kit (STEMdiff™ Cardiomyocyte Differentiation kit, Cat # 05010, Stem Cell Technologies). In preparation for a cardiomyocyte differentiation, the iPSCs were passaged into single cells using Accutase (Cat # 07922, Stem Cell Technologies). Areas of spontaneous differentiation were removed from the well via aspiration, and the well was washed using PBS to remove any dead cells. The PBS was then removed by aspiration, and 500 μL of Accutase was added (for a 6-well plate). The 6-well plate was then incubated for 8 minutes at 37 °C and 5% CO_2. After incubation in Accutase, the cells were observed under a microscope to ensure there were no clumps of cells and they had released from the plate. The Accutase was neutralized by adding 1 mL of E8. The cells were gently triturated up and down and then transferred to a 15 mL conical tube containing 5 mL of DMEM with no additives. The cells were then centrifuged at 300 x g for 5 minutes, the supernatant removed, and the cell pellet was resuspended in 1 mL of E8 medium supplemented with RHO/ROCK pathway inhibitor (10 μM, Y-27632; Cat # 72308, Stem Cell Technologies)

to promote single-cell survival. The media was replaced with E8 medium 24 hours after seeding.

For cardiomyocyte differentiation, iPSCs were seeded at a cell density of 2.0 x 10^5 cells/cm^2 into the desired vessel. Once the cells reached >95% confluency, mesoderm lineage specification was initiated as per the manufacturer's instructions by adding STEMdiff™ Cardiomyocyte Differentiation Basal Medium containing Supplement A and Corning™ Matrigel™ Membrane Matrix (1:100; Cat # 08-774-552, Thermo Fisher). Forty-eight hours later, the cells were committed to cardiac progenitors via the addition of STEMdiff™ Differentiation Medium B and incubated for another 48 hours. Finally, cells were differentiated into functional cardiomyocytes through STEMdiff™ Differentiation Medium C. Once differentiated, beating cardiomyocytes were fed every two days with STEMdiff™ Maintenance Medium until day 30 (immature beating cardiomyocytes) or day 90 (more mature beating cardiomyocytes).

2.7 Cycloheximide Time Course (TMEM43 Half-life)

The half-life of TMEM43 was determined in different cell types using a cycloheximide time course technique. Cells were seeded at a density of 2.5 x 10^4 cells/cm^2 and treated with 25 µM of cycloheximide (Cat # C1988, Sigma-Aldrich) for 0, 1, 2, 4, and 8 hours. Cell lysates were made from each experimental condition, and protein levels were determined using SDS-PAGE and Western blotting, as described in section 2.8.

2.8 Western Blot

2.8.1 Cell Lysis

When preparing protein lysate, all reagents and cells were kept as cold as possible by keeping everything on ice and cooling reagents in the fridge before preparing the protein lysate. The cell culture vessel was immediately placed on ice once taken out of the incubator. Cell culture medium was aspirated, and the cells were then washed twice with ice-cold PBS. PBS was aspirated and cells were lysed in ice-cold lysis buffer supplemented with protease and phosphatase inhibitors (150 mM NaCl; 50 mM Tris pH 8.0; 1.0% Triton X-100; 1 µg/mL Leupeptin; 1 µg/mL Aprotinin; 10 mM NaFl; 1 mM Na_3VO_4). Cells were scraped off the cell culture dish using a plastic cell scraper and transferred to a 1.5 mL microcentrifuge tube. The cell lysate was then centrifuged at 15000 RPMs for 10 minutes at 4 °C to pellet insoluble material. After centrifugation, the supernatant was transferred to a new microcentrifuge tube, and the pellet was discarded. At this point, the protein lysate could be stored at -20 °C until ready to proceed with the next step.

2.8.2 BCA Protein Assay

Protein concentration was determined using the commercially available Pierce BCA Protein Assay Kit (Cat # PI23225, Thermo Fisher) as per the manufacturer's instructions. Samples were measured in duplicate. Bovine Serum Albumin (BSA) protein standards were prepared by serial dilution in distilled water to obtain a final concentration range of 0 to 2 mg/mL. Colorimetric measurement was performed using a microplate spectrophotometer (model 2030, Perkin Elmer, Waltham, USA). The protein concentration of samples were interpolated based on the standard curve generated from the BSA standards

using the formula y = mx + b, where m is the slope, x is the sample concentration, and b is the y-intercept. Protein lysates were adjusted with PBS such that all samples contained equal protein concentrations. 4X Sample Loading Buffer [200 mM Tris HCl, pH 6.8; Sodium Dodecyl Sulfate 8% (w/v); Bromophenol Blue 0.4% (w/v); Glycerol 40% (v/v); 20% 2-mercaptoethanol] was added to the sample to a final concentration of 1X. The samples were allowed to solubilize at room temperature for at least 20 minutes before being loaded onto the gel.

2.8.3 SDS-Polyacrylamide Gel Electrophoresis

Protein samples were separated via sodium dodecyl sulfate-polyacrylamide gel electrophoresis (SDS-PAGE). Protein samples were run on a 7.5% polyacrylamide gel (Cat # EC-890, National Diagnostics, Atlanta, USA) at 100 volts using a Mini Trans-Blot Cell (Cat # 1658005, Bio-Rad, Hercules, USA). The gel was then transferred to a nitrocellulose membrane with a pore size of 0.45 µm (Cat # 1620115, Bio-Rad) at 100 volts for one hour at 4 °C.

2.8.4 Immunoblotting

After the protein was transferred to the nitrocellulose membrane, the membrane was simultaneously blocked and probed by incubating the primary antibody diluted in blocking buffer {3% w/v non-fat dry milk in Tris Buffered Saline with Tween 20 [TBS-T; 15.2 mM Tris HCL, 4.62 mM Tris base (Cat # 1610719, Bio Rad), 150 mM NaCl (Cat# 600-082-DG, Wisent), and 0.1% Tween 20 (Cat # BP337100, Fisher BioReagents, Ottawa, CA)]}. The membrane was placed on a rocker and incubated with primary antibody at 4 °C overnight. The following primary antibodies were used: Rabbit anti-TMEM43 [(1:5000),

Cat # ab230213, Abcam, Cambridge, USA]; Rabbit anti-Connexin43 [(1:5000), Cat # C6219, Sigma-Aldrich]; Mouse anti-Glyceraldehyde 3-phosphate dehydrogenase [(1:5000), Cat # CAB374, Thermo Fisher]. After incubation, the membrane was washed three times for five minutes in TBS-T to remove unbound primary antibody. Secondary antibody was added to the membrane for one hour at room temperature in the same blocking solution used for the primary antibody. The secondary antibodies were conjugated to horseradish peroxidase (HRP). The following secondary antibodies were used: goat anti-mouse-HRP [(1:5000), Cat # 31430, Thermo Fisher] and goat anti-rabbit-HRP [(1:5000), Cat # 31460, Thermo Fisher]. After the second incubation, the membrane was washed three times for five minutes to remove any excess secondary antibody. Membranes were exposed using Clarity™ Western ECL Substrate (Cat # 1705061, Bio-Rad), and proteins were visualized using the ImageQuant LAS 4000 (Cat # 28 9558 10, GE Healthcare, Chicago, USA).

2.8.5 Immunoblotting Analysis

Images of immunoblots were analyzed by densitometry using Fiji software (version 1.53c). Every immunoblot was normalized to the house-keeping protein Glyceraldehyde 3-phosphate dehydrogenase (GAPDH) when performing densitometric analysis.

2.9 Brefeldin A Time Course

Protein trafficking within AD293 and iPSCs was analyzed to determine how TMEM43 is trafficked in the cell. Cells were seeded at a density of 2.5 x 10^4 cells/cm^2 in all eight wells of an eight-well chamber slide (Cat # C7057, Thermo Fisher). Cells were treated with 5 µg/mL of Brefeldin A (BFA, Cat # 11861-5, Cayman Chemicals, Ann Arbor,

USA) for 6, 4, 2, 1, and 0.5 hours. The following controls were performed: untreated, vehicle control, 6-hour BFA plus 2-hour washout. Following BFA treatment, cells were fixed and immunofluorescently labeled to visualize protein trafficking, as described in section 2.10.

2.10 Immunofluorescence Cell Imaging

2.10.1 Cell Fixation

Two different methods of cell fixation have been used throughout this project. The first method is formalin fixation. This method was used when TMEM43 was not being immunofluorescently stained in cell culture. Cells to be fixed were grown on glass coverslips or Lab-Tek™ II CC^2™ 8-well chamber slides (Cat # 154941 Thermo Fisher). Cells to be fixed first had the culture medium aspirated and were washed twice with PBS. After washing, the PBS was aspirated, and cells were incubated in 10% normal buffered formalin (Cat # HT501128, Sigma-Aldrich) for 30 minutes at room temperature. After fixation, the cells were washed twice with PBS. The coverslip could then be stored in a 12-well dish filled with approximately 1 to 2 mL/well of PBS and sealed with parafilm. Cells that were fixed on a Lab-Tek™ II CC^2™ chamber slide were stored in approximately 400 µL/well of PBS with the cover sealed with parafilm. Fixed cells were stored at 4 °C until ready to stain.

The second method that was used was methanol fixation. This method was used when immunofluorescently staining for TMEM43 in cell culture. Cells to be fixed had the culture medium aspirated and were washed once with ice-cold PBS. Cells were then submerged in -30 °C methanol and placed in the freezer for 8 minutes. After the incubation, the methanol

was immediately removed, and the cells were washed once with PBS. Fixed cells could then be stored as previously described in section 2.10.1 until ready to stain.

2.10.2 Immunofluorescent Cell Staining

Primary antibodies were diluted in blocking/permeabilization buffer [3% BSA (Cat # B4287, Sigma-Aldrich)/0.1% Triton X-100 (Cat # 93426, Sigma-Aldrich) in PBS]. Cells were incubated with primary antibodies for 1 hour at room temperature or overnight at 4 °C. The following primary antibodies were used: rabbit anti-TMEM43 [(1:1000), Cat # ab230213, Abcam], rabbit anti-connexin43 [(1:1000), Cat # C6219, Sigma-Aldrich], mouse anti-lamin [(1:1000), Cat # ab238303, Abcam], mouse anti-EEA1 [(1:100), Cat # 48453S, New England Biolabs, Whitby, CA], and mouse anti-LAMP1 [(1:500), Cat # 15665T, New England Biolabs] mouse anti-gamma catenin [(1:1000), Cat # ab231304, Abcam], mouse anti-GM130 [(1:1000), Cat # ab169276, Abcam], mouse anti-Calnexin [(1:1000), Cat # MA3027, Thermo Fisher]. After incubation with the primary antibody, the cells were washed 3 times for 5 minutes to remove any excess primary antibody.

Fluorescently-conjugated secondary antibodies and dyes were diluted in the same blocking buffer described above and were incubated away from direct sunlight (covered with tinfoil) for 1 hour at room temperature. The following secondary antibodies and dyes were used: Alexa Fluor 488 Donkey anti-Rabbit [(1:5000), Cat # A21206, Invitrogen], Alexa Fluor 555 Donkey anti-Rabbit [(1:500), Cat # A31572, Invitrogen], Alexa Fluor 555 Donkey anti-Mouse [(1:500), Cat # A31570, Invitrogen] Alexa Fluor Plus 647 Goat anti-Mouse [(1:500), Cat # A32728, Invitrogen], Hoechst 33342 [(1:1000), Cat # H3570, Invitrogen]. After incubation, the secondary antibodies and dyes were aspirated, and the

cells were washed 3 times for 5 minutes to remove any excess secondary antibody or dye. The slides were then mounted onto a microscope slide using mounting media: Mowiol 4-88 (Cat # 81381, Sigma-Aldrich) DABCO (Cat # AAA1400314, Thermo Fisher).

2.10.3 Confocal Microscopy

Immunofluorescent images were taken on a Fluoview FV10i-W3 confocal laser scanning microscope using either the 60X water immersion lens (1.2 NA) or 10X lens (0.4 NA) using system version 2.1.1.7 (Olympus, Shinjuku, Tokyo, JP). Immunofluorescent images in figure 12 were taken on a Zeiss LSM 900 with Airyscan confocal laser scanning microscope using either the 20X lens (0.8 NA), 40X lens (0.8 NA), or 63X oil immersion lens (1.4 NA) using Zen Blue version 3.4 software (Carl Zeiss Canada Ltd., Toronto, CA) The lasers used to excite fluorescently labeled secondary antibodies were: 405 nm, 473 nm, 559 nm, and 635 nm laser. All images taken were analyzed and processed using Fiji software (version 1.53c).

2.11 Calcium Imaging

Contracting iPSC-CMs were incubated with Fluo-4 AM dye (10 µmol/L, Cat # F14201, Thermo Fisher) for 30 minutes in conditioned medium at 37°C and 5% CO_2. After incubation, iPSC-CMs were washed with HEPES balanced salt solution (HBSS, Cat # 14025092, Thermo Fisher) 3 times to remove excess dye from wells. Fresh cardiomyocyte maintenance medium was then added to wells. Calcium transients were measured using the Fluoview FV1000 confocal laser scanning microscope using the 20X water immersion lens and 473 nm laser. In addition to recording calcium transients without external stimulation,

iPSC-CM calcium transients were measured after being treated with 1 μM isoproterenol. Isoproterenol is a β-adrenergic receptor agonist that stimulates cardiomyocytes to contract.

2.11.1 Calcium Imaging Analysis

Images were taken over a 60 second time period at 5.33 frames per second (2.0 μs/pixel). They were all individually analyzed using Fiji software to determine fluorescent intensity in each region of interest. The lowest fluorescent intensity signal was used as a baseline fluorescence of Fluor-4 AM (F_0) when free calcium was not present in the cell. All measurements above this threshold (F_1) were considered to be proportional to intracellular calcium concentration $[Ca^{2+}]_i$. The ratio of fluorescent intensity at each time point was calculated using the equation F_1/F_0. Data were plotted using GraphPad Prism version 8.0.2 (GraphPad Software Inc, San Diego, USA).

2.12 Quantitative Reverse Transcription Polymerase Chain Reaction (qRT-PCR)

2.12.1 RNA Extraction and cDNA Synthesis

Total RNA was isolated using Invitrogen PureLink RNA Mini Kit (12183020, Thermo Fisher) according to the manufacturer's instructions. Genomic DNA was degraded through on-column DNaseI digestion (Cat # EN0521, Thermo Fisher). Extracted RNA was stored at -80 °C. The quantity and quality of isolated RNA of each sample were measured by nanodrop (NanoDrop™ 2000/2000c Spectrophotometers, Thermo Fisher). High-quality RNA was assessed as having a λ260/280 ratio of ~2.0 and a λ260/230 ratio of ~2.2. 500 ng of extracted RNA was used to generate cDNA using the High-Capacity cDNA Reverse Transcription Kit (Cat # 4387406, Thermo Scientific). cDNA was stored at -30°C until use.

2.12.2 Quantitative Polymerase Chain Reaction

Gene expression was assessed using semi-quantitative reverse transcription-polymerase chain reaction (qPCR) using SYBR Green fluorescent dye (Cat # 1725124, Bio-Rad). qPCR experiments were carried out using a ViiA 7 Real-Time PCR Thermocycler (Applied Biosystems, Waltham, USA). All primer sequences used are outlined in Table 1. *GAPDH* was used as a reference gene as it was stably expressed across all cell lines used in this study (refer to Appendix B) and has been proven to be stable in fibroblast cell lines[165–167], while target genes included *TMEM43, GJA1* (Cx43), *LMNA, JUP* (Plakoglobin), *MMP1, ITGA5* (Integrin α5)*, ITGB1* (Integrin β1), *COL1A1* (Collagen-1)*, LAMA1* (Laminin). Primers for GAPDH, TMEM43, Cx43, lamin, and plakoglobin were previously validated by the Esseltine laboratory. All other primers were acquired from Esseltine *et al.* 2015[168]. Cycle conditions were as follows: hold at 50°C for 2 minutes, pre-denaturation at 95°C for 30 seconds, initial denaturation at 95°C for 10 seconds, primer annealing/extension at 60°C for 60 seconds. The PCR was set to 40 cycles. The melting curves of amplicons were obtained using temperatures that ranged from 60°C to 95°C with a temperature increase of 0.05°C per second to analyze primer specificity.

Table 1. Primer sequences for qPCR

Gene	Sequence (5' to 3')	Annealing Temperature (°C)	Reference
GAPDH	F: TGCTTTTAACTCTGGTAAAG R: CACTTGATTTTGGAGGGATC	60	
TMEM43	F: TGGCCGCGAATTATTCCAGT R: CGTAAGGCGCCAATGATGTG	60	
Cx43	F: GGTCTGAGTGCCTGAACTTGCCT R: AGCCACACCTTCCCTCCAGCA	60	
Lamin	F: ATGAGGACCAGGTGGAGCAGTA R: ACCAGGTTGCTGTTCCTCTCAG	60	
Plakoglobin	F: ACCAGCATCCTGCACAACCTCT R: GGTGATGGCATAGAACAGGACC	60	
MMP-1	F: CTGGCCACAACTGCCAAATG R: CTGTCCCTGAACAGCCCAGTACTTA	60	[168]
Integrin α5	F: TGCTGGACTGTGGAGAAGACAACA R: TCTGGGCATGGAAAGTGAGGTTCA	60	[168]
Integrin β1	F: GACCTGCCTTGGTGTCTGTGC R: AGCAACCACACCAGCTACAAT	60	[168]
Collagen-1	F: AGACATCCCACCAATCACCTG R: GGCAGTTCTTGGTCTCGTCAC	60	[168]
Laminin	F: GCTCTGTGACTGCAAACCAA R: TTTCTGGGTCGCAGGTATTC	60	[168]

2.13 Statistical Analysis

All statistical analyses were performed using GraphPad Prism version 8.0.2. Data were presented as mean ± standard error of the mean values. When comparing two groups, an unpaired two-tailed t-test was used to analyze data and determine significance. When evaluating three or more groups, one-way analysis of variance (ANOVA) with Tukey's post hoc multiple comparisons test was used to determine statistical significance. A p-value of less than 0.05 was considered significant in this study.

3 Results

3.1 TMEM43 Gene Ablation in iPSCs

There is significant evidence linking the TMEM43-S358L mutation to ARVC5[116]; however, the disease mechanism is not understood. To test whether TMEM43 is essential in the normal function of iPSCs and iPSC-CMs, the Esseltine laboratory created a *TMEM43-/-* iPSC model using CRISPR-Cas9 gene ablation (Figure 7A). Immunofluorescence and Western blot analysis confirmed TMEM43 protein loss in the *TMEM43-/-* iPSC line (Figure 7B, C). Knocking out the TMEM43 protein did not present any apparent effects on iPSC morphology, viability, or proliferation (Figure 7D, Data not shown). Additionally, cardiomyocyte differentiation of *TMEM43-/-* iPSC-CMs in culture resulted in synchronously contracting cells at approximately the same time points as wild-type control cells. As would be expected from the adult presentation of *TMEM43*-associated ARVC, *TMEM43* gene knockout does not appear to negatively impact iPSC proliferation, survival, or cardiomyocyte lineage specification.

3.2 TMEM43 Life Cycle in iPSCs

3.2.1 TMEM43 Localization

Many studies report that TMEM43 localization depends on the scientific model used[118,119,120,122,123]. Researchers have shown TMEM43 residing in the nuclear envelope[118,119], endoplasmic reticulum[118], adherens junctions[122], and the sarcolemma[123]. Although there are many reports of TMEM43 localization in cell culture models, some of these reports use overexpression models[118,119] susceptible to protein localization artifacts, and there have not been any reports of endogenous localization in human-iPSCs. To fill

Figure 7 TMEM43 CRISPR-Cas9 gene ablation

(A) Two guide RNAs were designed targeting the TMEM43 gene in the 3rd exon for CRISPR-Cas9 gene ablation in human cells. (B) Representative immunofluorescent micrographs of TMEM43 (green) in wild type (WT) and *TMEM43-/-* iPSC-CMs. Nuclei (Hoechst, blue). Scale bar = 50 μm. (C) Representative Western blot of TMEM43 and GAPDH protein in WT and *TMEM43-/-* iPSCs. (D) Representative phase contrast images of WT and *TMEM43-/-* iPSC colonies. Scale bar = 200 μm.

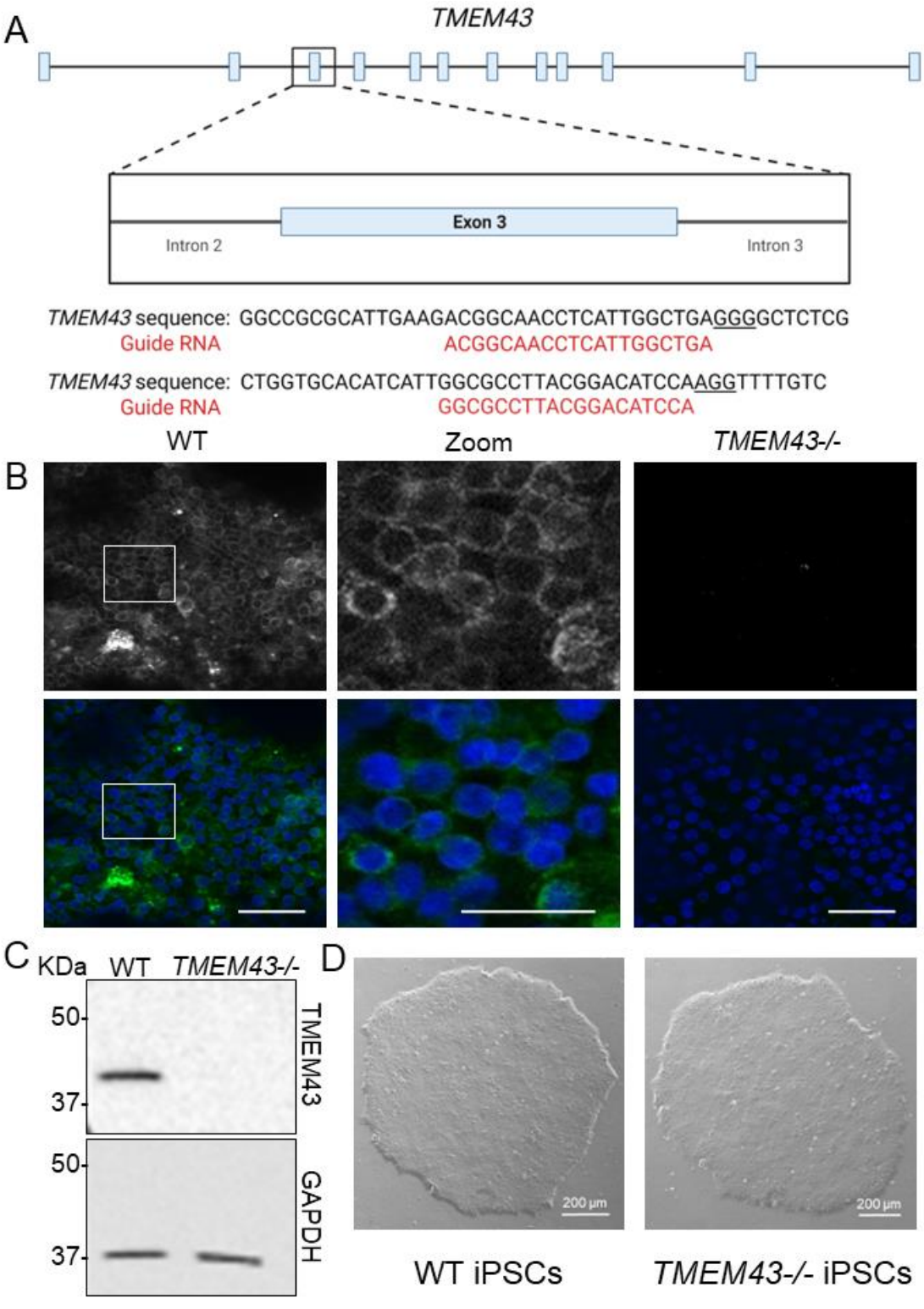
A
TMEM43
Exon 3
Intron 2
Intron 3
TMEM43 sequence: GGCCGCGCATTGAAGACGGCAACCTCATTGGCTGAGGGGCTCTCG
Guide RNA
ACGGCAACCTCATTGGCTGA
TMEM43 sequence: CTGGTGCACATCATTGGCGCCTTACGGACATCCAAGGTTTTGTC
Guide RNA
GGCGCCTTACGGACATCCA
WT
Zoom
TMEM43-/-
B
C
KDa
WT
TMEM43-/-
50
37
TMEM43
50
37
GAPDH
D
200 µm
200 µm
WT iPSCs
TMEM43-/- iPSCs

this gap in knowledge, I set out to determine where TMEM43 is located in iPSCs using immunofluorescence confocal microscopy. Immunofluorescent confocal microscopy demonstrated a drastically different TMEM43 staining pattern compared to previous reports and what our laboratory has seen in human AD293 cells (Figure 8). In contrast to all previous reports, TMEM43 localized to large puncta within the cytoplasm rather than the nuclear envelope, which suggested that the protein is not interacting with the nuclear envelope in undifferentiated iPSCs. To determine what subcellular compartment TMEM43 was residing in, iPSCs were labeled with markers for the nuclear envelope, Golgi apparatus, gap junctions, desmosomes, lysosomes, early endosomes, and endoplasmic reticulum. Co-staining showed that TMEM43 strongly colocalized with the early endosome marker early endosome antigen 1 (EEA1) with lesser colocalization with the other makers tested (Figure 8). Mander's Colocalization Coefficient analysis confirmed relatively little colocalization between TMEM43 and Cx43 (0.0038 ± 0.00095), GM130 (0.12 ± 0.028), and lamin (0.29 ± 0.028). There was a moderate amount of colocalization with the markers lysosomal-associated membrane protein 1 (LAMP1) (0.41 ± 0.084), plakoglobin (0.54 ± 0.059), and calnexin (0.56 ± 0.028). As highlighted by our images, TMEM43 and EEA1 had the highest colocalization with a Manders coefficient of 0.91 ± 0.016 (Figure 9A). The high degree of co-localization as revealed through the Mander's coefficient suggests that the majority of endogenous wild-type TMEM43 protein resides within early endosomes of undifferentiated human iPSCs.

Figure 8 TMEM43 localization with cellular compartments in iPSCs

Representative immunofluorescence confocal micrographs of TMEM43 (green), various intracellular compartment markers (red), and nuclei (Hoechst, blue) in undifferentiated human iPSCs. Intracellular compartments include early endosomes (EEA1), lysosomes (LAMP1), Golgi apparatus (GM130), endoplasmic reticulum (calnexin), nuclear envelope (lamin), desmosomes (plakoglobin), and gap junctions (connexin43). Arrows highlight regions of co-localization. n = 3. Scale bar = 50 μm.

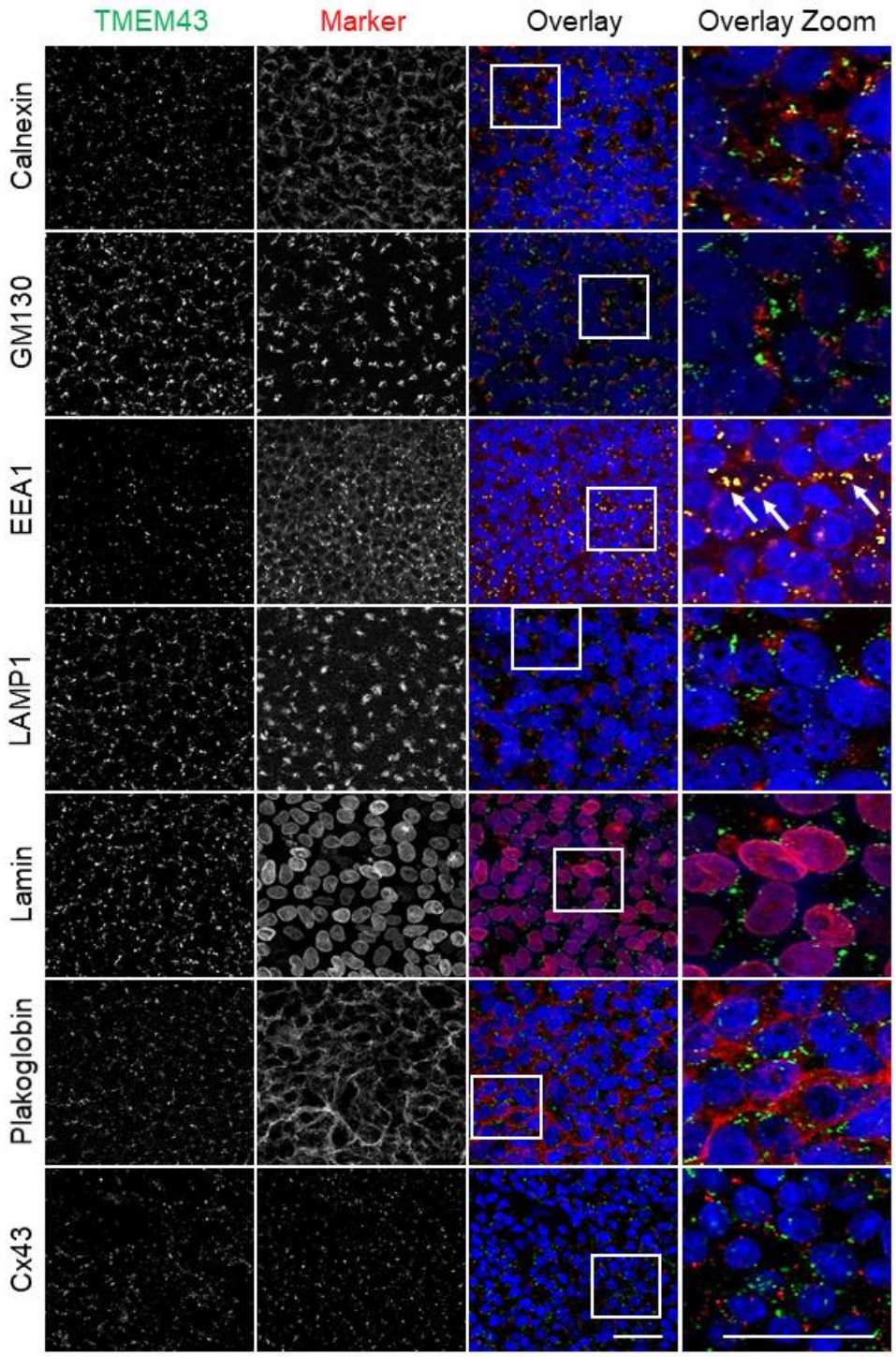
TMEM43
Marker
Overlay
Overlay Zoom
Calnexin
GM130
EEA1
LAMP1
Lamin
Plakoglobin
Cx43

Figure 9 TMEM43 colocalization with early endosomes in iPSCs

(A) Manders' Colocalization Coefficient (M1) analysis of immunofluorescent micrographs shown in Figure 8. (B) Representative images and (C) Manders' Colocalization analysis of TMEM43 (green) and EEA1 (red) in iPSCs treated with BFA (5 µg/mL) for 2 hr, 4 hr, and 6 hr. Nuclei (Hoechst, blue). Scale bar = 50 µm. (D) Representative images and (E) Manders' Colocalization analysis of Cx43 (green) and Actin (Phalloidin, red) in iPSCs treated with BFA (5 µg/mL) for 2 hr, 4 hr, and 6 hr. Nuclei (Hoechst, blue). Scale bar = 50 µm. Colocalization was determined by the Manders' Coefficient (M1) and the Costes' automatic threshold. Data represents the standard error of the mean of 3 independent experiments. Each experiment measured the colocalization of TMEM43 and EEA1 in 5 separate regions of interest (total of 15 images analyzed). *, $p < 0.05$; **, $p < 0.01$.

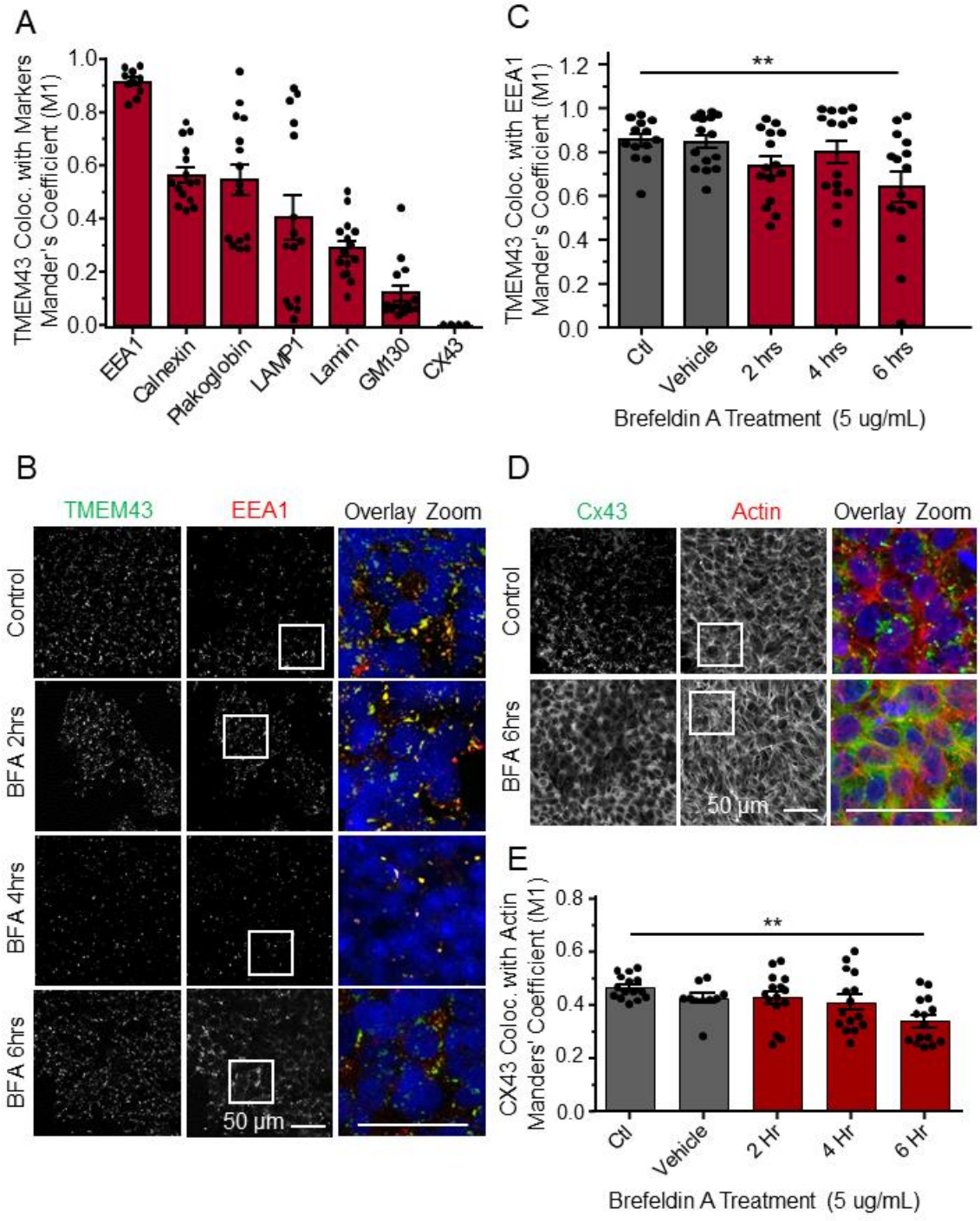
A
TMEM43 Coloc. with Markers
Mander's Coefficient (M1)
1.0
0.8
0.6
0.4
0.2
0.0
EEA1
Calnexin
Plakoglobin
LAMP1
Lamin
GM130
CX43
C
TMEM43 Coloc. with EEA1
Mander's Coefficient (M1)
1.2
1.0
0.8
0.6
0.4
0.2
0.0
**
Ctl
Vehicle
2 hrs
4 hrs
6 hrs
Brefeldin A Treatment (5 ug/mL)
B
TMEM43
EEA1
Overlay Zoom
Control
BFA 2hrs
BFA 4hrs
BFA 6hrs
50 µm
D
Cx43
Actin
Overlay Zoom
Control
BFA 6hrs
50 µm
E
CX43 Coloc. with Actin
Manders' Coefficient (M1)
0.8
0.6
0.4
0.2
0.0
**
Ctl
Vehicle
2 Hr
4 Hr
6 Hr
Brefeldin A Treatment (5 ug/mL)

3.2.2 TMEM43 Trafficking within the Cell

To follow up on our finding of TMEM43 localization with early endosomes, I investigated TMEM43 protein trafficking within the cell. Brefeldin A (BFA) is an antibiotic produced by a species of toxic fungi that inhibits endoplasmic reticulum to Golgi apparatus protein trafficking in eukaryotic cells. Thus, BFA treatment in iPSCs allows us to determine how long TMEM43 occupies the early endosomes without the confounding variable of newly synthesized protein trafficking to the early endosome. BFA treatments ranged from 2 hours to 6 hours. Colocalization analysis showed that TMEM43 localization with EEA1 was significantly decreased after 6 hours of BFA treatment (Figure 9B, C). However, although there was a significant decrease, 63.55 ± 6.918% of TMEM43 remained co-localized with EEA1 even after 6 hours of BFA treatment (Figure 9C). Cx43 was used as a positive control as this protein is known to exhibit rapid turnover at gap junction plaques (Figure 9D, E). The movement of Cx43 localization from the cell surface to the cytoplasm confirms that BFA is inhibiting protein trafficking in iPSCs (Figure 9D, E). These data suggest that TMEM43 trafficking away from the early endosome is relatively slow in undifferentiated iPSCs.

3.3 TMEM43 in iPSC-derived Cardiomyocytes

3.3.1 TMEM43 Localization in iPSC-derived Cardiomyocytes

Although I had determined that TMEM43 resides within the early endosome of undifferentiated iPSCs, numerous reports show that this protein is localized to the nuclear envelope of cardiomyocytes[169,124,125]. Therefore, I sought to determine when in differentiation TMEM43 makes the shift from early endosomes to the nuclear envelope

(Figure 10). Successful differentiation of iPSC-cardiomyocytes (iPSC-CM) was confirmed by staining for the well-known cardiac marker cardiac troponin T (cTnT; Figure 10A). In iPSC-CMs that were in culture for 1 to 2 weeks post first signs of contraction, TMEM43 appeared to form large puncta similar to the staining pattern in iPSCs (Figure 10B). iPSC-CMs are well-known to be immature when compared to adult human heart tissue[170].To address potential differences in cell development stages, I maintained the cardiomyocytes in culture for up to 6 weeks to determine if an extended maturation period would affect TMEM43 localization. Interestingly, four weeks after the onset of contraction (contraction began at approximately day 10 to 12 of the iPSC-CM differentiation protocol), TMEM43 had moved from large puncta within the cytoplasm to the nuclear envelope (Figure 10B). TMEM43 retains this nuclear envelope localization up to 6 weeks and beyond after the onset of contraction (Figure 10B). These findings suggest that iPSC-cardiomyocytes need at least four weeks of maturation *in vitro* to ensure TMEM43 nuclear envelope trafficking within the cell.

3.3.2 Calcium handling in iPSC-derived Cardiomyocytes

Calcium handling is an essential component of cardiomyocyte excitation-contraction coupling and other forms of arrhythmogenic cardiomyopathy exhibit alterations in calcium release. A normal calcium trace in cardiomyocytes should have a rapid increase in calcium signal upon cellular depolarization and contraction, followed by a rapid decrease in calcium signal as calcium is pumped into the sarcoplasmic reticulum and out of the cell. The spike-like pattern should be uniform and consistent without any extra spikes or missed spikes in the calcium signal. The steep increase in signal in the trace is due to the rapid increase in

Figure 10 TMEM43 expression and localization in human iPSC-CMs

(A) Representative immunofluorescent confocal micrographs of cardiac troponin T (red), and nuclei (Hoechst, blue) in iPSC-CMs that have been contracting *in vitro* for 2 weeks. Scale bar = 50 μm. (B) Immunofluorescent confocal micrographs of TMEM43 (green), lamin (red), and nuclei (Hoechst, blue) in iPSC-CMs after 2, 4, and 6 weeks of contraction *in vitro*. Scale bar = 25 μm.

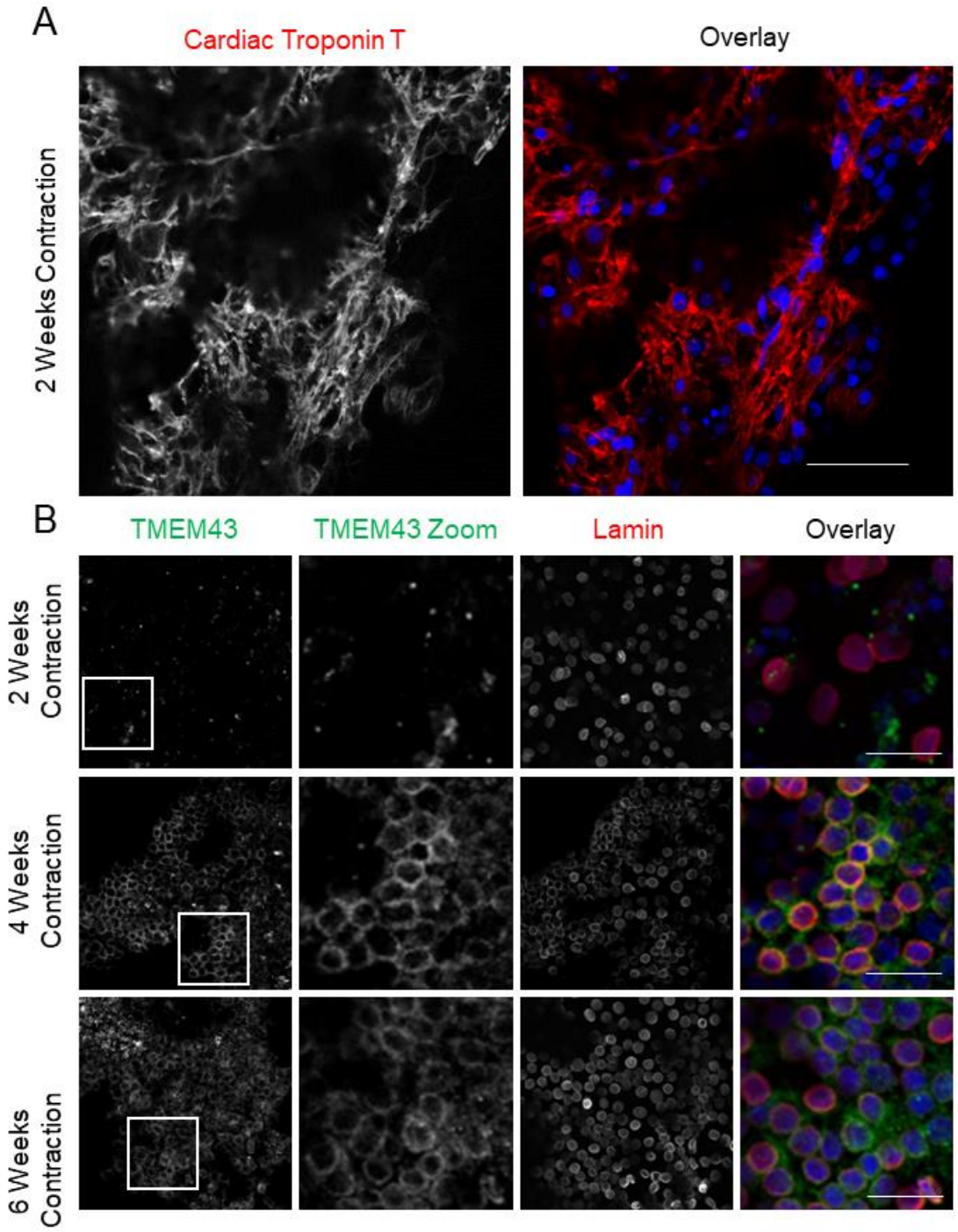
A
Cardiac Troponin T
Overlay
2 Weeks Contraction
B
TMEM43
TMEM43 Zoom
Lamin
Overlay
2 Weeks Contraction
4 Weeks Contraction
6 Weeks Contraction

the intracellular calcium concentration within the cardiomyocyte upon depolarization. The drop in calcium signal is due to the rapid clearance of calcium by SERCA in the sarcoplasmic reticulum and sodium-calcium exchangers in the sarcolemma. Therefore, I examined the calcium transients in contracting WT and *TMEM43-/-* iPSC-CMs using the calcium-sensitive fluorescent dye Fluo-4 AM[7]. iPSC-CMs cultured for four weeks were loaded with Fluo-4 AM, and calcium transients were recorded in the WT and *TMEM43-/-* iPSC-CMs. Figure 11A-D shows representative calcium recordings of contracting WT and *TMEM43-/-* iPSC-CMs under unstimulated and stimulated (1 μM isoproterenol) conditions. In the WT iPSC-CM, baseline recordings displayed uniform contractions with a rate of 25.05 ± 1.51 contractions per minute and maximum fluorescence intensity of 1.436 ± 0.069. After stimulation with isoproterenol, the WT iPSC-CMs contractions per minute were increased to 39.12 ± 2.85 contractions per minute, and the maximum fluorescence intensity was 1.297 ± 0.051. As expected, both genotypes exhibited increased contraction frequency upon isoproterenol stimulation (Figure 11F). However, I observed no significant differences in the contraction rates between WT and *TMEM43-/-* iPSC-CMs (Figure 11E). On the other hand, *TMEM43-/-* iPSC-CMs displayed slightly more abnormal calcium traces at baseline and after stimulation with isoproterenol, with either missing spikes or premature spikes (Figure 11C, D). Blinded grading of the calcium traces revealed that unstimulated *TMEM43-/-* iPSC-CMs exhibited 8.78% more pro-arrhythmic events compared to WT cells, which was exacerbated after treatment with isoproterenol leading to a 15.87% increase in pro-arrhythmic events compared to isoproterenol treated WT iPSCs-CMs. However, the increase in pro-arrhythmic events is not statistically significant (Figure 11G). Although no statistical significance was found using our *TMEM43* knockout model, it

Figure 11 Intracellular calcium handling in WT and *TMEM43-/-* iPSC-CMs

Intracellular calcium transients in (A) unstimulated contracting wild-type iPCS-CMs and (B) after stimulation with 1 μM isoproterenol. (C) Intracellular calcium transients in unstimulated contracting *TMEM43-/-* iPCS-CMs and (D) after stimulation with 1 μM isoproterenol. Data were plotted as the increase in fluorescence intensity (F_1) divided by the basal fluorescence (F_0). (E) Quantification of the maximum fluorescence intensity and (F) contraction frequency of wild-type and *TMEM43-/-* iPCS-CMs while unstimulated or stimulated with isoproterenol (1 μM). (G) Fold change of percentage of abnormal calcium traces of WT and *TMEM43-/-* iPSC-CMs after blinded calcium trace grading. Abnormal calcium traces are defined as having one or more abnormal calcium spikes. Data represented as the mean ± SEM. *, $p < 0.05$, **, $p < 0.01$ ***. $p < 0.001$. $n = 3$.

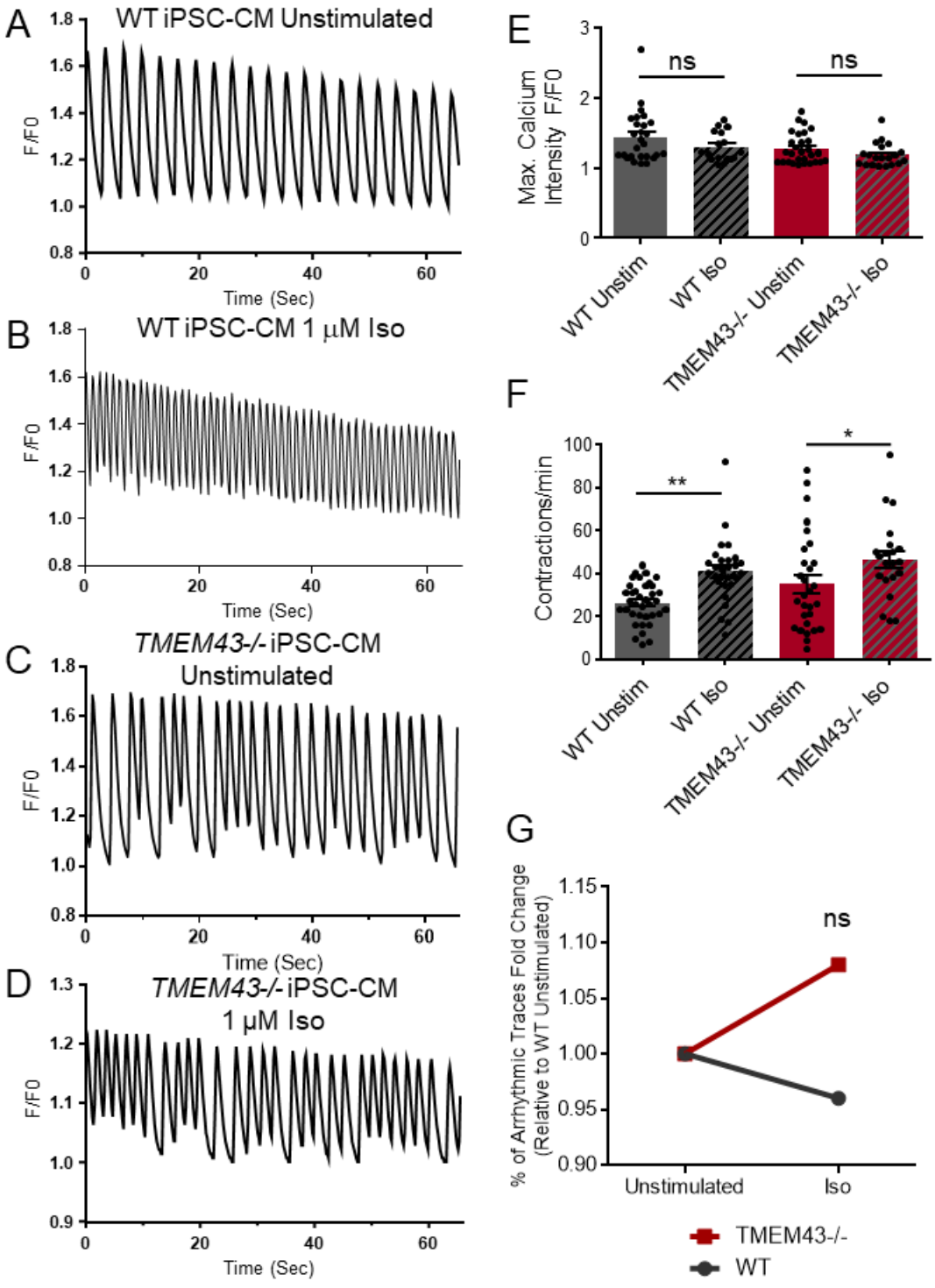
A
WT iPSC-CM Unstimulated
F/F0
Time (Sec)
B
WT iPSC-CM 1 μM Iso
C
TMEM43-/- iPSC-CM
Unstimulated
D
TMEM43-/- iPSC-CM
1 μM Iso
E
Max. Calcium Intensity F/F0
ns
WT Unstim
WT Iso
TMEM43-/- Unstim
TMEM43-/- Iso
F
Contractions/min
**
*
G
% of Arrhythmic Traces Fold Change (Relative to WT Unstimulated)
Unstimulated
Iso
TMEM43-/-
WT

remains to be seen whether the introduction of the mutant TMEM43-S358L protein will perturb iPSC-cardiomyocyte function.

3.4 The Effect of TMEM43 Knockout on Intracellular Organelles

TMEM43 is known to interact with nuclear envelope proteins lamin and emerin, and TMEM43 mutations have been shown to negatively impact multiple organelles, including the nuclear envelope, desmosomes, and gap junctions[171,126]. Therefore, we examined our *TMEM43-/-* iPSC-CMs to determine if any of the above-mentioned organelles were compromised in the absence of TMEM43. iPSC-CMs that had been contracting in culture for four weeks were stained with cTnT, plakoglobin, and lamin to examine sarcomere, desmosome, and nuclear envelop structures, respectively. (Figure 12A, B). In the WT iPSC-CMs, cTnT staining demonstrated that the sarcomeres had aligned Z-discs and were well organized within the cardiomyocytes. The desmosomes were primarily located at the cell edges where cardiomyocytes meet. Lamin staining was observed to tightly outline the nucleus as expected for the nuclear envelope. Immunofluorescence confocal microscopy revealed no apparent abnormalities in the *TMEM43-/-* knockout iPSC-CMs compared to the wild-type cell line. Additionally, the markers for the cellular structures did not appear to be localized to alternate areas of the cell. The desmosomal protein plakoglobin was present along the edges of the cells, and lamin was strictly localized around the nucleus. The Z-discs within the sarcomeres are often an affected area in myocardial diseases. Unorganized Z-discs are a common phenotype, yet the Z-discs within the sarcomeres of the knockout cell line are uniform in spacing and similar to those found in the wild-type

Figure 12 Intracellular organelles in WT and *TMEM43-/-* iPSC-CMs

(A) Immunofluorescent micrographs of WT iPSC-CMs that have been cultured for 4 weeks after the onset of contraction *in vitro*. Images show cardiac troponin T, plakoglobin, and lamin in green and nuclei (Hoechst) in blue. (B) Immunofluorescent micrographs of *TMEM43-/-* iPSC-CMs that have been cultured for 4 weeks post contraction. Images show cardiac troponin T, plakoglobin, and lamin in green and nuclei in blue. n=3. Scale bar = 25 μm.

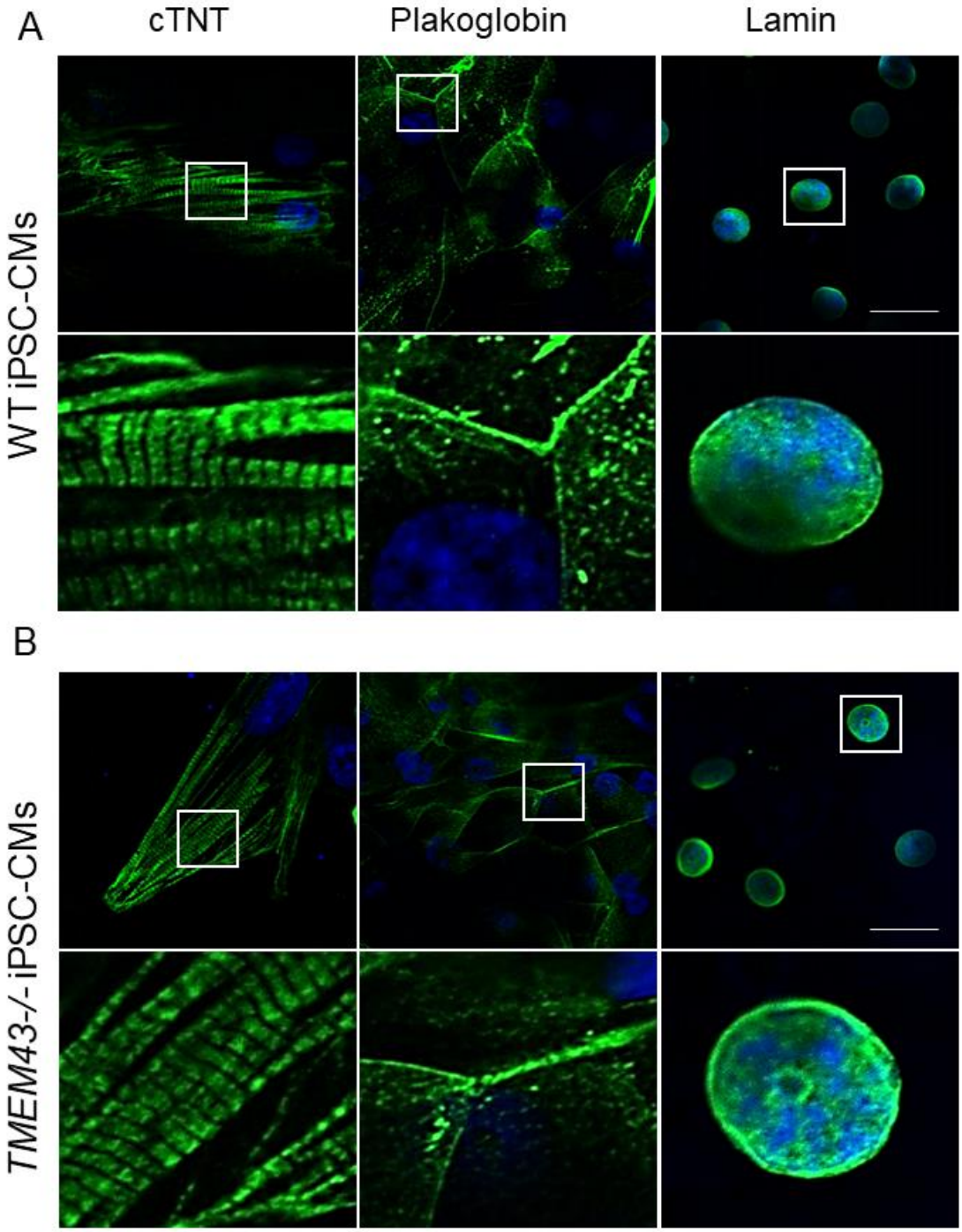
A
cTNT
Plakoglobin
Lamin
WT iPSC-CMs
B
TMEM43-/- iPSC-CMs

cell line. From these findings, knocking out TMEM43 in iPSC-CMs does not appear to negatively affect the organization of important cardiac structures within the cell.

3.5 ARVC patient-derived Fibroblast Gene Expression

Fibrosis is a hallmark feature of ARVC that causes problems such as decreased electrical conductivity of the myocardium and increased rate of re-entry arrhythmias[172]. Since the fibroblast's primary function is maintaining the extracellular matrix and producing scar tissue, it would be useful to know if ARVC fibroblasts have any differentially expressed genes. Human fibroblasts were derived from male and female ARVC patients with varying levels of disease severity. All experiments were blinded to sex and disease severity. mRNA levels of *TMEM43*, *GJA1* (Cx43), *JUP* (plakoglobin), *LMNA* (lamin), and the extracellular matrix (ECM) associated proteins *MMP1* (matrix metalloprotease-1), *ITGA5* (integrin α5), *ITGB1* (integrin β1), *COL1A1* (collagen-1), and *LAMA1* (laminin) were measured to elucidate any differences between the fibroblast cell lines.

The cell lines that were used in this study included an ARVC5 affected male (ARVC#1) and their unaffected brother (CNTRL#1), an affected male (ARVC#4), affected females (ARVC#2 and ARVC#3), and two control fibroblast cell lines (CNTRL#2 – Female, CNTRL#3 – Male). Fibroblast cell lines ARVC#2, ARVC#3, and ARVC#4 were paired with the control cell lines. The identity of the ARVC cell lines were unknown throughout the study so to ensure control cell lines were paired with all ARVC fibroblasts CNTRL#2 and CNTRL#3 were included in all experiments.

I first investigated if there were any changes in mRNA expression in *TMEM43* in control and ARVC patient primary fibroblasts. ARVC#1 (affected male) displayed a significant decrease in *TMEM43,* while the other affected male, ARVC#4, showed an increase in *TMEM43* mRNA compared to the male control cell line (Figure 13A, B). Similarly, *TMEM43* expression was significantly increased in the two ARVC female patient cell lines, ARVC#2 and ARVC#3, compared to the female control (Figure 13C). Overall, there was a trend of increased *TMEM43* gene expression in the majority of ARVC samples apart from ARVC#1.

Next, I sought to determine whether ARVC patient fibroblasts exhibited any differences in nuclear envelope or intercalated disc gene expression. *GJA1* (Cx43) or *LMNA* (lamin) expression was not significantly altered in the examined ARVC patient fibroblasts compared to control (Figure 13D, E, F, G). On the other hand, ARVC#1 had a significant increase in *JUP* (plakoglobin) compared to CNTL#1 (Figure 13H). Knowing that fibroblasts play an essential role in maintaining the extracellular matrix, I investigated the gene expression of ECM-related genes *MMP1* [matrix metalloprotease-1 (MMP-1)], *ITGA5* (integrin α5), *ITGB1* (integrin β1), *COL1A1* (collagen-1), and *LAMA1* (laminin) for any changes in expression at the mRNA level. MMP-1 showed no significant changes between ARVC#1 and CNTRL#1 (Figure 14A); however, there was a significant decrease in MMP-1 expression in the male (ARVC#4) and female (ARVC#2 and ARVC#3) ARVC cell lines compared to the control male and female cell lines (Figure 14B, C). Integrin α5 expression in CNTRL#1 and ARVC#1 was also not changed, while expression in ARVC#4, ARVC#2, and ARVC#3 were higher than their respective controls (Figure 14D,

Figure 13 mRNA expression of ARVC patient fibroblasts

qPCR analysis demonstrating mRNA levels of *TMEM43* (A, B, C), *GJA1* (Cx43; D, E, F), *LMNA* (lamin; G), and *JUP* (plakoglobin; H) in patient-derived fibroblast cell lines ARVC#1 (affected male), CNTRL#1 (unaffected brother of ARVC#1), ARVC#2 (mildly affected female), ARVC#3 (mildly affected female), and ARVC#4 (mildly affected male). Control fibroblast cell lines were cell lines CNTRL#2 (female) and CNTRL#3 (male). Data were presented as the mean ± SEM. *, $p < 0.05$; **, $p < 0.01$; ***, $p < 0.001$;. $n = 5$. Statistical significance was determined using unpaired two-tailed t-test (A, B, D, E, G, H) and one-way ANOVA with Tukey's multiple comparisons test (C, F).

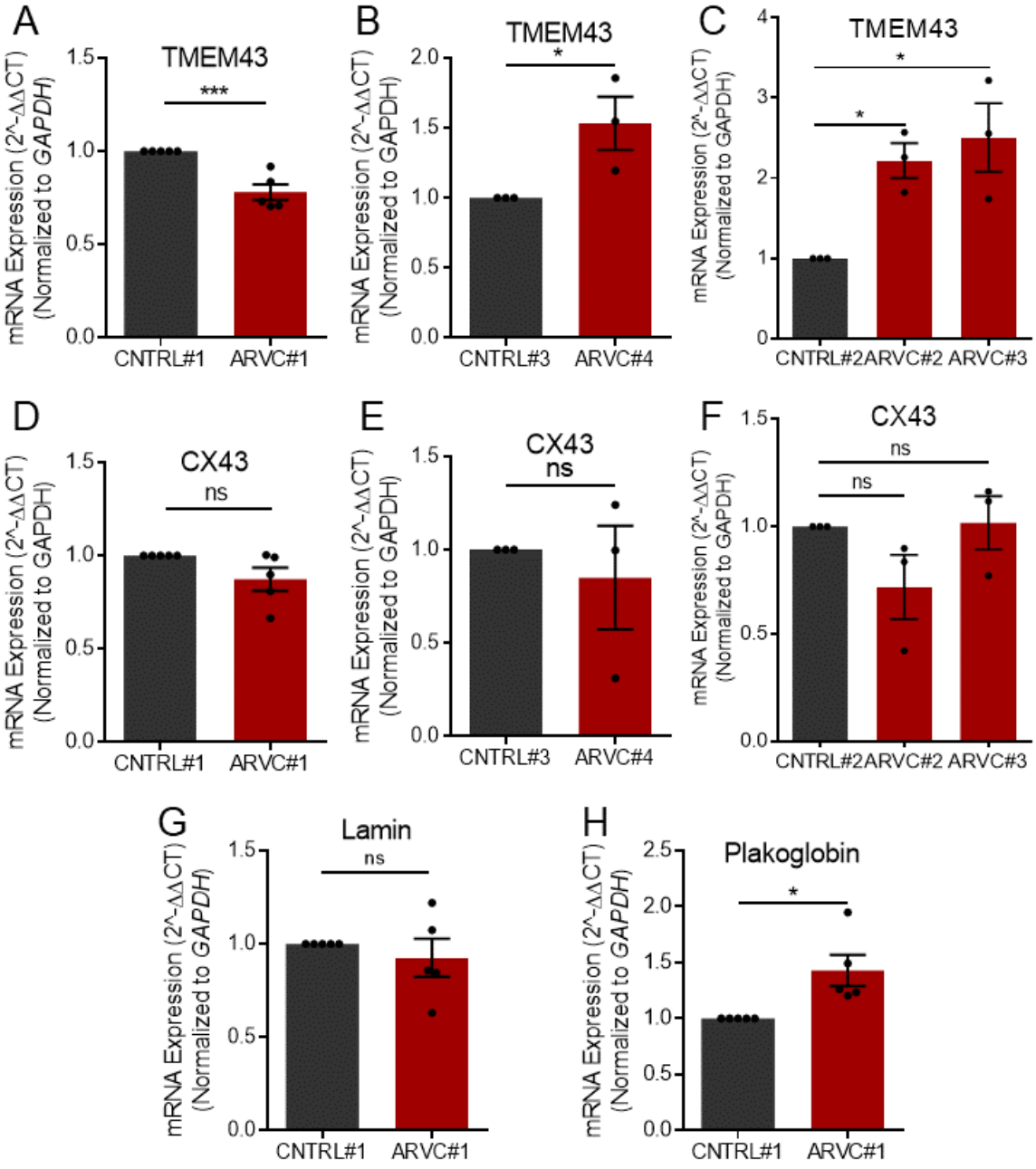
A
TMEM43
***
mRNA Expression (2^-ΔΔCT)
(Normalized to GAPDH)
1.5
1.0
0.5
0.0
CNTRL#1
ARVC#1
B
TMEM43
*
mRNA Expression (2^-ΔΔCT)
(Normalized to GAPDH)
2.0
1.5
1.0
0.5
0.0
CNTRL#3
ARVC#4
C
TMEM43
*
*
mRNA Expression (2^-ΔΔCT)
(Normalized to GAPDH)
4
3
2
1
0
CNTRL#2
ARVC#2
ARVC#3
D
CX43
ns
mRNA Expression (2^-ΔΔCT)
(Normalized to GAPDH)
1.5
1.0
0.5
0.0
CNTRL#1
ARVC#1
E
CX43
ns
mRNA Expression (2^-ΔΔCT)
(Normalized to GAPDH)
1.5
1.0
0.5
0.0
CNTRL#3
ARVC#4
F
CX43
ns
ns
mRNA Expression (2^-ΔΔCT)
(Normalized to GAPDH)
1.5
1.0
0.5
0.0
CNTRL#2
ARVC#2
ARVC#3
G
Lamin
ns
mRNA Expression (2^-ΔΔCT)
(Normalized to GAPDH)
1.5
1.0
0.5
0.0
CNTRL#1
ARVC#1
H
Plakoglobin
*
mRNA Expression (2^-ΔΔCT)
(Normalized to GAPDH)
2.5
2.0
1.5
1.0
0.5
0.0
CNTRL#1
ARVC#1

E, F). Integrin β1 was significantly changed in all fibroblasts that were tested. Integrin β1 was decreased in ARVC#1 compared to CNTRL#1. In contrast to ARVC#1, integrin β1 was significantly increased in ARVC#4, ARVC#2, and ARVC#3 (Figure 14G, H, I). The collagen-1 qPCR data showed a similar theme seen in the integrin β1 data as the ARVC#1 had a significantly lower amount of collagen-1 mRNA while ARVC#4, ARVC#2, and ARVC#3 all had increased levels of collagen-1 compared to the controls (Figure 14J, K, L). Finally, ARVC#1 did not have significantly different mRNA expression of laminin compared to CNTRL#1. Compared to the male and female control cell lines, Laminin mRNA was significantly lower in ARVC#4, ARVC#2, and ARVC#3 (Figure 14M, N, O). These data demonstrate significant changes in mRNA expression of ECM-related genes between control and affected fibroblasts.

In addition to comparing the individual ARVC5 fibroblasts to the control cell lines, all ARVC cell lines were grouped to determine if individual or sex variation contributes to the data's significance. Furthermore, CNTRL#1, CNTRL #2, and CNTRL#3 were plotted together to examine if there were any differences between the male ARVC5 control, the generic male control, and generic female control. mRNA expression of TMEM43 when all ARVC cell lines were grouped was not significantly different from the controls. (Figure 15A). Cx43 showed no significant differences when the ARVC cell lines were combined Figure 15B). When the ARVC cell lines were pooled, mRNA expression of MMP-1 and integrin α5 were significantly different than the control. MMP-1 was decreased in ARVC cell lines, while integrin α5 was increased (Figure 15C, D). Integrin β1, collagen-1, and lamin were not significantly changed (Figure 15E, F, G). Interestingly, the expression of

Figure 14 ECM-associated protein mRNA expression in ARVC patient fibroblasts

qPCR analysis demonstrating mRNA levels of extracellular matrix proteins *MMP1* (matrix metalloprotease-1; A, B, C), *ITGA5* (integrin α5; D, E, F), *ITGB1* (integrin β1; G, H, I), *COL1A1* (collagen-1; J, K, L), and *LAMA1* (laminin; M, N, O) in patient-derived fibroblast cell lines ARVC#1 (affected male), CNTRL#1 (unaffected brother of ARVC#1), ARVC#2 (mildly affected female), ARVC#3 (mildly affected female), and ARVC#4 (mildly affected male). Control fibroblast cell lines were cell lines CNTRL#2 (female) and CNTRL#3 (male). Data were presented as the mean ± SEM. *, $p < 0.05$; **, $p < 0.01$; ***, $p < 0.001$; ****, $p < 0.0001$. $n = 5$. Statistical significance was determined using unpaired two-tailed t-test and one-way ANOVA with Tukey's multiple comparisons test (C, F, I, L, O).

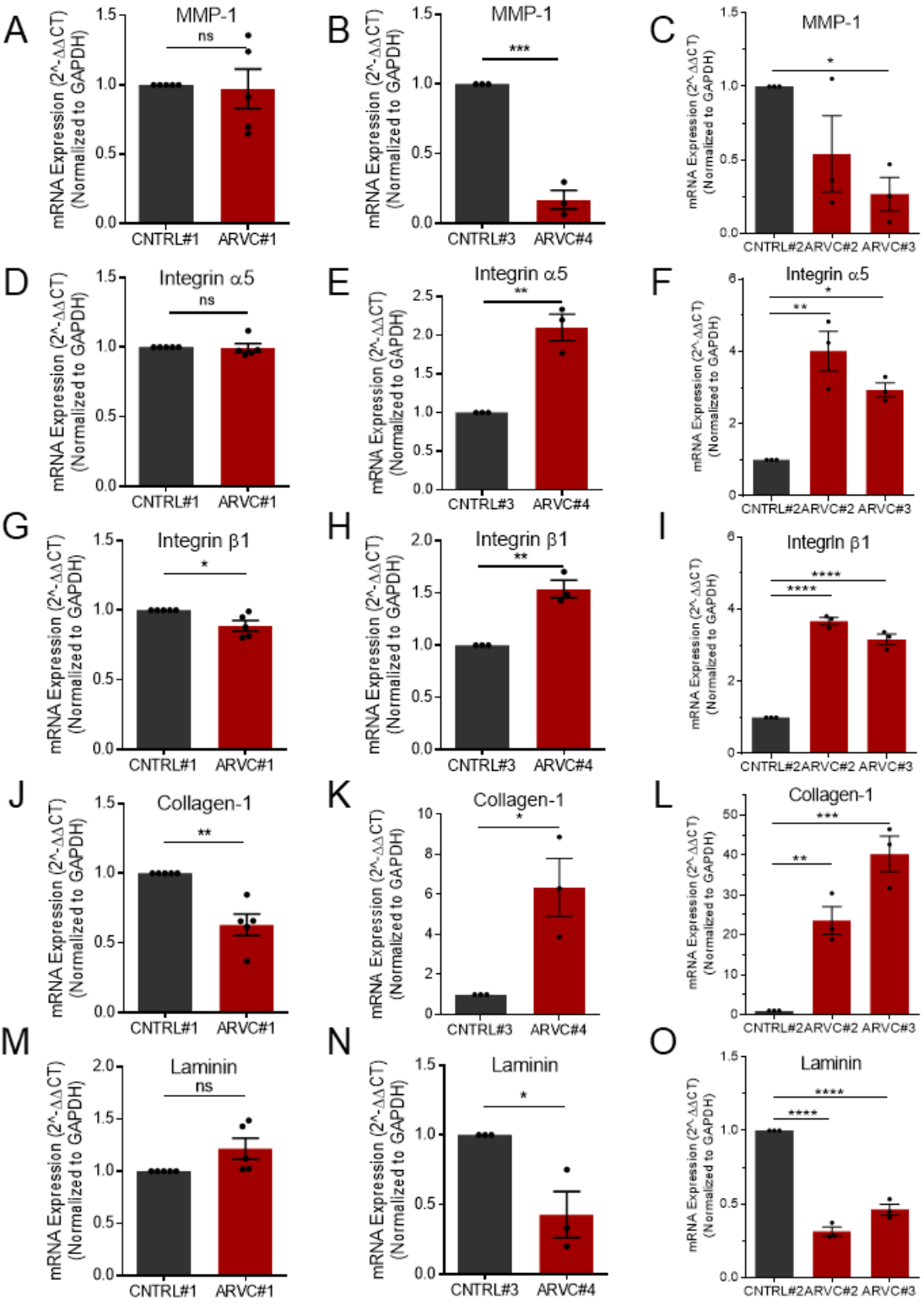
A
MMP-1
ns
mRNA Expression (2^-ΔΔCT) (Normalized to GAPDH)
CNTRL#1
ARVC#1
B
MMP-1
***
CNTRL#3
ARVC#4
C
MMP-1
*
CNTRL#2
ARVC#2
ARVC#3
D
Integrin α5
ns
E
Integrin α5
**
F
Integrin α5
*
**
G
Integrin β1
*
H
Integrin β1
**
I
Integrin β1
****
****
J
Collagen-1
**
K
Collagen-1
*
L
Collagen-1
***
**
M
Laminin
ns
N
Laminin
*
O
Laminin
****
****

Figure 15 mRNA expression of ARVC and control fibroblasts when grouped

qPCR analysis demonstrating mRNA levels of *TMEM43* (A), *GJA1* (Cx43; B) *MMP1* (matrix metalloprotease-1; C), *ITGA5* (integrin α5; D), *ITGB1* (integrin β1; E), *COL1A1* (collagen-1; F), and *LAMA1* (laminin; G) with patient-derived fibroblast cell lines ARVC#1 (blue square, affected male), ARVC#2 (pink triangle, mildly affected female), ARVC#3 (pink diamond, mildly affected female), and ARVC#4 (blue circle, mildly affected male) data combined. Control fibroblast cell lines were cell lines CNTRL#1 (blue square, unaffected brother of ARVC#1), CNTRL#2 (pink triangle, female), and CNTRL#3 (blue circle male) were combined. Data were presented as the mean ± SEM. *, $p < 0.05$; **, $p < 0.01$. n = 3-5. Statistical significance was determined using unpaired two-tailed t-test.

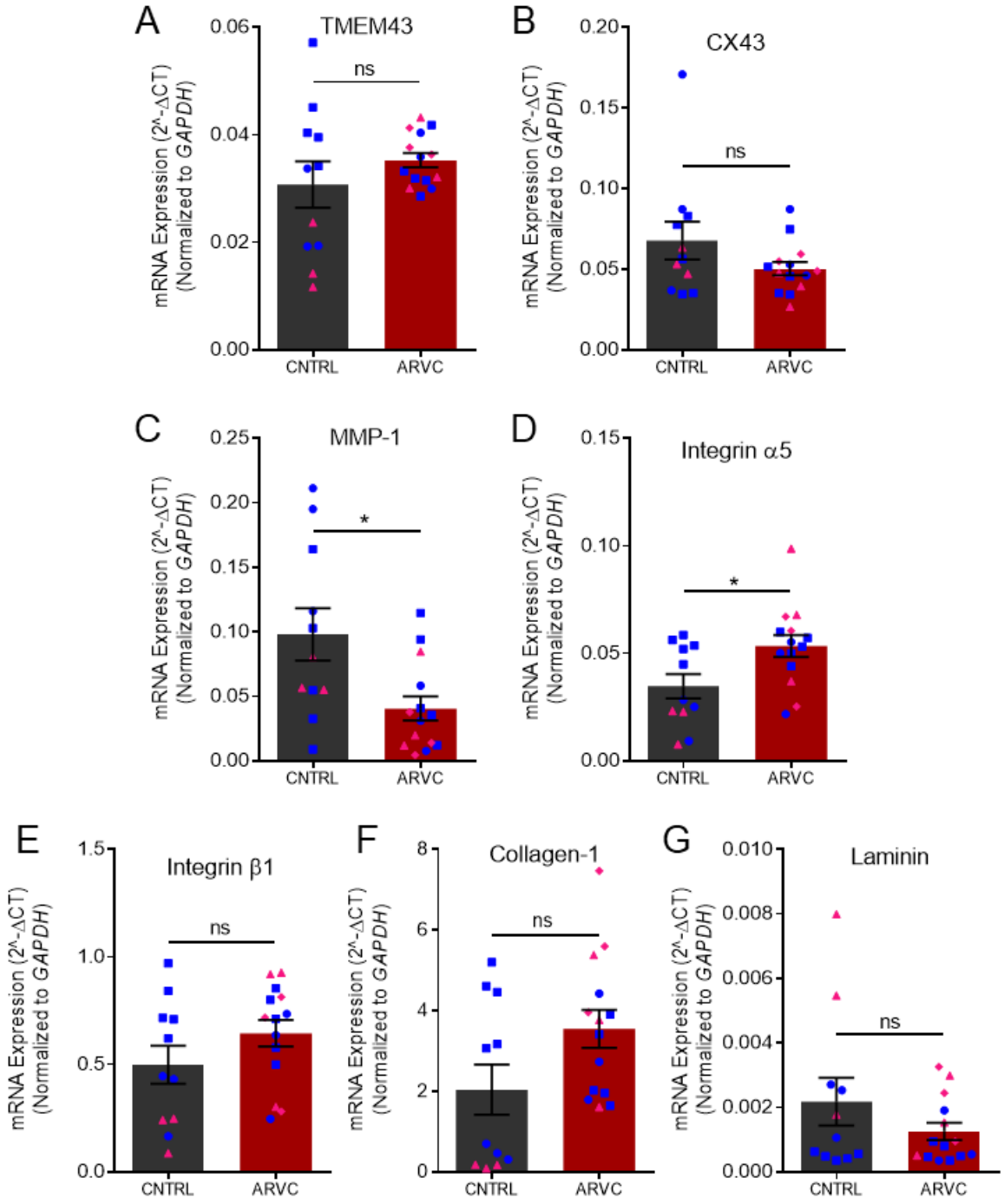
A
TMEM43
ns
mRNA Expression (2^-ΔCT)
(Normalized to GAPDH)
0.06
0.04
0.02
0.00
CNTRL
ARVC
B
CX43
ns
0.20
0.15
0.10
0.05
0.00
C
MMP-1
*
0.25
0.20
0.15
0.10
0.05
0.00
D
Integrin α5
*
0.15
0.10
0.05
0.00
E
Integrin β1
ns
1.5
1.0
0.5
0.0
F
Collagen-1
ns
8
6
4
2
0
G
Laminin
ns
0.010
0.008
0.006
0.004
0.002
0.000

TMEM43 in CNTRL#1 was significantly different than CNTRL#2 and CNTRL#3. CNTRL#2 and CNTRL#3 displayed lower levels of TMEM43 mRNA compared to CNTRL#1 (Figure 16A). Cx43 and MMP-1 mRNA expression was not significantly different between CNTRL#1, CNTRL#2, and CNTRL#3 (Figure 16B, C). Integrin α5, integrin β1, and collagen-1 had decreased mRNA levels in CNTRL#2 and CNTRL#3 compared to CNTRL#1 (Figure 16D, E, F). Finally, laminin mRNA was significantly higher in CNTRL#2 compared to CNTRL#1 (Figure 16G). Overall, the differences in expression of the extracellular matrix proteins may play a role in the fibrosis phenotype of ARVC. These data suggest that there could be dysregulation of specific genes in ARVC patient fibroblasts, which may play a part in disease progression and phenotype.

Figure 16 Comparison of mRNA expression in control fibroblasts cell lines

qPCR analysis demonstrating mRNA levels of *TMEM43* (A), *GJA1* (Cx43; B) *MMP1* (matrix metalloprotease-1; C), *ITGA5* (integrin α5; D), *ITGB1* (integrin β1; E), *COL1A1* (collagen-1; F), and *LAMA1* (laminin; G) in patient-derived fibroblast cell line CNTRL#1 (unaffected brother of ARVC#1) and commercial control fibroblast cell lines CNTRL#2 (female) and (CNTRL#3 (male). Data were presented as the mean ± SEM. *, $p < 0.05$; **, $p < 0.01$***, $p < 0.001$; ****, $p < 0.0001$. n = 3-5. Statistical significance was determined using one-way ANOVA with Tukey's multiple comparisons test.

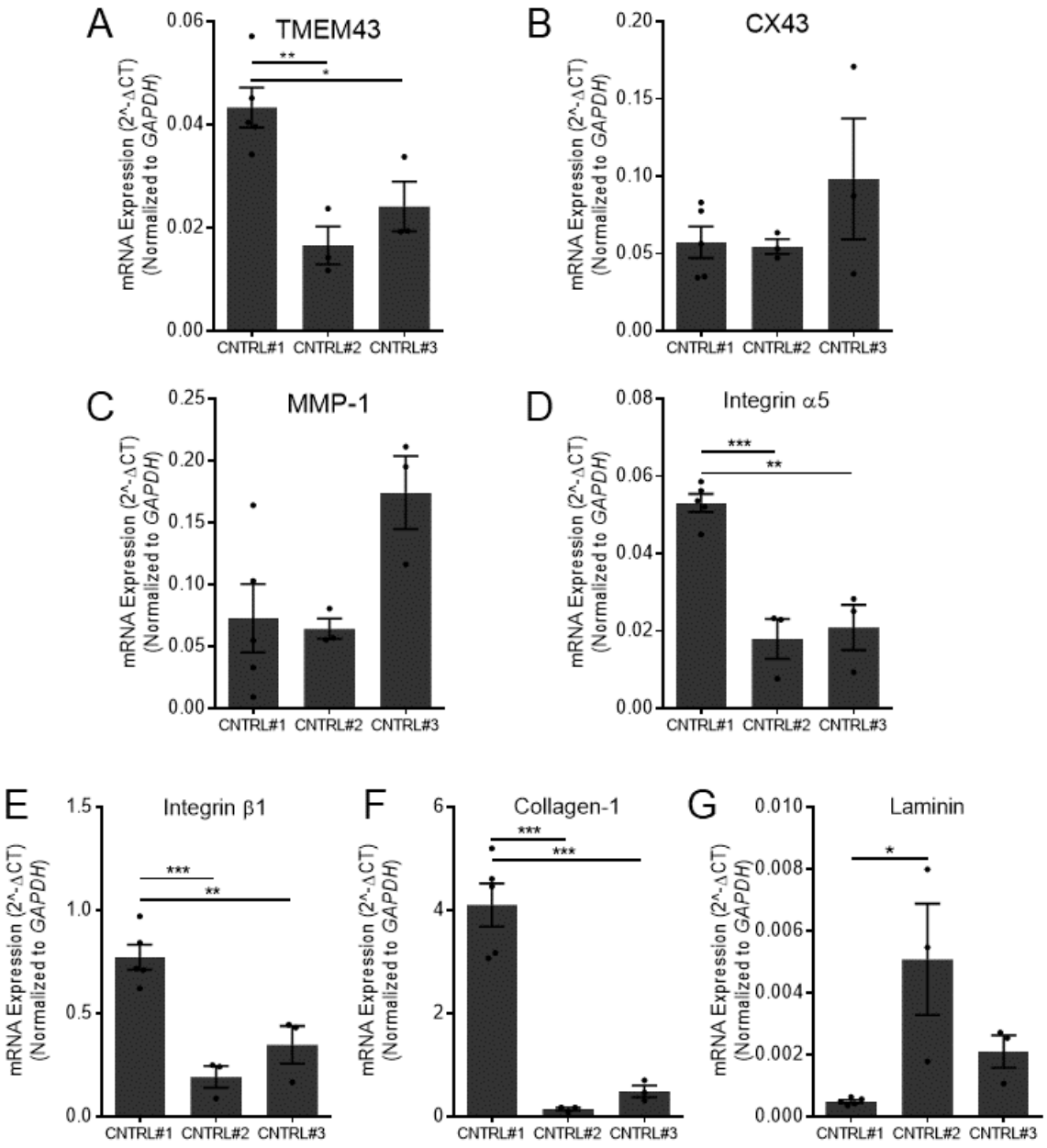
A
TMEM43
mRNA Expression (2^-ΔCT) (Normalized to GAPDH)
0.06
0.04
0.02
0.00
**
*
CNTRL#1 CNTRL#2 CNTRL#3
B
CX43
0.20
0.15
0.10
0.05
0.00
C
MMP-1
0.25
0.20
0.15
0.10
0.05
0.00
D
Integrin α5
0.08
0.06
0.04
0.02
0.00
***
**
E
Integrin β1
1.5
1.0
0.5
0.0
***
**
F
Collagen-1
6
4
2
0
***
***
G
Laminin
0.010
0.008
0.006
0.004
0.002
0.000
*

4 Discussion

In this study, I examined the expression, localization, and trafficking of wild-type TMEM43 protein in undifferentiated iPSCs and at specific time points during cardiomyocyte differentiation. Using *TMEM43* CRISPR-Cas9 knockout iPSCs, I investigated how TMEM43 influences cardiomyocyte differentiation and calcium handling in human iPSC-CMs. Finally, I explored if extracellular matrix protein gene expression was altered in ARVC patient primary dermal fibroblasts compared to unaffected controls.

4.1 TMEM43 is not Essential for iPSC Growth or Differentiation

This study took advantage of CRISPR-Cas9 gene editing to study the effects of knocking out *TMEM43* in human iPSCs. *TMEM43-/-* iPSCs are viable in culture and exhibit similar morphology to wild-type iPSCs, including growing as colonies of tightly packed cells with a small cytoplasmic to nuclear ratio and limited amounts of spontaneous differentiation or death. *TMEM43-/-* iPSCs successfully differentiated into cardiomyocytes and closely mimicked the differentiation timeline of the wild-type iPSCs. These findings are not surprising given that *TMEM43-/-* mice matured to adulthood without developmental issues, and human patients with the TMEM43-S358L mutation do not usually manifest cardiac symptoms until adulthood[125,117].

4.2 TMEM43 is Localized in Early Endosomes in iPSCs

The cellular localization of TMEM43 is debated in the literature. TMEM43 has been reported to reside in cellular compartments such as the nuclear envelope[119,120], endoplasmic reticulum[118,121], and adherens junctions[122]. This variability across studies could be

attributed to a number of different factors, including overexpression systems versus endogenous expression, species differences, or different cell or tissue types. To date, no one has examined endogenous TMEM43 protein expression or localization in human iPSCs. To our surprise, I found a large proportion of TMEM43 protein colocalizing with EEA1, a marker for early endosomes. This study is the first time TMEM43 has been reported to localize within early endosomes in any cell or tissue type. As the early endosome is primarily a sorting center for membrane-bound molecules from the plasma membrane and the Golgi apparatus, it is unclear why or how TMEM43 came to reside in this compartment[173]. There have been reports of cell surface proteins being translocated to the nuclear envelope[174,175], some of which through "nuclear envelope-associated endosomes"[176,177]; however, the pathway is poorly understood, and the function of many cell surface proteins in the nucleus is not known either. It is unlikely TMEM43 is ever located in the cell membrane in our iPSCs, as I saw little evidence of TMEM43 colocalization with actin or surface structures such as gap junctions, or desmosomes (Figure 8, 9A). Additionally, it is unclear if the TMEM43-positive endosomes are associated with the nuclear envelope. iPSCs have very little cytoplasmic space, making organelles appear as though they are in close proximity to one another. It is possible that TMEM43 could be housed in the early endosomes while the cells are still in a pluripotent state and will only be directed to another organelle once the iPSCs begin lineage specification.

In addition to discovering that TMEM43 colocalizes with early endosomes, I demonstrated that TMEM43 resides within the endosomes for approximately 6 hours before TMEM43 levels begin to decrease (Figure 9B, C). Despite this significant reduction

in early endosome occupation, 74% of TMEM43 protein remained colocalized with the early endosomes after 6 hours of BFA treatment. The decrease in TMEM43 localization with EEA1 could be due to TMEM43 protein degradation or by TMEM43 trafficking out of the endosome to an alternate intracellular location. The latter may be a more plausible explanation for why I see a decrease in localization after six hours because the Esseltine laboratory has demonstrated that TMEM43 is stable in the cell for greater than eight hours[178]. Degradation after six hours seems unlikely when TMEM43 expression levels remain unchanged for more than eight hours. The effect of BFA on other cellular proteins must be considered when discussing TMEM43 trafficking out of early endosomes. It is unknown what proteins are involved in TMEM43 trafficking. Therefore, I cannot fully determine the effect BFA has on TMEM43 trafficking. It is currently unknown where TMEM43 is trafficked to after leaving the early endosomes. Early endosomes generally transition into either late endosomes or recycling endosomes. The late endosomes would be a likely candidate if TMEM43 were destined for degradation within the lysosomal compartment. I did see some TMEM43 localization within LAMP1-positive lysosomal compartment, but again with a half-life of greater than 8 hours, it is likely that TMEM43 is trafficked to other cellular compartments. Ras-like proteins in brain (Rab) proteins are a family of small GTPases that regulate anterograde and retrograde endosomal transport throughout the cell[179] and could play a role in TMEM43 trafficking. Future studies will uncover whether TMEM43 transitions from early endosomes (Rab5)[180] toward recycling endosomes (Rabs 4, 11)[181,182], late endosomes (Rabs 7, 9)[183,184], or some other endosomal pathway.

4.3 TMEM43 Trafficking to the Nuclear Envelope in iPSC-CMs

TMEM43 has been widely reported to localize to the nuclear envelope in human and rodent cardiac tissue[169,124,125]. iPSC-CMs begin to contract in culture after approximately 14 days of differentiation. Interestingly, I discovered that TMEM43 remained localized to early endosomes in these early contracting iPSC-CMs rather than the nuclear envelope as I had anticipated. iPSC-CMs are known to be immature and resemble fetal cardiomyocytes rather than adult cardiomyocytes[144]. Knowing this, I allowed the iPSC-CMs to mature *in vitro* for six weeks after the iPSC-CMs were differentiated and contracting to determine if there was any change in TMEM43 localization in more mature cardiomyocytes. Indeed, I observed a transition to the nuclear envelope approximately four weeks after the iPSC-CMs were differentiated and contracting. The late movement of TMEM43 suggests that TMEM43 trafficking may be influenced by the maturation of the cardiomyocytes *in vitro*. Early contracting iPSC-CMs may not express the correct genes to direct TMEM43 to the nuclear envelope, or post-translational modification may influence when TMEM43 migrates to the nuclear envelope. There are several other cardiomyocyte maturation protocols, including applying mechanical strain, metabolic maturation protocols, and incorporating iPSC-CMs into 3-dimensional engineered heart tissue[185]. It would be interesting in the future to discover whether these maturation techniques encourage TMEM43 to traffic to the nuclear envelope of iPSC-CMs.

This delayed transport could potentially have implications for ARVC. In mice harboring the TMEM43-S358L mutation, a significant increase in serum cardiac troponin I levels was detected when the mice were five weeks old, indicating cardiomyocyte

necrosis[124]. It is likely that the detrimental effects of the TMEM43-S358L mutation on cardiomyocytes only begin once TMEM43 fully traffics to the nuclear envelope. Future studies examining cell death markers such as cleaved caspase 3 will shed light on whether *TMEM43-/-* or ARVC patient iPSC-CMs undergo apoptosis.

4.4 Altered Calcium Handling in *TMEM43-/-* iPSC-CMs

Life-threatening ventricular arrhythmias are a hallmark of ARVC. One pathway in which arrhythmias can occur is through dysregulation of calcium within the working myocardium. There is little literature on the effects of knocking out TMEM43 on calcium handling in human iPSC-CMs. Padron-Barth *et al.* 2019 demonstrated that iPSC-CMs expressing TMEM43-S358L exhibited dysregulated calcium; however, they did not investigate how knocking out the protein would affect calcium handling[124]. Therefore, I investigated *TMEM43-/-* iPSC-CMs to determine if this genotype would recapitulate the disease phenotype. I accomplished this by measuring the calcium handling dynamics of the *TMEM43-/-* iPSC-CMs. The relationship between intracellular calcium concentration and contraction (discussed in section 1.3.1) allows us to track the cells' contraction rhythm and frequency. I found that *TMEM43-/-* iPSC-CMs exhibited slightly more abnormal calcium traces compared to wild type, which was exacerbated with application of the β-adrenergic receptor agonist, isoproterenol. Importantly, although there was a subtle perturbation in calcium handling, these results did not reach significance. This data suggests that the loss of TMEM43 is not entirely responsible for cardiomyocyte calcium dysregulation. It has been reported in other disease models that the presence of a mutated protein can be more detrimental to cell physiology than simple gene knockout[186]. Based on our findings using

TMEM43 knockout iPSC-CMs, I expect that the TMEM43-S358L mutant protein in ARVC patient cells may function abnormally, causing severe calcium disturbances. Ongoing studies in the Esseltine laboratory are investigating this very issue using ARVC patient iPSC-CMs.

Exercise and increased heart rate are connected with sudden cardiac death in patients with ARVC[187]. This risk is so great that children in NL with the TMEM43-S358L mutation are restricted from engaging in competitive sports, even though the disease does not usually manifest until early adulthood[130]. Epinephrine is a catecholamine released during exercise and binds to α-adrenergic and β-adrenergic receptors, leading to increased heart rate and increased contraction force. Isoproterenol stimulation of dilated cardiomyopathy patient-derived iPSC-CMs showed a dampening of β-adrenergic signaling and an increased expression of phosphodiesterases (PDE) 2A and PDE3A[151]. Additionally, integrin β1D-/- mouse cardiomyocytes stimulated with isoproterenol were shown to be more susceptible to calcium-dependent arrhythmogenesis[188]. In our study, isoproterenol was used to stimulate the iPSC-CMs to study how activation of the β-adrenergic receptor would affect calcium handling in *TMEM43-/-* iPSC-CMs. Our calcium imaging demonstrates that TMEM43 may have a small role in calcium handling, contraction-coupling, and pro-arrhythmic risk within our iPSC-CMs. The results from this study are not as prominent as other iPSC-CM studies. This could be the result of many factors. For example, the iPSC-CM cell line used in this study was derived from female somatic cells. There is a known sex difference between males and females with ARVC. Males commonly have a more severe ARVC phenotype. Therefore, a female iPSC-CM cell line could display a milder phenotype than a male cell

line. The genetic mutation could play a role in the mild phenotype. ARVC patients have the TMEM43-S358L mutated version of the protein, which could be more pathogenic than a complete knockout model. Finally, patient-specific cell lines encompass the genetic background of the patients, for which the iPSC model used here does not account. It will be interesting to see how the TMEM43-S358L mutant affects calcium handling and contraction coupling in ARVC patient-derived iPSC-CMs. Early evidence from the Esseltine laboratory indicates that male ARVC patient iPSC-CMs exhibit significantly higher contraction rates and dramatically more pro-arrhythmic traces compared to unaffected sibling control (Noort and Esseltine, unpublished). Although the protein structure has not been resolved, *in silico* modeling suggests that TMEM43 oligomerizes[124]. Potential interactions between wild-type and mutant TMEM43 proteins may prove to be more arrhythmogenic than no protein at all. The TMEM43-S358L mutant could influence cardiomyocytes' gene regulation or signaling pathways, which could increase arrhythmogenicity.

4.5 Intracellular Localization of Key Proteins in Cardiac Function is Unchanged after Knocking out TMEM43

TMEM43 is known to have protein interacting partners such as lamin and emerin[125]. TMEM43 was found to be important in the positioning of chromatin in one study, which may lead to altered chromatin distribution and gene expression in *TMEM43*-/- cardiomyocytes[118]. A TMEM43-S358L expressing HL-1 cardiac cell line showed a redistribution of desmosomal proteins plakoglobin and α-catenin into the cytoplasm and altered phosphorylation states Cx43, leading to reduced conduction velocity[171]. Since there

was a slight increase in abnormal calcium handling events in our iPSC-CMs, I decided to look at important cardiac structures to see if there were any apparent structural defects in the *TMEM43-/-* iPSC-CMs. Using specific antibodies for plakoglobin, cardiac troponin T, and lamin A/C, I could not find any structural differences in the desmosomes, sarcomeres, or nuclear envelope between the wild-type and *TMEM43-/-* cardiomyocytes. These findings should be followed up with additional experiments since the effects of *TMEM43-/-* may not be detectable by immunofluorescence staining of one protein. There are many different proteins that make up the structures studied. Looking at just one does not warrant the conclusion that knocking out TMEM43 does not affect them. As mentioned previously, the expression of the TMEM43-S358L mutant protein may be more harmful to the cell's cardiac structures. Further studies will fully elucidate the consequences of mutating or knocking out TMEM43 by characterizing additional proteins in the mentioned organelles.

4.6 ARVC patient-derived Fibroblasts show Differential Gene Expression

Fibrofatty invasion of the myocardium in ARVC patients' hearts results in a build-up of fat and scar tissue in the muscle and results in a weakening and decreased conductivity of the myocardium. A large contributor to fibrosis in ARVC is the resident epicardial fibroblasts responsible for producing and maintaining the extracellular matrix (ECM) that provides structure and strength to the cardiomyocytes[189]. Collagen-1 and laminin are two major ECM proteins produced by fibroblasts while cardiac ECM-interacting/modifying proteins include MMP-1, α-integrin, and β-integrin[190].

Our laboratory recently isolated dermal fibroblasts from ARVC patient skin biopsies. Although epicardial fibroblasts are obviously different from dermal fibroblasts, important

information can still be gathered using these primary patient cells. Using these primary patient cells, I examined the gene expression of TMEM43 as well as several key proteins previously identified to be impacted by TMEM43 mutations. My results were not consistent among the different groups tested. For example, while one ARVC patient exhibited a decrease in TMEM43 expression, the other three examined patients all demonstrated a significant increase in TMEM43 expression compared to the control. I secured unaffected sibling controls for several of our ARVC patients; however, I had not secured sibling controls for all ARVC patient fibroblasts at the time of examination. For these fibroblasts, I used commercially available primary dermal fibroblasts from middle-aged male or female Caucasian donors with no known disease. Therefore, the differences in gene expression could be a consequence of comparing some patient cells to the commercially available fibroblast cell lines while others were compared directly to an unaffected family member of the ARVC patient. The genetic background of the unaffected family member could play a role in the level of TMEM43 mRNA in the control compared to the control cell line with no genetic connections to ARVC. When the control cell lines were directly compared in figure 16, it was clear that there were differences in TMEM43 expression. Significantly different expression levels of integrin α5, integrin β1, collagen-1, and laminin mRNA were observed between the ARVC control and the commercially available control cell lines. This data highlights the importance of the genetic background of cell lines used. Additionally, the differences in gene expression between an unaffected individual from an ARVC family and an unrelated individual point toward other genetic factors that may play a role in ARVC5. Plakoglobin mRNA levels were higher in the male ARVC cell line tested, while Cx43 levels were either lower or not significantly different in male and female fibroblasts;

however, the significance of this is unknown. No significant differences were observed in TMEM43 and Cx43 mRNA expression when the data from both male and female ARVC cell lines were combined. Other ARVC studies have shown that plakoglobin and Cx43 expression is decreased in ARVC myocardium[191,192], and patients with low levels of plakoglobin and Cx43 were shown to have a higher frequency of ventricle tachycardia[193]. Lamin mRNA levels did not change, which is interesting as TMEM43 is known to interact with lamin, and other studies have shown that TMEM43 mutation causes stiffening of the nucleus[194]. My results from ARVC patient dermal fibroblasts suggest that the presence of the TMEM43-S358L mutant does not influence mRNA expression of lamin in fibroblasts. Future studies will uncover whether lamin protein expression or localization is altered in ARVC patient fibroblasts with the TMEM43-S358L mutation.

4.7 Extracellular matrix-associated gene expression in ARVC patient-derived Fibroblasts

A major function of fibroblasts is the production and remodeling of extracellular matrix proteins; to that end, I examined the gene expression of several ECM and ECM-interacting proteins between control and ARVC patient cell lines. There were several significant changes in ECM protein mRNA levels in the ARVC fibroblast paired with control cell lines. Collagen-1, integrin α5, and integrin 1β were upregulated, while MMP-1 and laminin were downregulated in the ARVC fibroblasts. MMP-1 mRNA was down-regulated, and integrin α5 mRNA was upregulated when all ARVC samples were combined. This is interesting as collagen-1 is an important structural protein while MMP-1 is responsible for degrading collagen-1[195]. Downregulation of MMP-1 may indicate that

collagen-1 is not being correctly regulated, leading to an excess of collagen-1 buildup. Excess collagen-1 would support the fibrosis phenotype that is often seen in ARVC hearts and could be a potential mechanism that causes the disease. TGFβ3 is involved in ECM production, and mutant TGFβ3 was found to be associated with ARVC[196]. Additionally, mice harboring the TMEM43-S358L mutation were found to upregulate TGFβ expression[135] suggesting TGFβ could be involved in ARVC. With this study, a growing body of literature points to dysregulation in ECM pathways as a potential mechanism for the fibrofatty invasion phenotype of ARVC.

4.8 Sex differences in ARVC Patient Gene Expression

TMEM43-associated ARVC is known to be more severe in males compared to females[116]. In the current study, there were no apparent differences in ECM mRNA expression between male and female fibroblasts. The fibroblast used in this study was dermal fibroblast, so it is possible that we would not observe sex-related differences since ARVC5 patients have not been described to develop skin conditions. Measuring the mRNA levels of these proteins in differentiated cardiac fibroblasts moving forward will allow us to better assess the role of ECM proteins in ARVC. Males diagnosed with ARVC have an increased likelihood of life-threatening arrhythmias and sudden cardiac death compared to females[116]. The mechanisms behind the segregation of sexes in ARVC are still unclear. There are hypotheses that differences in physical exercise between sexes and/or the effects of varying levels of sex hormones play a role[197,198]. Moving forward, incorporating sex hormones into our experimental protocols could help better mimic the hormonal levels that cardiomyocytes experience *in vivo.* Male hormones may exacerbate our findings as a study

has shown that elevated testosterone levels and decreased estradiol levels are independently linked to major arrhythmic cardiovascular events *in vivo* and *in vitro*[197].

4.9 Study Limitations

My study brings many strengths to the table, including the ability to account for genetic background in patient-derived fibroblasts, well-characterized patient samples from the Newfoundland and Labrador ARVC5 population, high reproducibility of cell culture models, and easy manipulation and pharmacological treatment of the cells. However, no study is perfect, and we must acknowledge the weakness in our research. We employed a 2-dimensional cell culture model system to study the fundamental characteristics of TMEM43 and its role in cardiomyocytes. 2-dimensional cell culture comes with its limitations, especially when differentiating iPSC into cardiomyocytes. In contrast to *in vivo* embryonic development of cardiac tissue, iPSC-CMs do not receive 3-dimensional signaling since they are cultured on a flat surface. Additionally, our cell cultures contained a single cell type that was directed towards a cardiac cell fate. *in vivo* development involves the interaction of multiple different cell types. iPSC-CMs are known to represent a very immature cardiomyocyte – approximately the same as embryonic or early fetal cardiomyocytes. They spontaneously contract, have poorly established calcium dynamics, and lack T-tubules[144]. The shortcomings of the iPSC-CM model must be considered when drawing conclusions from experiments; however, this model is still very valuable for its ease of manipulation and ability to account for genetic background in the case of patient-derived iPSC-CMs.

Extracellular matrix protein mRNA analysis was conducted on ARVC patient-derived dermal fibroblast. This should be noted as they are not the exact cell type found in the heart, although very similar. These cells are still worth investigating as TMEM43-S358L may have a similar effect on both cells.

4.10 Conclusion

This study has discovered novel characteristics of the wild-type TMEM43 protein in human iPSCs and iPSC-CMs. Interestingly, TMEM43 is located in the early endosomes of iPSCs and stays associated with this organelle for longer than 6 hours. After 6 hours, the levels of TMEM43 in the early endosomes begin to decrease, although it is unknown where TMEM43 is going at that point. I demonstrated that TMEM43 is trafficked from the cytoplasm to the nuclear envelope in iPSC-CMs after the cells have been maturing *in vitro* for 4 weeks after the onset of contraction. *TMEM43-/-* iPSC-CMs demonstrated a slight increase in abnormal calcium handling compared to wild-type iPSC-CMs. This phenotype was exacerbated after stimulation with the β-adrenergic receptor agonist isoproterenol. Additionally, knocking out TMEM43 in iPSC-CMs did not appear to affect the localization of protein markers for desmosomes, sarcomeres, or the nuclear envelope. This study demonstrates that TMEM43-S358L likely gains an abnormal function not possessed by the wild-type protein as our knockout model did not appear to dramatically inhibit cardiomyocyte function or development.

qPCR analysis of mRNA levels in ARVC patient-derived primary dermal fibroblasts showed differential expression of TMEM43, Cx43, plakoglobin, lamin, and ECM genes. Important components of the ECM, such as collagen-1, α-integrin, and β-integrin, were

upregulated, while MMP-1 and laminin were down-regulated. However, the expression of mRNA was not consistent across all ARVC patient fibroblasts. Conclusions about the role of sex differences cannot be made at this point in the study, and additional work will have to be done.

I found for the first time that wild-type TMEM43 localizes to early endosomes in undifferentiated human iPSCs. This finding supports my hypothesis that TMEM43 may be differentially trafficked across different cell and tissue types. This differential trafficking pattern may play a role in ARVC disease progression. For example, the cytoplasmic to nuclear envelope transition I observed as iPSCs mature into cardiomyocytes presents an interesting question regarding when TMEM43 becomes functional in the cell after being trafficked in iPSC-CMs. TMEM43 trafficking in most cell types, including cardiomyocytes, is poorly understood. My observations are some of the first made for endogenous TMEM43 in iPSCs and iPSC-CMs. The mutant TMEM43 protein causes up-regulation of the NF-κB-TGFβ signaling pathway. The function of the PPARγ response element in the *TMEM43* gene is unknown. TMEM43 may play a role in gene expression since ECM genes were differentially expressed in ARVC patient fibroblasts. Differential gene expression in ARVC patient fibroblasts may be associated with the increased levels of fibrosis found in the myocardium of ARVC patients. Figure 17 depicts our current knowledge about TMEM43 in different model systems and the contributions to the literature that this thesis provides.

Figure 17 Current knowledge and new contributions for wild-type and p.S358L TMEM43

An overview of the current literature concerning TMEM43 and TMEM43-S358L is highlighted on the left side of the figure. Knowledge depicted in the figure includes the localization of wild-type TMEM43 at the nuclear envelope, endoplasmic reticulum, and adherens junctions in different cell types and mutant TMEM43 in the cytoplasm and intracellular puncta in cardiomyocytes. TMEM43 interacts with lamin A/C and emerin. TMEM43-S358L mutation enhances the NF-κβ-TFGβ signaling cascade in heart tissue and primary cardiomyocyte cells. Here I have discovered that wild-type TMEM43 localizes to the early endosomes in undifferentiated human iPSCs. Furthermore, TMEM43 undergoes an endosomal-to-nuclear transition during iPSC-CM maturation. Finally, my study demonstrates that ARVC patient-derived fibroblasts exhibit altered mRNA expression of extracellular matrix proteins. Figure 17 was created using BioRender Premium software, *biorender.com*.

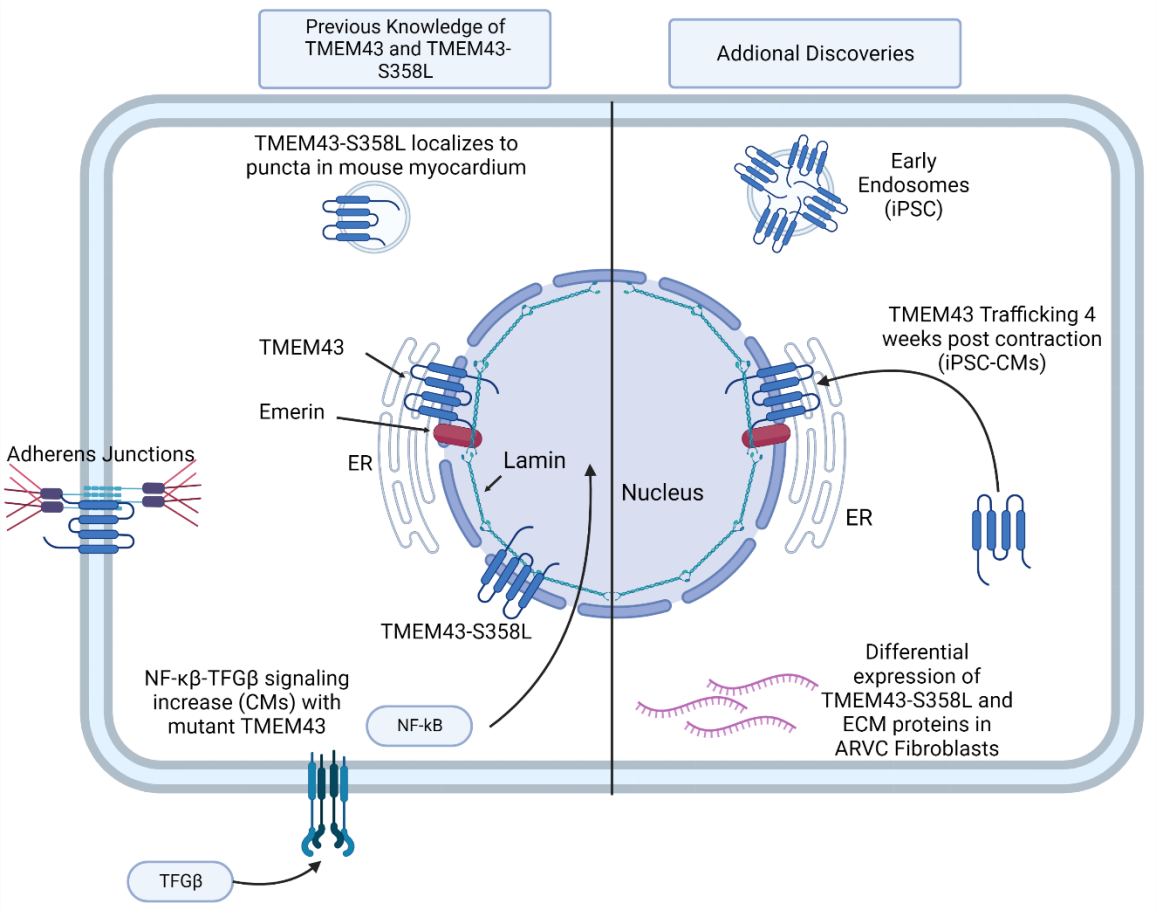
Previous Knowledge of TMEM43 and TMEM43-S358L
Addional Discoveries
TMEM43-S358L localizes to puncta in mouse myocardium
Early Endosomes (iPSC)
TMEM43
Emerin
ER
Lamin
Nucleus
ER
TMEM43 Trafficking 4 weeks post contraction (iPSC-CMs)
Adherens Junctions
TMEM43-S358L
NF-κβ-TFGβ signaling increase (CMs) with mutant TMEM43
NF-kB
Differential expression of TMEM43-S358L and ECM proteins in ARVC Fibroblasts
TFGβ

4.11 Future Directions and Outlook

Studying the role of TMEM43 in ARVC5 will certainly need more work. This research project has many promising avenues that we will investigate. Learning more about wild-type TMEM43 protein function, trafficking, protein interactions, and involvement in signaling pathways is essential to better understanding how the TMEM43-S358L mutant causes disease. It is still unknown why TMEM43 is located in early endosomes in iPSCs or how the protein gets to the nuclear envelope after cardiac lineage specification. We would like to determine what proteins TMEM43 interacts with in iPSCs and iPSC-CMs.

The Esseltine laboratory is currently in the process of reprogramming the ARVC patient-derived dermal fibroblast described in this study into iPSCs and using CRISPR-Cas9 to "repair" the mutated allele in the iPSCs. These cell lines will be instrumental in teasing out sex differences in ARVC. ARVC patient-derived iPSC-CMs will be used to study calcium handling, electrophysiology, TMEM43-S358L protein life cycle, and critical cardiac cell structures such as the sarcomere, desmosomes, and gap junctions. To better simulate the microenvironment of cardiomyocytes in the heart, multicell cultures, including cardiac fibroblasts and cardiomyocytes, should be used to see what effect it has on arrhythmogenesis and fibrofatty invasion. Another possible technique that could be integrated into the long-term project is the use of engineered heart tissues or organoids. These cell culture techniques are great for mimicking the 3-dimensional aspect of *in vivo* heart tissue.

The generation of TMEM43-associated ARVC iPSCs from patient fibroblasts is the best possible way to study this disease in a cell culture model. We are able to manipulate

these cell lines much easier than an animal model and can account for genetic variability in our study. This project moving forward, is poised to make significant contributions to our knowledge of TMEM43 and ARVC in the coming years.

References

1. Cleveland Clinic. Body Systems and Organs: Heart. Published 2021. Accessed February 18, 2022. *https://my.clevelandclinic.org/health/body/21704-heart*

2. Paige SL, Plonowska K, Xu A, Wu SM. Molecular regulation of cardiomyocyte differentiation. *Circ Res*. 2015;116(2):341-353. doi:10.1161/circresaha.116.302752

3. Buijtendijk MF, Barnett P, van den Hoff MJ. Development of the human heart. *Am J Med Genet Part C Semin Med Genet*. 2020;184C(1):7-22. doi:10.1002/ajmg.c.31778

4. Buckberg G, Nanda N, Nguyen C, Kocica M. What is the heart? Anatomy, function, pathophysiology, and misconceptions. *J Cardiovasc Dev Dis*. 2018;5(2):33. doi:10.3390/jcdd5020033

5. Rajendran P, Rengarajan T, Thangavel J, et al. The vascular endothelium and human diseases. *Int J Biol Sci*. 2013;9(10):1057-1069. doi:10.7150/ijbs.7502

6. Sherwood L, Ward C. *Human Physiology: From Cells to Systems*. 4th ed. (Jongeward C, ed.). Nelson; 2019.

7. Tallquist MD, Molkentin JD. Redefining the identity of cardiac fibroblasts. *Nat Rev Cardiol*. 2017;14(8):484-491. doi:10.1038/nrcardio.2017.57

8. Kanisicak O, Khalil H, Ivey MJ, et al. Genetic lineage tracing defines myofibroblast origin and function in the injured heart. *Nat Commun*. 2016;7(1):12260. doi:10.1038/ncomms12260

9. Vincent SD, Buckingham ME. How to make a heart: The origin and regulation of cardiac progenitor cells. *Curr Top Dev Biol*. 2010;90:1-41. doi:10.1016/S0070-2153(10)90001-X

10. Wang Z, Oron E, Nelson B, Razis S, Ivanova N. Distinct lineage specification roles for NANOG, OCT4, and SOX2 in human embryonic stem cells. *Cell Stem Cell*.

2012;10(4):440-454. doi:10.1016/j.stem.2012.02.016

11. Schier AF. Nodal signaling in vertebrate development. *Annu Rev Cell Dev Biol*. 2003;19(1):589-621. doi:10.1146/annurev.cellbio.19.041603.094522

12. Ben-Haim N, Lu C, Guzman-Ayala M, et al. The nodal precursor acting via activin receptors induces mesoderm by maintaining a source of its convertases and BMP4. *Dev Cell*. 2006;11(3):313-323. doi:10.1016/j.devcel.2006.07.005

13. Lindsley RC, Gill JG, Kyba M, Murphy TL, Murphy KM. Canonical Wnt signaling is required for development of embryonic stem cell-derived mesoderm. *Development*. 2006;133(19):3787-3796. doi:10.1242/dev.02551

14. Inman KE, Downs KM. Localization of brachyury (T) in embryonic and extraembryonic tissues during mouse gastrulation. *Gene Expr Patterns*. 2006;6(8):783-793. doi:10.1016/j.modgep.2006.01.010

15. Wilkinson DG, Bhatt S, Herrmann BG. Expression pattern of the mouse T gene and its role in mesoderm formation. *Nature*. 1990;343(6259):657-659. doi:10.1038/343657a0

16. Beddington RSP, Rashbass P, Wilson V. Brachyury - a gene affecting mouse gastrulation and early organogenesis. *Development*. 1992;116(Supplement):157-165. doi:10.1242/dev.116.Supplement.157

17. Pearce JJH, Evans MJ. Mml, a mouse Mix-like gene expressed in the primitive streak. *Mech Dev*. 1999;87(1-2):189-192. doi:10.1016/S0925-4773(99)00135-5

18. Hart AH, Hartley L, Sourris K, et al. Mixl1 is required for axial mesendoderm morphogenesis and patterning in the murine embryo. *Development*. 2002;129(15):3597-3608. doi:10.1242/dev.129.15.3597

19. Barron M, Gao M, Lough J. Requirement for BMP and FGF signaling during cardiogenic induction in non-precardiac mesoderm is specific, transient, and cooperative. *Dev Dyn*. 2000;218(2):383-393. doi:10.1002/(SICI)1097-

0177(200006)218:2<383::AID-DVDY11>3.0.CO;2-P

20. Jang J, Ku SY, Kim JE, et al. Notch inhibition promotes human embryonic stem cell-derived cardiac mesoderm differentiation. *Stem Cells*. 2008;26(11):2782-2790. doi:10.1634/stemcells.2007-1053

21. Saga Y, Kitajima S, Miyagawa-Tomita S. Mesp1 expression is the earliest sign of cardiovascular development. *Trends Cardiovasc Med*. 2000;10(8):345-352. doi:10.1016/S1050-1738(01)00069-X

22. Saga Y, Miyagawa-Tomita S, Takagi A, Kitajima S, Miyazaki J i., Inoue T. MesP1 is expressed in the heart precursor cells and required for the formation of a single heart tube. *Development*. 1999;126(15):3437-3447. doi:10.1242/dev.126.15.3437

23. Yang L, Soonpaa MH, Adler ED, et al. Human cardiovascular progenitor cells develop from a KDR+ embryonic-stem-cell-derived population. *Nature*. 2008;453(7194):524-528. doi:10.1038/nature06894

24. Lints TJ, Parsons LM, Hartley L, Lyons I, Harvey RP. Nkx-2.5: a novel murine homeobox gene expressed in early heart progenitor cells and their myogenic descendants. *Development*. 1993;119(2):419-431. doi:10.1242/dev.119.2.419

25. Lyons I, Parsons LM, Hartley L, et al. Myogenic and morphogenetic defects in the heart tubes of murine embryos lacking the homeo box gene Nkx2-5. *Genes Dev*. 1995;9(13):1654-1666. doi:10.1101/gad.9.13.1654

26. Cai C-L, Liang X, Shi Y, et al. Isl1 identifies a cardiac progenitor population that proliferates prior to differentiation and contributes a majority of cells to the heart. *Dev Cell*. 2003;5(6):877-889. doi:10.1016/S1534-5807(03)00363-0

27. Cohen ED, Wang Z, Lepore JJ, et al. Wnt/β-catenin signaling promotes expansion of Isl-1–positive cardiac progenitor cells through regulation of FGF signaling. *J Clin Invest*. 2007;117(7):1794-1804. doi:10.1172/JCI31731

28. Lin L, Cui L, Zhou W, et al. β-Catenin directly regulates Islet1 expression in

cardiovascular progenitors and is required for multiple aspects of cardiogenesis. *Proc Natl Acad Sci*. 2007;104(22):9313-9318. doi:10.1073/pnas.0700923104

29. Nakamura T, Sano M, Songyang Z, Schneider MD. A Wnt- and β-catenin-dependent pathway for mammalian cardiac myogenesis. *Proc Natl Acad Sci*. 2003;100(10):5834-5839. doi:10.1073/pnas.0935626100

30. Ueno S, Weidinger G, Osugi T, et al. Biphasic role for Wnt/beta-catenin signaling in cardiac specification in zebrafish and embryonic stem cells. *Proc Natl Acad Sci*. 2007;104(23):9685-9690. doi:10.1073/pnas.0702859104

31. Wang RN, Green J, Wang Z, et al. Bone Morphogenetic Protein (BMP) signaling in development and human diseases. *Genes Dis*. 2014;1(1):87-105. doi:10.1016/j.gendis.2014.07.005

32. Tirosh-Finkel L, Zeisel A, Brodt-Ivenshitz M, et al. BMP-mediated inhibition of FGF signaling promotes cardiomyocyte differentiation of anterior heart field progenitors. *Development*. 2010;137(18):2989-3000. doi:10.1242/dev.051649

33. Vanwijk B, Moorman A, Vandenhoff M. Role of bone morphogenetic proteins in cardiac differentiation. *Cardiovasc Res*. 2007;74(2):244-255. doi:10.1016/j.cardiores.2006.11.022

34. Akazawa H, Komuro I. Cardiac transcription factor Csx/Nkx2-5: Its role in cardiac development and diseases. *Pharmacol Ther*. 2005;107(2):252-268. doi:10.1016/j.pharmthera.2005.03.005

35. Nishii K, Morimoto S, Minakami R, et al. Targeted disruption of the cardiac troponin T gene causes sarcomere disassembly and defects in heartbeat within the early mouse embryo. *Dev Biol*. 2008;322(1):65-73. doi:10.1016/j.ydbio.2008.07.007

36. Park DS, Fishman GI. Development and function of the cardiac conduction system in health and disease. *J Cardiovasc Dev Dis*. 2017;4(2):7. doi:10.3390/jcdd4020007

37. Kockskämper J. Excitation–contraction coupling of cardiomyocytes. In:

Cardiomyocytes – Active Players in Cardiac Disease. Springer International Publishing; 2016:67-96. doi:10.1007/978-3-319-31251-4_3

38. Fabiato A. Calcium-induced release of calcium from the cardiac sarcoplasmic reticulum. *Am J Physiol Physiol*. 1983;245(1):C1-C14. doi:10.1152/ajpcell.1983.245.1.C1

39. Niggli E, Lederer WJ. Voltage-independent calcium release in heart muscle. *Science (80-)*. 1990;250(4980):565-568. doi:10.1126/science.2173135

40. Henderson CA, Gomez CG, Novak SM, Mi-Mi L, Gregorio CC. Overview of the muscle cytoskeleton. In: *Comprehensive Physiology*. Wiley; 2017:891-944. doi:10.1002/cphy.c160033

41. Blaustein MP, Lederer WJ. Sodium/calcium exchange: Its physiological implications. *Physiol Rev*. 1999;79(3):763-854. doi:10.1152/physrev.1999.79.3.763

42. Periasamy M, Kalyanasundaram A. SERCA pump isoforms: Their role in calcium transport and disease. *Muscle Nerve*. 2007;35(4):430-442. doi:10.1002/mus.20745

43. Garrod D, Chidgey M. Desmosome structure, composition and function. *Biochim Biophys Acta - Biomembr*. 2008;1778(3):572-587. doi:10.1016/j.bbamem.2007.07.014

44. Patel DM, Green KJ. Desmosomes in the heart: A review of clinical and mechanistic analyses. *Cell Commun Adhes*. 2014;21(3):109-128. doi:10.3109/15419061.2014.906533

45. Bolling MC, Jonkman MF. Skin and heart: Une liaison dangereuse. *Exp Dermatol*. 2009;18(8):658-668. doi:10.1111/j.1600-0625.2009.00908.x

46. Rickman L. N-terminal deletion in a desmosomal cadherin causes the autosomal dominant skin disease striate palmoplantar keratoderma. *Hum Mol Genet*. 1999;8(6):971-976. doi:10.1093/hmg/8.6.971

47. Samuelov L, Sarig O, Harmon RM, et al. Desmoglein 1 deficiency results in severe

dermatitis, multiple allergies and metabolic wasting. *Nat Genet*. 2013;45(10):1244-1248. doi:10.1038/ng.2739

48. Amagai M, Klaus-Kovtun V, Stanley JR. Autoantibodies against a novel epithelial cadherin in pemphigus vulgaris, a disease of cell adhesion. *Cell*. 1991;67(5):869-877. doi:10.1016/0092-8674(91)90360-B

49. Pilichou K, Nava A, Basso C, et al. Mutations in desmoglein-2 gene are associated with arrhythmogenic right ventricular cardiomyopathy. *Circulation*. 2006;113(9):1171-1179. doi:10.1161/circulationaha.105.583674

50. McGrath JA, McMillan JR, Shemanko CS, et al. Mutations in the plakophilin 1 gene result in ectodermal dysplasia/skin fragility syndrome. *Nat Genet*. 1997;17(2):240-244. doi:10.1038/ng1097-240

51. Corrado D, Thiene G. Arrhythmogenic right ventricular cardiomyopathy/dysplasia. *Circulation*. 2006;113(13):1634-1637. doi:10.1161/circulationaha.105.616490

52. Noorman M, van der Heyden MAG, van Veen TAB, et al. Cardiac cell–cell junctions in health and disease: Electrical versus mechanical coupling. *J Mol Cell Cardiol*. 2009;47(1):23-31. doi:10.1016/j.yjmcc.2009.03.016

53. Vite A, Radice GL. N-cadherin/catenin complex as a master regulator of intercalated disc function. *Cell Commun Adhes*. 2014;21(3):169-179. doi:10.3109/15419061.2014.908853

54. Vermij SH, Abriel H, van Veen TAB. Refining the molecular organization of the cardiac intercalated disc. *Cardiovasc Res*. 2017;113(3):259-275. doi:10.1093/cvr/cvw259

55. Li J, Levin MD, Xiong Y, Petrenko N, Patel V V., Radice GL. N-cadherin haploinsufficiency affects cardiac gap junctions and arrhythmic susceptibility. *J Mol Cell Cardiol*. 2008;44(3):597-606. doi:10.1016/j.yjmcc.2007.11.013

56. Swope D, Cheng L, Gao E, Li J, Radice GL. Loss of cadherin-binding proteins β-

catenin and plakoglobin in the heart leads to gap junction remodeling and arrhythmogenesis. *Mol Cell Biol*. 2012;32(6):1056-1067. doi:10.1128/MCB.06188-11

57. Kanno S, Saffitz JE. The role of myocardial gap junctions in electrical conduction and arrhythmogenesis. *Cardiovasc Pathol*. 2001;10(4):169-177. doi:10.1016/S1054-8807(01)00078-3

58. Willecke K, Hennemann H, Dahl E, Jungbluth S, Heynkes R. The diversity of connexin genes encoding gap junctional proteins. *Eur J Cell Biol*. 1991;56(1):1-7.

59. Paznekas WA, Karczeski B, Vermeer S, et al. GJA1 mutations, variants, and connexin 43 dysfunction as it relates to the oculodentodigital dysplasia phenotype. *Hum Mutat*. 2009;30(5):724-733. doi:10.1002/humu.20958

60. Judisch GF. Oculodentodigital dysplasia: four new reports and a literature review. *Arch Ophthalmol*. 1979;97(5):878-884. doi:10.1001/archopht.1979.01020010436007

61. Zhao G, Qiu Y, Zhang HM, Yang D. Intercalated discs: cellular adhesion and signaling in heart health and diseases. *Heart Fail Rev*. 2019;24:115-132. doi:10.1007/s10741-018-9743-7

62. Gros DB, Jongsma HJ. Connexins in mammalian heart function. *BioEssays*. 1996;18(9):719-730. doi:10.1002/bies.950180907

63. Severs NJ, Bruce AF, Dupont E, Rothery S. Remodelling of gap junctions and connexin expression in diseased myocardium. *Cardiovasc Res*. 2008;80(1):9-19. doi:10.1093/cvr/cvn133

64. Reaume AG, de Sousa PA, Kulkarni S, et al. Cardiac malformation in neonatal mice lacking connexin43. *Science (80-)*. 1995;267(5205):1831-1834. doi:10.1126/science.7892609

65. Government of Canada. About Heart Disease and Conditions. Published 2017.

https://www.canada.ca/en/public-health/services/diseases/heart-health/heart-diseases-conditions/about-heart-diseases-conditions.html

66. Government of Canada. Heart Disease in Canada. Published 2017. *https://www.canada.ca/en/public-health/services/publications/diseases-conditions/heart-disease-canada.html#shr-pg0*

67. American Heart Association. Bradycardia: Slow Heart Rate. Published 2016. Accessed January 23, 2022. *https://www.heart.org/en/health-topics/arrhythmia/about-arrhythmia/bradycardia--slow-heart-rate*

68. Rubenstein JJ, Schulman CL, Yurchak PM, DeSanctis RW. Clinical spectrum of the sick sinus syndrome. *Circulation*. 1972;46(1):5-13. doi:10.1161/01.cir.46.1.5

69. Mangrum JM, DiMarco JP. The evaluation and management of bradycardia. *N Engl J Med*. 2000;342(10):703-709. doi:10.1056/nejm200003093421006

70. Wung S-F. Bradyarrhythmias: Clinical presentation, diagnosis, and management. *Crit Care Nurs Clin North Am*. 2016;28(3):297-308. doi:10.1016/j.cnc.2016.04.003

71. Yeung C, Enriquez A, Suarez-Fuster L, Baranchuk A. Atrial fibrillation in patients with inherited cardiomyopathies. *EP Eur*. 2019;21(1):22-32. doi:10.1093/europace/euy064

72. Bun S-S, Latcu G, Marchlinski F, Saoudi N. Atrial flutter: more than just one of a kind. *Eur Heart J*. 2015;36:2356-2363. doi:10.1093/eurheartj/ehv118

73. Page RL, Joglar JA, Caldwell MA, et al. 2015 ACC/AHA/HRS guideline for the management of adult patients with supraventricular tachycardia: Executive summary. *Circulation*. 2016;133(14):471-505. doi:10.1161/cir.0000000000000310

74. Anter E, Tschabrunn CM, Buxton AE, Josephson ME. High-resolution mapping of postinfarction reentrant ventricular tachycardia: Electrophysiological characterization of the circuit. *Circulation*. 2016;134(4):314-327. doi:10.1161/circulationaha.116.021955

75. Martinez BK, Baker WL, Konopka A, et al. Systematic review and meta-analysis of catheter ablation of ventricular tachycardia in ischemic heart disease. *Hear Rhythm*. 2020;17(1):e206-e219. doi:10.1016/j.hrthm.2019.04.024

76. Cherry EM, Fenton FH, Gilmour RF. Mechanisms of ventricular arrhythmias: A dynamical systems-based perspective. *Am J Physiol - Hear Circ Physiol*. 2012;302(12):H2451-H2463. doi:10.1152/ajpheart.00770.2011

77. Koplan BA, Stevenson WG. Ventricular tachycardia and sudden cardiac death. In: *Mayo Clinic Proceedings*. Vol 84. ; 2009:289-297. doi:10.4065/84.3.289

78. Heart&Stroke. Cardiomyopathy. *https://www.heartandstroke.ca/heart-disease/conditions/cardiomyopathy*

79. Maron BJ, Towbin JA, Thiene G, et al. Contemporary definitions and classification of the cardiomyopathies. *Circulation*. 2006;113(14):1807-1816. doi:10.1161/circulationaha.106.174287

80. Nihoyannopoulos P, Dawson D. Restrictive cardiomyopathies. *Eur J Echocardiogr*. 2009;10(8):iii23–iii33. doi:10.1093/ejechocard/jep156

81. Luk A, Ahn E, Soor GS, Butany J, Butany J. Dilated cardiomyopathy: a review. *J Clin Pathol*. 2008;62(3):219-225. doi:10.1136/jcp.2008.060731

82. Maron BJ, Maron MS. Hypertrophic cardiomyopathy. *Lancet*. 2013;381(9862):242-255. doi:10.1016/S0140-6736(12)60397-3

83. Calkins H, Corrado D, Marcus F. Risk stratification in arrhythmogenic right ventricular cardiomyopathy. *Circulation*. 2017;136(21):2068-2082. doi:10.1161/circulationaha.117.030792

84. López-Ayala JM, Gómez-Milanés I, Sánchez Muñoz JJ, et al. Desmoplakin truncations and arrhythmogenic left ventricular cardiomyopathy: characterizing a phenotype. *EP Eur*. 2014;16(12):1838-1846. doi:10.1093/europace/euu128

85. Bao J, Wang J, Yao Y, et al. Correlation of ventricular arrhythmias with genotype

in arrhythmogenic right ventricular cardiomyopathy. *Circ Cardiovasc Genet*. 2013;6(6):552-556. doi:10.1161/circgenetics.113.000122

86. Mayo Clinic. Diseases & conditions: Cardiomyopathy. Published 2021. Accessed February 20, 2022. *https://www.mayoclinic.org/diseases-conditions/cardiomyopathy/symptoms-causes/syc-20370709*

87. McNally EM, Barefield DY, Puckelwartz MJ. The genetic landscape of cardiomyopathy and its role in heart failure. *Cell Metab*. 2015;21(2):174-182. doi:10.1016/j.cmet.2015.01.013

88. Jacoby D, McKenna WJ. Genetics of inherited cardiomyopathy. *Eur Heart J*. 2012;33(3):296-304. doi:10.1093/eurheartj/ehr260

89. Marian AJ, Braunwald E. Hypertrophic cardiomyopathy: genetics, pathogenesis, clinical manifestations, diagnosis, and therapy. *Circ Res*. 2017;121(7):749-770. doi:10.1161/circresaha.117.311059

90. MedlinePlus. Arrhythmogenic right ventricular cardiomyopathy. Bethesda (MD): National Library of Medicine (US); [updated 2018 Feb 1]. Published 2018. Accessed June 5, 2022. *https://medlineplus.gov/genetics/condition/arrhythmogenic-right-ventricular-cardiomyopathy/#references*

91. Brieler J, Breeden MA, Tucker J. Cardiomyopathy: An overview. *Am Fam Physician*. 2017;96(10):640-646. http://www.ncbi.nlm.nih.gov/pubmed/29431384

92. Ommen SR, Mital S, Burke MA, et al. 2020 AHA/ACC guideline for the diagnosis and treatment of patients with hypertrophic cardiomyopathy: Executive summary. *Circulation*. 2020;142(25):E23-E106. doi:10.1161/cir.0000000000000938

93. Gandjbakhch E, Redheuil A, Pousset F, Charron P, Frank R. Clinical diagnosis, imaging, and genetics of arrhythmogenic right ventricular cardiomyopathy/dysplasia: JACC state-of-the-art review. *J Am Coll Cardiol*. 2018;72(7):784-804. doi:10.1016/j.jacc.2018.05.065

94. Gemayel C, Pelliccia A, Thompson PD. Arrhythmogenic right ventricular cardiomyopathy. *J Am Coll Cardiol*. 2001;38(7):1773-1781. doi:10.1016/S0735-1097(01)01654-0

95. Prior D, La Gerche A. Exercise and arrhythmogenic right ventricular cardiomyopathy. *Hear Lung Circ*. 2020;29(4):547-555. doi:10.1016/j.hlc.2019.12.007

96. Te Riele ASJM, Hauer RN. Arrhythmogenic right ventricular dysplasia/cardiomyopathy: Clinical challenges in a changing disease spectrum. *Trends Cardiovasc Med*. 2015;25(3):191-198. doi:10.1016/j.tcm.2014.11.003

97. Sen-Chowdhry S, Syrris P, Ward D, Asimaki A, Sevdalis E, McKenna WJ. Clinical and genetic characterization of families with arrhythmogenic right ventricular dysplasia/cardiomyopathy provides novel insights into patterns of disease expression. *Circulation*. 2007;115(13):1710-1720. doi:10.1161/circulationaha.106.660241

98. Berte B, Denis A, Amraoui S, et al. Characterization of the left-sided substrate in arrhythmogenic right ventricular cardiomyopathy. *Circ Arrhythmia Electrophysiol*. 2015;8(6):1403-1412. doi:10.1161/circep.115.003213

99. Tansey DK, Aly Z, Sheppard MN. Fat in the right ventricle of the normal heart. *Histopathology*. 2005;46(1):98-104. doi:10.1111/j.1365-2559.2005.02054.x

100. te Riele ASJM, Tandri H, Sanborn DM, Bluemke DA. Noninvasive multimodality imaging in ARVD/C. *JACC Cardiovasc Imaging*. 2015;8(5):597-611. doi:10.1016/j.jcmg.2015.02.007

101. Lahtinen AM, Lehtonen E, Marjamaa A, et al. Population-prevalent desmosomal mutations predisposing to arrhythmogenic right ventricular cardiomyopathy. *Hear Rhythm*. 2011;8(8):1214-1221. doi:10.1016/j.hrthm.2011.03.015

102. Basso C, Corrado D, Marcus FI, Nava A, Thiene G. Arrhythmogenic right ventricular cardiomyopathy. *Lancet*. 2009;373(9671):1289-1300.

doi:10.1016/S0140-6736(09)60256-7

103. Porter KE, Turner NA. Cardiac fibroblasts: At the heart of myocardial remodeling. *Pharmacol Ther*. 2009;123(2):255-278. doi:10.1016/j.pharmthera.2009.05.002

104. Girolami F, Iascone M, Tomberli B, et al. Novel α-actinin 2 variant associated with familial hypertrophic cardiomyopathy and juvenile atrial arrhythmias. *Circ Cardiovasc Genet*. 2014;7(6):741-750. doi:10.1161/circgenetics.113.000486

105. Purevjav E, Varela J, Morgado M, et al. Nebulette mutations are associated with dilated cardiomyopathy and endocardial fibroelastosis. *J Am Coll Cardiol*. 2010;56(18):1493-1502. doi:10.1016/j.jacc.2010.05.045

106. Finkbeiner S. The autophagy lysosomal pathway and neurodegeneration. *Cold Spring Harb Perspect Biol*. 2020;12(3):a033993. doi:10.1101/cshperspect.a033993

107. Vite A, Gandjbakhch E, Prost C, et al. Desmosomal cadherins are decreased in explanted arrhythmogenic right ventricular dysplasia/cardiomyopathy patient hearts. Mohanraj R, ed. *PLoS One*. 2013;8(9):e75082. doi:10.1371/journal.pone.0075082

108. Asimaki A, Syrris P, Wichter T, Matthias P, Saffitz JE, McKenna WJ. A novel dominant mutation in plakoglobin causes arrhythmogenic right ventricular cardiomyopathy. *Am J Hum Genet*. 2007;81(5):964-973. doi:10.1086/521633

109. Rahman P. The Newfoundland population: a unique resource for genetic investigation of complex diseases. *Hum Mol Genet*. 2004;13(12):1287-1287. doi:10.1093/hmg/ddh143

110. Grewal KK, Stefanelli MG, Meijer IA, Hand CK, Rouleau GA, Ives EJ. A founder effect in three large Newfoundland families with a novel clinically variable spastic ataxia and supranuclear gaze palsy. *Am J Med Genet*. 2004;131A(3):249-254. doi:10.1002/ajmg.a.30397

111. Pater JA, Benteau T, Griffin A, et al. A common variant in CLDN14 causes precipitous, prelingual sensorineural hearing loss in multiple families due to founder

effect. *Hum Genet*. 2017;136(1):107-118. doi:10.1007/s00439-016-1746-7

112. Dawson LM, Smith KN, Werdyani S, et al. A dominant RAD51C pathogenic splicing variant predisposes to breast and ovarian cancer in the Newfoundland population due to founder effect. *Mol Genet Genomic Med*. 2020;8(2):1070. doi:10.1002/mgg3.1070

113. Martin LJ, Crawford MH, Koertvelyessy T, Keeping D, Collins M, Huntsman R. The population structure of ten Newfoundland outports. *Hum Biol*. 2000;72(6):997-1016.

114. Zhai G, Zhou J, Woods MO, et al. Genetic structure of the Newfoundland and Labrador population: founder effects modulate variability. *Eur J Hum Genet*. 2016;24(7):1063-1070. doi:10.1038/ejhg.2015.256

115. Ada Hamosh. Online Mendelian Inheritance of Man. Published January 16, 2022. Accessed January 17, 2022. *https://www.ncbi.nlm.nih.gov/omim/?term=Newfoundland*

116. Merner ND, Hodgkinson KA, Haywood AFM, et al. Arrhythmogenic right ventricular cardiomyopathy type 5 is a fully penetrant, lethal arrhythmic disorder caused by a missense mutation in the TMEM43 Gene. *Am J Hum Genet*. 2008;82(4):809-821. doi:10.1016/j.ajhg.2008.01.010

117. Hodgkinson KA, Connors SP, Merner N, et al. The natural history of a genetic subtype of arrhythmogenic right ventricular cardiomyopathy caused by a p.S358L mutation in TMEM43. *Clin Genet*. 2013;83(4):321-331. doi:10.1111/j.1399-0004.2012.01919.x

118. Bengtsson L, Otto H. LUMA interacts with emerin and influences its distribution at the inner nuclear membrane. *J Cell Sci*. 2008;121(4):536-548. doi:10.1242/jcs.019281

119. Dreger M, Bengtsson L, Schöneberg T, Otto H, Hucho F. Nuclear envelope proteomics: Novel integral membrane proteins of the inner nuclear membrane. *Proc*

Natl Acad Sci U S A. 2001;98(21):11943-11948. doi:10.1073/pnas.211201898

120. Rajkumar R, Sembrat JC, McDonough B, Seidman CE, Ahmad F. Functional effects of the TMEM43 Ser358Leu mutation in the pathogenesis of arrhythmogenic right ventricular cardiomyopathy. *BMC Med Genet*. 2012;13:21. doi:10.1186/1471-2350-13-21

121. Shinomiya H, Kato H, Kuramoto Y, et al. Aberrant accumulation of TMEM43 accompanied by perturbed transmural gene expression in arrhythmogenic cardiomyopathy. *FASEB J*. 2021;35(11):e21994. doi:10.1096/fj.202100800R

122. Franke WW, Dörflinger Y, Kuhn C, et al. Protein LUMA is a cytoplasmic plaque constituent of various epithelial adherens junctions and composite junctions of myocardial intercalated disks: A unifying finding for cell biology and cardiology. *Cell Tissue Res*. 2014;357(1):159-172. doi:10.1007/s00441-014-1865-1

123. Christensen A, Andersen C, Tybjærg-Hansen A, et al. Mutation analysis and evaluation of the cardiac localization of TMEM43 in arrhythmogenic right ventricular cardiomyopathy. *Clin Genet*. 2011;80(3):256-264. doi:10.1111/j.1399-0004.2011.01623.x

124. Padrón-Barthe L, Villalba-Orero M, Gómez-Salinero JM, et al. Severe cardiac dysfunction and death caused by arrhythmogenic right ventricular cardiomyopathy type 5 are improved by inhibition of glycogen synthase kinase-3β. *Circulation*. 2019;140(14):1188-1204. doi:10.1161/circulationaha.119.040366

125. Stroud MJ, Fang X, Zhang J, et al. Luma is not essential for murine cardiac development and function. *Cardiovasc Res*. 2018;114(3):378-388. doi:10.1093/cvr/cvx205

126. Liang W-C, Mitsuhashi H, Keduka E, et al. TMEM43 mutations in emery-dreifuss muscular dystrophy-related myopathy. *Ann Neurol*. 2011;69(6):1005-1013. doi:10.1002/ana.22338

127. Jang MW, Oh D-Y, Yi E, et al. A nonsense TMEM43 variant leads to disruption of

connexin-linked function and autosomal dominant auditory neuropathy spectrum disorder. *Proc Natl Acad Sci*. 2021;118(22):e2019681118. doi:10.1073/pnas.2019681118

128. Jang MW, Kim TY, Sharma K, Kwon J, Yi E, Lee CJ. A deafness associated protein TMEM43 interacts with KCNK3 (TASK-1) two-pore domain K + (K2P) channel in the cochlea. *Exp Neurobiol*. 2021;30(5):319-328. doi:10.5607/en21028

129. Baskin B, Skinner JR, Sanatani S, et al. TMEM43 mutations associated with arrhythmogenic right ventricular cardiomyopathy in non-Newfoundland populations. *Hum Genet*. 2013;132(11):1245-1252. doi:10.1007/s00439-013-1323-2

130. Paulin FL, Hodgkinson KA, MacLaughlan S, et al. Exercise and arrhythmic risk in TMEM43 p.S358L arrhythmogenic right ventricular cardiomyopathy. *Hear Rhythm*. 2020;17(7):1159-1166. doi:10.1016/j.hrthm.2020.02.028

131. Dominguez F, Zorio E, Jimenez-Jaimez J, et al. Clinical characteristics and determinants of the phenotype in TMEM43 arrhythmogenic right ventricular cardiomyopathy type 5. *Hear Rhythm*. 2020;17(6):945-954. doi:10.1016/j.hrthm.2020.01.035

132. Hodgkinson KA, Howes AJ, Boland P, et al. Long-term clinical outcome of arrhythmogenic right ventricular cardiomyopathy in individuals with a p.S358L mutation in TMEM43 following implantable cardioverter defibrillator therapy. *Circ Arrhythmia Electrophysiol*. 2016;9(3):e003589. doi:10.1161/circep.115.003589

133. Syrris P, Ward D, Asimaki A, et al. Desmoglein-2 mutations in arrhythmogenic right ventricular cardiomyopathy: a genotype-phenotype characterization of familial disease. *Eur Heart J*. 2006;28(5):581-588. doi:10.1093/eurheartj/ehl380

134. Kim C, Wong J, Wen J, et al. Studying arrhythmogenic right ventricular dysplasia with patient-specific iPSCs. *Nature*. 2013;494(7435):105-110. doi:10.1038/nature11799

135. Zheng G, Jiang C, Li Y, et al. TMEM43-S358L mutation enhances NF-κB-TGFβ signal cascade in arrhythmogenic right ventricular dysplasia/cardiomyopathy. *Protein Cell*. 2019;10(2):104-119. doi:10.1007/s13238-018-0563-2

136. Lowry WE, Richter L, Yachechko R, et al. Generation of human induced pluripotent stem cells from dermal fibroblasts. *Proc Natl Acad Sci*. 2008;105(8):2883-2888. doi:10.1073/pnas.0711983105

137. Ran FA, Hsu PD, Wright J, Agarwala V, Scott DA, Zhang F. Genome engineering using the CRISPR-Cas9 system. *Nat Protoc*. 2013;8(11):2281-2308. doi:10.1038/nprot.2013.143

138. Platt RJ, Chen S, Zhou Y, et al. CRISPR-Cas9 knockin mice for genome editing and cancer modeling. *Cell*. 2014;159(2):440-455. doi:10.1016/j.cell.2014.09.014

139. Fontaine V, Duboscq-Bidot L, Jouve C, et al. Generation of iPSC line from MYH7 R403L mutation carrier with severe hypertrophic cardiomyopathy and isogenic CRISPR/Cas9 corrected control. *Stem Cell Res*. 2021;52:102245. doi:10.1016/j.scr.2021.102245

140. Jiang F, Doudna JA. CRISPR–Cas9 structures and mechanisms. *Annu Rev Biophys*. 2017;46(1):505-529. doi:10.1146/annurev-biophys-062215-010822

141. Lino CA, Harper JC, Carney JP, Timlin JA. Delivering CRISPR: a review of the challenges and approaches. *Drug Deliv*. 2018;25(1):1234-1257. doi:10.1080/10717544.2018.1474964

142. Lian X, Zhang J, Azarin SM, et al. Directed cardiomyocyte differentiation from human pluripotent stem cells by modulating Wnt/β-catenin signaling under fully defined conditions. *Nat Protoc*. 2013;8(1):162-175. doi:10.1038/nprot.2012.150

143. Olson EN, Schneider MD. Sizing up the heart: development redux in disease. *Genes Dev*. 2003;17(16):1937-1956. doi:10.1101/gad.1110103

144. Karbassi E, Fenix A, Marchiano S, et al. Cardiomyocyte maturation: advances in

knowledge and implications for regenerative medicine. *Nat Rev Cardiol*. 2020;17(6):341-359. doi:10.1038/s41569-019-0331-x

145. Mordwinkin NM, Lee AS, Wu JC. Patient-specific stem cells and cardiovascular drug discovery. *JAMA*. 2013;310(19):2039. doi:10.1001/jama.2013.282409

146. Matsa E, Burridge PW, Wu JC. Human stem cells for modeling heart disease and for drug discovery. *Sci Transl Med*. 2014;6(239):239ps6. doi:10.1126/scitranslmed.3008921

147. Karakikes I, Ameen M, Termglinchan V, Wu JC. Human induced pluripotent stem cell–derived cardiomyocytes. *Circ Res*. 2015;117(1):80-88. doi:10.1161/circresaha.117.305365

148. Lieu DK, Liu J, Siu C-W, et al. Absence of transverse tubules contributes to non-uniform Ca 2+ wavefronts in mouse and human embryonic stem cell–derived cardiomyocytes. *Stem Cells Dev*. 2009;18(10):1493-1500. doi:10.1089/scd.2009.0052

149. Lan F, Lee AS, Liang P, et al. Abnormal calcium handling properties underlie familial hypertrophic cardiomyopathy pathology in patient-specific induced pluripotent stem cells. *Cell Stem Cell*. 2013;12(1):101-113. doi:10.1016/j.stem.2012.10.010

150. Sun N, Yazawa M, Liu J, et al. Patient-specific induced pluripotent stem cells as a model for familial dilated cardiomyopathy. *Sci Transl Med*. 2012;4(130):130ra47. doi:10.1126/scitranslmed.3003552

151. Wu H, Lee J, Vincent LG, et al. Epigenetic regulation of phosphodiesterases 2A and 3A underlies compromised β-adrenergic signaling in an iPSC model of dilated cardiomyopathy. *Cell Stem Cell*. 2015;17(1):89-100. doi:10.1016/j.stem.2015.04.020

152. Hawthorne RN, Blazeski A, Lowenthal J, et al. Altered electrical, biomolecular, and immunologic phenotypes in a novel patient-derived stem cell model of desmoglein-

2 mutant ARVC. *J Clin Med*. 2021;10(14):3061. doi:10.3390/jcm10143061

153. Caspi O, Huber I, Gepstein A, et al. Modeling of arrhythmogenic right ventricular cardiomyopathy with human induced pluripotent stem cells. *Circ Cardiovasc Genet*. 2013;6(6):557-568. doi:10.1161/circgenetics.113.000188

154. Chen P, Xiao Y, Wang Y, et al. Intracellular calcium current disorder and disease phenotype in OBSCN mutant iPSC-based cardiomyocytes in arrhythmogenic right ventricular cardiomyopathy. *Theranostics*. 2020;10(24):11215-11229. doi:10.7150/thno.45172

155. Ratnavadivel S, Szymanski de Toledo M, Rasmussen TB, et al. Human pluripotent stem cell line (HDZi001-A) derived from a patient carrying the ARVC-5 associated mutation TMEM43-p.S358L. *Stem Cell Res*. 2020;48:101957. doi:10.1016/j.scr.2020.101957

156. El-Battrawy I, Zhao Z, Lan H, et al. Electrical dysfunctions in human-induced pluripotent stem cell-derived cardiomyocytes from a patient with an arrhythmogenic right ventricular cardiomyopathy. *EP Eur*. 2018;20(FI1):f46-f56. doi:10.1093/europace/euy042

157. Smith AST, Macadangdang J, Leung W, Laflamme MA, Kim D-H. Human iPSC-derived cardiomyocytes and tissue engineering strategies for disease modeling and drug screening. *Biotechnol Adv*. 2017;35(1):77-94. doi:10.1016/j.biotechadv.2016.12.002

158. Lemoine MD, Mannhardt I, Breckwoldt K, et al. Human iPSC-derived cardiomyocytes cultured in 3D engineered heart tissue show physiological upstroke velocity and sodium current density. *Sci Rep*. 2017;7(1):5464. doi:10.1038/s41598-017-05600-w

159. Esseltine JL, Shao Q, Brooks C, et al. Connexin43 mutant patient-derived induced pluripotent stem cells exhibit altered differentiation potential. *J Bone Miner Res*. 2017;32(6):1368-1385. doi:10.1002/jbmr.3098

160. Chen G, Gulbranson DR, Hou Z, et al. Chemically defined conditions for human iPSC derivation and culture. *Nat Methods*. 2011;8(5):424-429. doi:10.1038/nmeth.1593

161. Vangipuram M, Ting D, Kim S, Diaz R, Schüle B. Skin punch biopsy explant culture for derivation of primary human fibroblasts. *J Vis Exp*. 2013;(77):e3779. doi:10.3791/3779

162. Rittié L, Fisher GJ. Isolation and culture of skin fibroblasts. *Methods Mol Med*. 2005;17:83-98. doi:10.1385/1-59259-940-0:083

163. Esseltine JL, Brooks CR, Edwards NA, et al. Dynamic regulation of connexins in stem cell pluripotency. *Stem Cells*. 2020;38(1):52-66. doi:10.1002/stem.3092

164. Shao Q, Esseltine JL, Huang T, et al. Connexin43 is dispensable for early stage human mesenchymal stem cell adipogenic differentiation but is protective against cell senescence. *Biomolecules*. 2019;9(9):474. doi:10.3390/biom9090474

165. Brugè F, Venditti E, Tiano L, Littarru GP, Damiani E. Reference gene validation for qPCR on normoxia- and hypoxia-cultured human dermal fibroblasts exposed to UVA: Is β-actin a reliable normalizer for photoaging studies? *J Biotechnol*. 2011;156(3):153-162. doi:10.1016/j.jbiotec.2011.09.018

166. Zainuddin A, Chua KH, Rahim NA, Makpol S. Effect of experimental treatment on GAPDH mRNA expression as a housekeeping gene in human diploid fibroblasts. *BMC Mol Biol*. 2010;11(1):59. doi:10.1186/1471-2199-11-59

167. Maioli M, Rinaldi S, Santaniello S, et al. Radio electric conveyed fields directly reprogram human dermal skin fibroblasts toward cardiac, neuronal, and skeletal muscle-like lineages. *Cell Transplant*. 2013;22(7):1227-1235. doi:10.3727/096368912X657297

168. Esseltine JL, Shao Q, Huang T, Kelly JJ, Sampson J, Laird DW. Manipulating Cx43 expression triggers gene reprogramming events in dermal fibroblasts from oculodentodigital dysplasia patients. *Biochem J*. 2015;472(1):55-69.

doi:10.1042/BJ20150652

169. Rouhi L, Cheedipudi SM, Chen SN, et al. Haploinsufficiency of Tmem43 in cardiac myocytes activates the DNA damage response pathway leading to a late-onset senescence-associated pro-fibrotic cardiomyopathy. *Cardiovasc Res*. 2021;117(11):2377-2394. doi:10.1093/cvr/cvaa300

170. Kolanowski TJ, Antos CL, Guan K. Making human cardiomyocytes up to date: Derivation, maturation state and perspectives. *Int J Cardiol*. 2017;241:379-386. doi:10.1016/j.ijcard.2017.03.099

171. Siragam V, Cui X, Masse S, et al. TMEM43 mutation p.S358L alters intercalated disc protein expression and reduces conduction velocity in arrhythmogenic right ventricular cardiomyopathy. Ai X, ed. *PLoS One*. 2014;9(10):e109128. doi:10.1371/journal.pone.0109128

172. de Jong S, van Veen TAB, van Rijen HVM, de Bakker JMT. Fibrosis and cardiac arrhythmias. *J Cardiovasc Pharmacol*. 2011;57(6):630-638. doi:10.1097/FJC.0b013e318207a35f

173. Jovic M, Sharma M, Rahajeng J, Caplan S. The early endosome: a busy sorting station for proteins at the crossroads. *Histol Histopathol*. 2010;25(1):99-112. doi:10.14670/HH-25.99

174. Podlecki DA, Smith RM, Kao M, et al. Nuclear translocation of the insulin receptor. A possible mediator of insulin's long term effects. *J Biol Chem*. 1987;262(7):3362-3368. doi:10.1016/S0021-9258(18)61511-X

175. Maher PA. Nuclear Translocation of fibroblast growth factor (FGF) receptors in response to FGF-2. *J Cell Biol*. 1996;134(2):529-536. doi:10.1083/jcb.134.2.529

176. Chaumet A, Wright GD, Seet SH, Tham KM, Gounko N V., Bard F. Nuclear envelope-associated endosomes deliver surface proteins to the nucleus. *Nat Commun*. 2015;6(1):8218. doi:10.1038/ncomms9218

177. Shah, Chaumet, Royle, Bard. The NAE pathway: Autobahn to the nucleus for cell surface receptors. *Cells*. 2019;8(8):915. doi:10.3390/cells8080915

178. Sadighian H. Cellular mechanisms underlying inherited arrhythmogenic right ventricular cardiomyopathy in the newfoundland population. Published online 2021.

179. Bucci C, Thomsen P, Nicoziani P, McCarthy J, van Deurs B. Rab7: A key to lysosome biogenesis. *Mol Biol Cell*. 2000;11(2):467-480. doi:10.1091/mbc.11.2.467

180. Bucci C, Parton RG, Mather IH, et al. The small GTPase rab5 functions as a regulatory factor in the early endocytic pathway. *Cell*. 1992;70(5):715-728. doi:10.1016/0092-8674(92)90306-W

181. McCaffrey MW, Bielli A, Cantalupo G, et al. Rab4 affects both recycling and degradative endosomal trafficking. *FEBS Lett*. 2001;495(1-2):21-30. doi:10.1016/S0014-5793(01)02359-6

182. Ullrich O, Reinsch S, Urbé S, Zerial M, Parton RG. Rab11 regulates recycling through the pericentriolar recycling endosome. *J Cell Biol*. 1996;135(4):913-924. doi:10.1083/jcb.135.4.913

183. Feng Y, Press B, Wandinger-Ness A. Rab 7: an important regulator of late endocytic membrane traffic. *J Cell Biol*. 1995;131(6):1435-1452. doi:10.1083/jcb.131.6.1435

184. Lombardi D, Soldati T, Riederer MA, Goda Y, Zerial M, Pfeffer SR. Rab9 functions in transport between late endosomes and the trans Golgi network. *EMBO J*. 1993;12(2):677-682. doi:10.1002/j.1460-2075.1993.tb05701.x

185. Machiraju P, Greenway SC. Current methods for the maturation of induced pluripotent stem cell-derived cardiomyocytes. *World J Stem Cells*. 2019;11(1):33-43. doi:10.4252/wjsc.v11.i1.33

186. Thyagarajan T, Totey S, Danton MJS, Kulkarni AB. Genetically altered mouse models: the good, the bad, and the ugly. *Crit Rev Oral Biol Med*. 2003;14(3):154-174. doi:10.1177/154411130301400302

187. Corrado D, Basso C, Rizzoli G, Schiavon M, Thiene G. Does sports activity enhance the risk of sudden death in adolescents and young adults? *J Am Coll Cardiol*. 2003;42(11):1959-1963. doi:10.1016/j.jacc.2003.03.002

188. Wang Y, Li C, Shi L, et al. Integrin β1D deficiency–mediated RyR2 dysfunction contributes to catecholamine-sensitive ventricular tachycardia in arrhythmogenic right ventricular cardiomyopathy. *Circulation*. 2020;141(18):1477-1493. doi:10.1161/circulationaha.119.043504

189. Moore-Morris T, Guimarães-Camboa N, Banerjee I, et al. Resident fibroblast lineages mediate pressure overload–induced cardiac fibrosis. *J Clin Invest*. 2014;124(7):2921-2934. doi:10.1172/JCI74783

190. Chang CW, Dalgliesh AJ, López JE, Griffiths LG. Cardiac extracellular matrix proteomics: Challenges, techniques, and clinical implications. *PROTEOMICS - Clin Appl*. 2016;10(1):39-50. doi:10.1002/prca.201500030

191. Asimaki A, Tandri H, Huang H, et al. A new diagnostic test for arrhythmogenic right ventricular cardiomyopathy. *N Engl J Med*. 2009;360(11):1075-1084. doi:10.1056/NEJMoa0808138

192. Noorman M, Hakim S, Kessler E, et al. Remodeling of the cardiac sodium channel, connexin43, and plakoglobin at the intercalated disk in patients with arrhythmogenic cardiomyopathy. *Hear Rhythm*. 2013;10(3):412-419. doi:10.1016/j.hrthm.2012.11.018

193. Yoshida T, Kawano H, Kusumoto S, et al. Relationships between clinical characteristics and decreased plakoglobin and connexin 43 expressions in myocardial biopsies from patients with arrhythmogenic right ventricular cardiomyopathy. *Int Heart J*. 2015;56(6):626-631. doi:10.1536/ihj.15-144

194. Milting H, Klauke B, Christensen AH, et al. The TMEM43 Newfoundland mutation p.S358L causing ARVC-5 was imported from Europe and increases the stiffness of the cell nucleus. *Eur Heart J*. 2015;36(14):872-881. doi:10.1093/eurheartj/ehu077

195. Ricard-Blum S. The collagen family. *Cold Spring Harb Perspect Biol*. 2011;3(1):a004978-a004978. doi:10.1101/cshperspect.a004978

196. BEFFAGNA G, OCCHI G, NAVA A, et al. Regulatory mutations in transforming growth factor-beta3 gene cause arrhythmogenic right ventricular cardiomyopathy type 1. *Cardiovasc Res*. 2005;65(2):366-373. doi:10.1016/j.cardiores.2004.10.005

197. Akdis D, Saguner AM, Shah K, et al. Sex hormones affect outcome in arrhythmogenic right ventricular cardiomyopathy/dysplasia: from a stem cell derived cardiomyocyte-based model to clinical biomarkers of disease outcome. *Eur Heart J*. 2017;38(19):1498-1508. doi:10.1093/eurheartj/ehx011

198. Kirchhof P, Fabritz L, Zwiener M, et al. Age- and training-dependent development of arrhythmogenic right ventricular cardiomyopathy in heterozygous plakoglobin-deficient mice. *Circulation*. 2006;114(17):1799-1806. doi:10.1161/circulationaha.106.624502

Appendix A

Ethics approval for this study was granted to Dr. Jessica Esseltine (PI).

Subject **HREB - Approval of Ethics Renewal 559689**
From <administrator@hrea.ca>
To Esseltine Jessica(Principal Investigator) <jesseltine@mun.ca>
Cc Hodgkinson Kathleen(Co-Principal Investigator) <KHODGKIN@mun.ca>, <administrator@hrea.ca>
Date 2022-01-25 16:37

roundcube
open source webmail software

Researcher Portal File #: 20211181

Dear Dr. Jessica Esseltine:

This e-mail serves as notification that your ethics renewal for study HREB # 2020.301 – A personalized, translational approach using molecular mechanisms to understanding inherited Arrhythmogenic Right Ventricular Cardiomyopathy caused by TMEM43 p.S358L in Newfoundland and Labrador – has been **approved**. Please log in to the Researcher Portal to view the approved event.

Ethics approval for this project has been granted for a period of twelve months effective from January 13, 2022 to January 13, 2023.

Please note, it is the responsibility of the Principal Investigator (PI) to ensure that the Ethics Renewal form is submitted prior to the renewal date each year. Though the Research Ethics Office makes every effort to remind the PI of this responsibility, the PI may not receive a reminder. The Ethics Renewal form can be found on the Researcher Portal as an "Event".

The ethics renewal [will be reported] to the Health Research Ethics Board at their meeting dated February 8, 2021.

Thank you,

Research Ethics Office

(e) info@hrea.ca
(t) 709-777-6974
(f) 709-777-8776
(w) www.hrea.ca
Office Hours: 8:30 a.m. – 4:30 p.m. (NL TIME) Monday-Friday

Appendix B

Supplemental Figure 1 *GAPDH* gene expression across all cell lines used in this study

GAPDH was used as the reference gene for all qPCR transcript expression analysis as it was stably expressed in all cell lines assessed in this study.